Through-space higher dimensionality conjugation to enhance optical properties?; an exploratory computational investigation on a model system

Ou Xie, Carl W. Dirk*

Department of Chemistry

The University of Texas at El Paso

El Paso, TX 79968-0513

cwdirk@utep.edu

20000718 091

REPORT DOCUMENTATION PAGE

AFRL-SR-BL-TR-00-

0250

Public reporting burden for this collection of information is estimated to average 1 hour per response, including the data needed, and completing and reviewing the collection of information. ... collection of information, including suggestions for reducing this burden, to Washington Headquarters Service, Davis Highway, Suite 1204, Arlington, VA 22202-4302, and to the Office of Management and Budget, Paperwork Reduction Project (0704-0188), Washington, DC 20503.

1. AGENCY USE ONLY *(Leave blank)*	2. REPORT DATE	3. REPORT TYPE AND DATES COVERED
		Final - 01 May 96 - 31 Oct 97

4. TITLE AND SUBTITLE
Approaches Toward Systematic Enhancement and Developmentof Organic Electro-Optic and All-Optic Materials Possessing Unprecedented Magnitudes of Optical Nonlinearity

5. FUNDING NUMBERS
F49620-96-1-0013

6. AUTHOR(S)
Dr Carl W. Dirk

7. PERFORMING ORGANIZATION NAME(S) AND ADDRESS(ES)
University of Texas at El Paso
El Paso TX 79968-0513

8. PERFORMING ORGANIZATION REPORT NUMBER

9. SPONSORING/MONITORING AGENCY NAME(S) AND ADDRESS(ES)
AFOSR/NL
801 N. Randolph St.,Rm 732
Arlington VA 22203-1977

10. SPONSORING/MONITORING AGENCY REPORT NUMBER

11. SUPPLEMENTARY NOTES

12a. DISTRIBUTION AVAILABILITY STATEMENT
Approved for Public Release: Distribution Unlimited

12b. DISTRIBUTION CODE

13. ABSTRACT *(Maximum 200 words)*

AMPAC (Semichem Inc.) AMI semi-empirical calculations on stacked benzene delocalized ring systems suggest that very large order polarizabilities (y) can be obtained. Systems of +2 charge consisting of benzene rings separated by 3 A, display finite-field (FF) zero frequency y(0;0,0,0)s that are many orders of magnitude larger than any thus far commonly encountered or previously predicted for organics. The ratio of the FF Re[a] is an increasing function with system size for the +2 species and is a decreasing function for the neutral species. Up to 14 rings, the largest systems currently calculated, there is not yet a clear indication of leveling-off or saturation of or y/a. This is discussed in the context of the absence of electron correlation in these SCF-only calculations. The feasibility of such systems is discussed, as well as potentially significant limiatation to the calculations that need to be further investigated before the certainty of these predictions can be certified.

14. SUBJECT TERMS	15. NUMBER OF PAGES
	75
	16. PRICE CODE

17. SECURITY CLASSIFICATION OF REPORT	18. SECURITY CLASSIFICATION OF THIS PAGE	19. SECURITY CLASSIFICATION OF ABSTRACT	20. LIMITATION OF ABSTRACT
UNCLASS	UNCLASS	UNCLASS	

ABSTRACT

AMPAC (Semichem Inc.) AM1 semi-empirical calculations on stacked benzene delocalized ring systems suggest that very large third order polarizabilities (γ) can be obtained. Systems of +2 charge consisting of benzene rings separated by 3 Å, display finite-field (FF) zero frequency $\gamma(0;0,0;0)$s that are many orders of magnitude larger than any thus far commonly encountered or previously predicted for organics. The ratio of the FF Re{γ} to Re{α} is an increasing function with system size for the +2 species and is a decreasing function for the neutral species. Up to 14 rings, the largest systems currently calculated, there is not yet a clear indication of leveling-off or saturation of γ or γ/α. This is discussed in the context of the absence of electron correlation in these SCF-only calculations. The feasibility of such systems is discussed, as well as potentially significant limitations to the calculations that need to be further investigated before the certainty of these predictions can be certified.

The pursuit of large third order optical polarizabilities ($\gamma(\omega_4, \omega_3, \omega_2, \omega_1)$ for microscopic systems, and $\chi^{(3)}(\omega_4, \omega_3, \omega_2, \omega_1)$ for macroscopic systems) in organic materials has been fraught with considerable frustration. Third order polarizabilities that have been achieved are relatively small or are small relative to linear optical losses so that the ideal materials appear unattainable, and good-enough materials with either sufficient γ (or bulk $\chi^{(3)}$) with low enough linear (or nonlinear multiphoton) losses are often on a borderline of real utility. Indeed, based on extensive work on conjugated hydrocarbons, the prediction has been that larger third order susceptibilities are unattainable, and that the loss problem cannot be overcome.[1]

The most recent intriguing work that appears to go beyond the neutral hydrocarbons - at least in apparent magnitude of γ or $\chi^{(3)}$ – is the investigation into bipolaronic systems broadly investigated by Spangler and co-workers.[2-12] Bipolaronic systems experience enhanced delocalization by removing two electrons chemically or electrochemically. The difference in filled and empty orbitals relative to the neutral leads to an apparent significant enhancement in third order (nonlinear) optical polarizabilities. The question of optical loss has not been fully resolved, since electronic transitions are shifted to lower in energy, which normally reduces the useful window in the visible and near IR. However, it is unresolved whether potentially useful windows of transparency may broaden in the visible or there may be other useful optical regions further into the near IR. Photonic switching devices based on third order processes are relatively primitive in practical concept such that the preferred frequency regions of operation are still not clearly defined, and more likely will depend on the availability of materials.

Largely, investigation into nonlinear optical materials based on organics has followed the lines of either readily available materials or traditionally well known simple dye chemistry variants. These systems, when viewed in terms of their electronic and optical dimensionality are either approximately one or two dimensional. Approximate one dimensional systems are for instance,

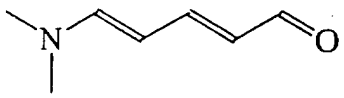

while two dimensional systems might be thought of in terms of phthalocyanines[13-17] as a model. There are of course few real one dimensional systems. Even p-nitroaniline, while extremely polar in its optical response, will display a non-zero response orthogonal to the polar axis, so that it may be considered one dimensional in one concept of approximation and somewhat two-dimensional in another. However, electronic delocalization and optical response dimensionality higher than two-dimensional is not commonly thought to be a significant contributor to these most commonly investigated systems. The main reason has likely been synthetic accessibility. Making molecules with interacting planes of conjugated atoms is not necessarily straightforward, though examples exist. In the solid state, molecular metals and conductive polymers display this higher dimensionality of interaction, though the interaction may be too long range usually leading to absorptions extending into the IR, or the aggregate size exceeds the light scattering limit. In principle, very one-dimensional neutral polydiacetylenes could as well display inter-chain delocalizations, though chains are likely too far away, and their filled shells do not promote band formation. Cyclophanes are examples of discrete molecular systems that can

offer higher dimensionality delocalization. Donor/acceptor cyclophane type systems show clear low energy transitions that suggest enhanced delocalization between the rings. [18,19]

An approach taken by us is to consider higher dimensional delocalized systems such as cyclophanes. Oxidative enhancement of delocalization such as in bipolarons is an obvious step. This report covers our preliminary work on investigating the calculational results of a model higher dimensional bipolaronic system.

The investigation of organic molecules for nonlinear optics has been fairly isolated to traditional conjugated structures, and the traditional modes of delocalization inherent to dye chemistry developed in the late 19th Century. These common modes of delocalization are:

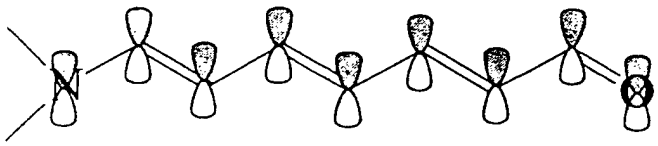

1D - Linear - commonly used in organic NLO molecules

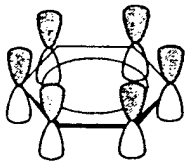

2D - Circular - commonly used in organic NLO molecules

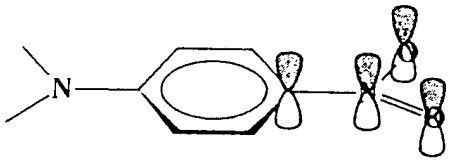

2D - Branched - commonly used in organic NLO molecules

The labeling as 1D or 2D is an approximate assertion, and is primarily for descriptive purposes. Less commonly investigated systems, especially in terms of organic nonlinear optics are as follows:

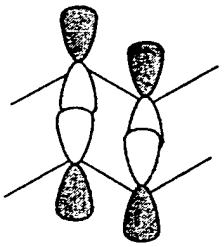

2D - p-pi / p-sigma

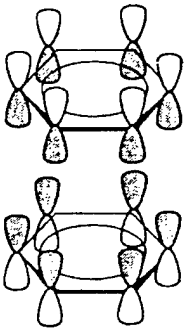

3D - Circular p-pi / p-sigma

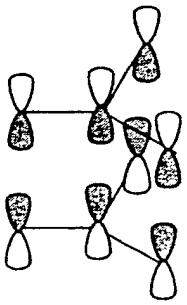

3D - Branched p-pi / p-sigma

Again, labeling is for descriptive purposes. The model system in which we are interested would fall into class 3D Circular p-pi/p-sigma. Our earlier work[20] in this area was on a series of dioxodiene cyclophanes,

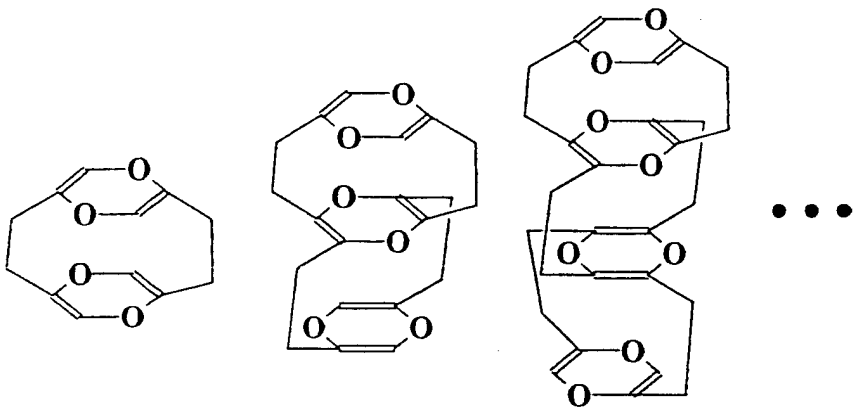

where calculation in the +2 state resulted in systems displaying large negative second hyperpolarizabilities, γ. The dioxodiene system is anti-aromatic as neutral, and expected to be aromatic as +2, thus implying the delocalization of aromaticity between rings in these +2 dioxodiene cyclophane systems. In the present work, the model system representing this higher dimensionality delocalization is merely a series of benzene rings stacked over each other and separated by 3 Å. This would be a system of aromatic rings which upon oxidation to +2 would be delocalizing anti-aromaticity. This system is also different from our earlier work on dioxodienes in that we are not covalently linking the rings through ethylenic bridges, but are fixing an interplanar distance between non-covalently linked rings.

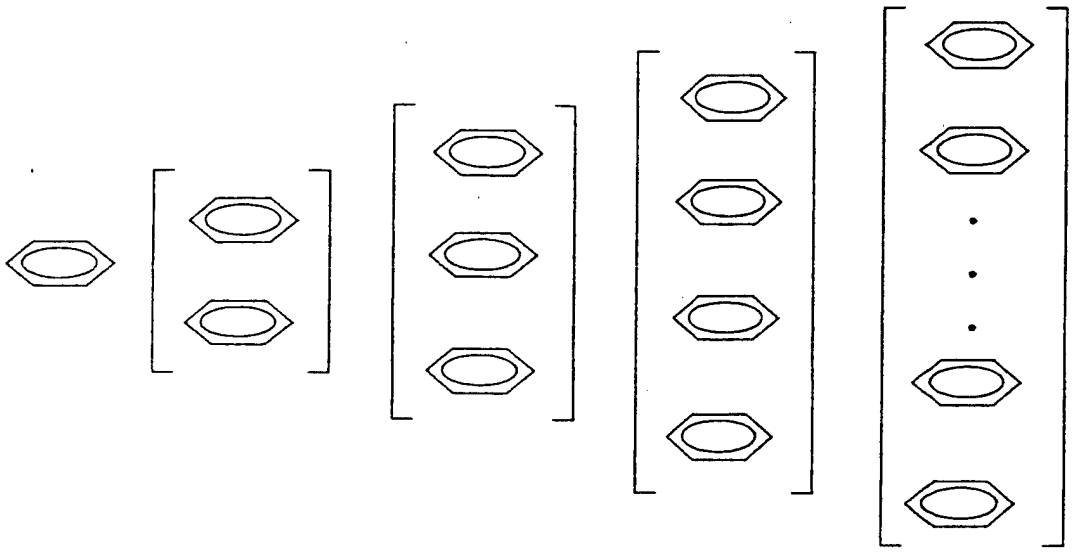

This different type of constraint was used to avoid what appeared to be inter-ring Jahn-Teller instabilities observed in the dioxodiene cyclophanes, which were allowed to fully optimize including their ethylenic bridges. By eliminating the bridge, and enforcing a fixed spacing, we can completely inhibit a distortion between the rings, at least for the purposes of clarifying the effect of delocalization in undistorted systems. This leads (*vide infra*) to a less likely distortion within the rings. This might be chemically and or physically unreasonable in this model system, but in-principle could be enforced in a system with significant covalent bridging.

Calculations on the model system have been done either as singlet neutral or singlet dications (bipolaronic) using AMPAC 5.0 licensed from Semichem. Inc., on SGI INDIGO2 workstations (either a R4400 with 48MB memory or a R4600 with 32MB memory). In all calculations the inter-ring distance of 3 Å was fixed, though all other coordinates were free to optimize. A distance of 3 Å is not unreasonable since real cyclophane distances are in some cases significantly less than this. The AM1 approximation was used, and all structures were fully SCF optimized, except for the fixed

inter-planar spacing. Results are reported for the E4 Energy expansion in the finite field and the DIP dipole expansion in the finite field. Calculations reported here were quite time consuming, and sometimes required up to 600-700 hours of CPU time to achieve refinement of the structure. Much of this time was the consequence of extensive use of virtual memory (in the absence of adequate RAM) for the largest systems reported here. Refined structures were then subject to AMPAC zero-frequency Finite Field analysis of polarizability properties up the 3rd order tensor γ.

Calculations reported here are for systems imposed to be singlets. This may not be realistic, and imposes further constraints that can affect the outcome of the calculations. It is however, a restriction imposed to assure a closed shell system. The combinations of choice of charge=+2, singlet, and not allowing optimization between rings is a deliberate attempt to ensure a systematic outcome of a particular type that in-principle could be synthetically accessible, necessarily, as pointed out earlier, with significant steric control of covalent bridging. Calculations of triplet or biradical type systems, etc., are also of importance. This study systematically deals with one case, and the other possible most likely circumstances remain to be investigated.

RESULTS:

Numerical results are summarized in Tables 1 & 2. The discussion which follows focuses primarily on graphical presentation of these results.

Structural results fall into two main categories of consideration: the symmetry of the collection of rings, and the structural variation in rings across the system.

Even though rings are permitted complete optimization freedom within the plane, final optimized structures do not differ, with some very slight angle of variation between overlapping rings. The very slight angle of variation (less than 0.2 degrees) depends on what atoms are being compared, and is a consequence of the distortion within all rings to an antiquinoidal bisallyl structure, the extent of which depends on the position of the ring within the stack.

Within the rings, the neutral systems largely remain aromatic as evidenced by their bond-length alternation. The dication systems however, clearly show a antiquinoidal bisallyl cation character:

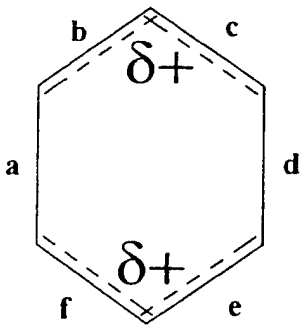

BLA= (a+d)/2 - (b+c+e+f)/4

Defining a bond-length alternation parameter of (a+d)/2-(b+c+e+f)/4 , and plotting (Figures 1 & 2) this parameter as a function of ring position within a given dicationic stack of benzenes shows that the BLA peaks at the penultimate - from either terminal end - benzene. Two figures are shown, one with all systems from one ring to 14 (Figure 1), the other (Figure 2) showing systems only larger than 4 rings to clearly show the effect in the larger systems. The positive charges are most localized on the penultimate-from-either-end rings, with terminal rings serving as a domain cap on either side. The implication is that

while there is some localization, the variation in BLA of antiquinoidal bisallylic structures suggests delocalization across these structures. This really is not an unexpected or startling conclusion since partial charge delocalization across many adjacent rings is commonly accepted for electrically conductive organic solids. The relative localization near the domain wall is perhaps a new detail not earlier identified in such systems. This intra-ring distortion, Jahn-Teller in origin, is a consequence of inhibition of the more likely inter-ring distortion. The distortion is expected and is a consequence of the creation of an open shell by removal of two electrons. The imposition of the singlet spin state then demands the distortion.

The average BLA per system size decreases smoothly with increasing system size (Figure 3), apparently just beginning to approach an asymptote at 14 rings for the +2 charged systems. It is clear that as we progress from smaller to larger dicationic stacks of benzenes, the BLA is reduced on all rings, again suggesting improved delocalization by way of the availability of more sites. The more the delocalization, the less charge that will exist on any given ring.

A plot (Figure 4) of ionization potential (IP) versus system size (number of stacked benzenes) shows that for the dicationic and neutral systems, there is a systematic monotonic reduction in IP with increase in the number of available benzenes. The implication is again that clear 'through-space' delocalization occurs, even for the neutral systems. In these plots, and as implied by the trends for BLA versus number of rings or system size, it is clear that a size of system of maximum effect has not been reached. Thus, and in other words, the delocalization effect is clearly not saturated at 13-14 rings. A saturation effect is anticipated, based on the observation of similar effects in delocalizing

excitons in conductive polyenes, and polyeneyne polymers. The barest hint of the onset of saturation may be observable in the BLA plot of the 14 ring dication. One can note that charge localization doesn't as clearly peak at the penultimate to the terminal rings as much as it does for smaller systems. This may be a first hint of a split to form relatively discrete electronic domains. If so, we might very roughly estimate that saturation will be observed in the range of 25-40 rings.

An analysis of the calculated heat of formations shows that the neutral system increase fairly linearly (Table 1) in ΔH_f, while the dication systems decrease then increases perhaps along an asymptote (Figure 5). If we calculate a hypothetical reaction between a dicationic system of a given size and a neutral benzene,

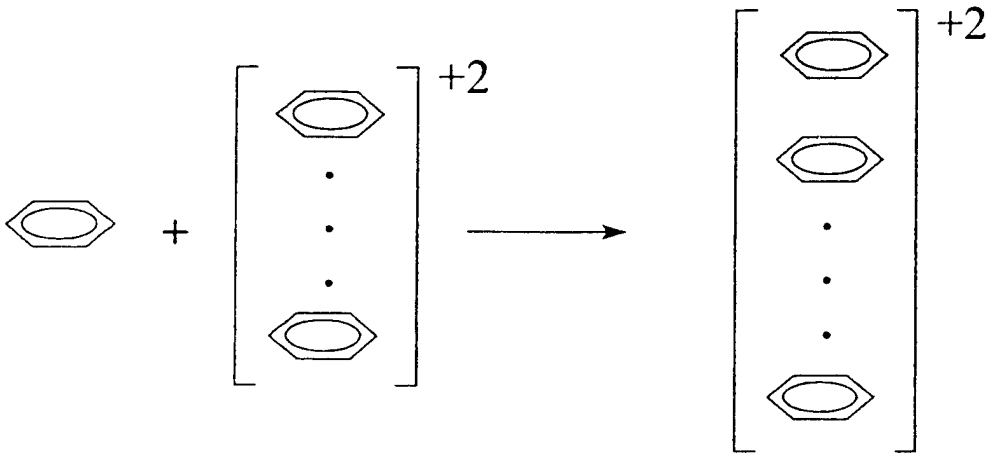

we can see in Figure 6 that such a reaction is favored, neglecting the effects of entropy, to self assemble up to five rings. This is not unexpected, since molecular metals must self assemble based on a favored thermodynamic situation. The results are of course gas-phase, but at least in the gas phase, oligomeric +2 systems should form spontaneously, upon +2 oxidation of a single ring, *neglecting* entropy. Whether solution effects would be favorable or unfavorable is unknown. However, benzene, being so purely 4n+2 aromatic,

is not a best case system for self assembly of dicationic stacks of antiaromatic character. Thus, a systematic way to construct such systems is to effect some sort of clever control of the self assembly to promote such, but limit the system size to maintain bandgaps or transparent windows in the visible or near-IR. This would be a challenge for synthetic chemists to consider.

For the system of neutral benzenes, the FF γ is seen in Figure 7 to increase linearly. The magnitude is not large, and is what might be expected. The DIP expansion results show some significant deviation from linearity at the large system sizes, which could be due to accuracy of the convergence in the field-applied SCF solution. The energy expansion results, typically more stable, are still fairly linear up to systems of 13 rings. A plot of γ/α in Figure 8 shows a decreasing value for this ratio with increased system size. This is not beneficial from device considerations because this implies that α (and potentially, linear loss if the imaginary quanity refelcts this behavior) increase faster than γ. These are zero frequency quantities, and of course are then real values for both α and γ, while the imaginary value for α is responsible for linear optical loss. Far off resonance, the real and imaginary quantities will track-with and be proportional to one another. As one approaches zero frequency, however, $\mathrm{Im}(\alpha)$ attains a limit of zero while $\mathrm{Re}(\alpha)$ tends toward a finite value, so one cannot use the ratio of zero frequency values to imply much about the true frequency dependent behavior.

The dicationic system displays a vastly different response when looking at γ versus system size. As the system becomes larger, γ is seen in Figure 9 to rapidly turn negative achieving huge magnitude values. These magnitudes dwarf typical known experimental systems that might be calculated under the AM1 model. The negative sign suggests that

two-photon effects are minimized (however, *vide infra*) relative to one-photon effects, which should in principle yield the largest possible magnitude of γ in the extreme of no two-photon influence. This would be a best case scenario for minimizing two-photon absorption while maximizing Re{γ} device effects. The magnitudes are startling, and just as startling is the apparent lack of saturation even up to 14 rings. A plot of γ/α shows in Figure 10 an increasing function with system size, which is opposite of the tend seen for the neutral system. Again, saturation effects are not seen up to 14 rings. Shown in Figure 11 is the ratio of Figure 10 to Figure 9. The improvement in (γ/α) upon oxidizing from neutral to +2 is as large as nearly 10000 up to the 13 ring system. Again, these are zero frequency quantities, so that a fundamental question exists as to the true behavior of the frequency dependent quantities. One expects the +2 systems to display significant low energy absorptions, which obviously shouldn't be present in the neutral systems, though their oscillator strength magnitude is unknown. An important issue is whether at some frequencies Re{γ} really does increase faster than Im{α}; a sum-over-states procedure is necessary to resolve this.

Some significant caveats are warranted for this work.

- Semi-empirical is a model of necessity for such kinds of exploratory work on these large systems. The suitability of the semi-empirical AM1 model is an issue. Rings as close as 3 Å and closer are certainly chemically viable as seen in cyclophanes, though the use of AM1 for such close systems has been relatively limited, and its use for conjugation through orbitals in the orthogonal-to-the-plane sense as shown here is probably unknown. The choice of the AM1 model here is primarily dictated by its availability in a package with a FF calculation, the ability to select specific spin states

to optimize, and the robustness of AMPAC for difficult optimization conditions. No semi-empirical calculation is likely a good choice for these kinds of systems. It is our intention to follow this work up at the *ab-initio* level where more extensive and complete basis functions can be employed, particularly to assess the participation of the core, which is frozen in the semi-empirical models, and diffuse electron contributions which are absent or at best embedded in the semiempirical parameterization. Obviously, present computer hardware dictates that *ab-initio* calculations will be on the smaller systems.

- Calculations reported here on charged systems have been performed in the absence of counter-ions. Obviously the counter-ion field will have some effect, and likely deleterious since it will promote localization. However, it is unclear what crystal field arrangements might be optimal, and might effectively mute the localization effect.
- Calculations have been performed at the SCF level without CI, primarily because of limits on available computational equipment. For SOS calculations it is clear that significant mutliply excited configurations of CI are necessary to properly characterize the γ tensor, particularly when two-photon effects must be calculated correctly. In fact, the apparent less significance of two-photon effects in these calculations implies either they really aren't there to the extent implied by the calculation, or the calculation was insufficient to adequately account for them. The major contributions to γ fall into three different types in terms of their sign. This is clearly seen in the three-level model we have defined[21-26] in earlier work.

$$\gamma \approx -(\mu_{01})^4 D_{11} + (\mu_{01})^2(\Delta\mu_{01})^2 D_{111} + (\mu_{01})^2(\mu_{12})^2 D_{121} + \ldots$$

$$\text{or,} \quad \gamma \approx \gamma_e + \gamma_n + \gamma_{tp} + \ldots$$

where μ_{rs} are transition moments between state *r* and *s*, $\Delta\mu_{01} = \mu_{11}-\mu_{00}$, and D_{lm} and D_{lmn} are perturbation type dispersion terms. In this equation, γ_c is negative, γ_n is positive, and γ_{tp} is positive. γ_n , proportional to dipole moments, is small due to the high degree of symmetry. γ_{tp} depends on the magnitude of the overlap between the one-photon and two-photon excited states. Negative perturbation contributions to γ (e.g. γ_c type components of the form $-(\mu_{0n})^4 D_{nn}$, where the notation is defined earlier[21-23]) that are large in magnitude can dominate inappropriately as a result of an inadequate calculation of two-photon contributions. This would lead to γ's that are too large in the negative sense, which would be consistent with our unusual results. However, the same methods have been applied to squarylium dyes with success at predicting both their negative γ as well as the relative differences between dyes. Also, it is unclear how much electronic correlation matters for zero frequency FF relative to standard frequency-dependent SOS results, at least in terms of characterizing two-photon effects.

- We did not allow the systems to fully optimize. Inter-ring distances were fixed at 3 Å. This may not be realistic as might be anticipated in a self assembly sense. However, known cyclophanes possess distances smaller than this, so such distances can be imposed if necessary to render a real analogous system, though not necessarily with the ability to inhibit distortions (*vide infra*). Earlier calculations[20] that we performed on potentially real systems such as dioxodiene cyclophanes showed problems in structure optimization when all degrees of freedom were allowed to optimize, which we interpreted as a Jahn-Teller instability. Real laboratory systems, either cyclophanic

or self-assembled rings may display similar instabilities, complicating a practical demonstration of the optical effects. In the present system, the calculational restraints confined the distortion to occurring within each ring in order to assure preservation of inter-ring delocalization. Our choice of singlet and charge=+2 was deliberate since real systems will tend to distort to close their shell. Choosing to inhibit the Jahn-Teller distortion between the rings in favor of one within the rings was also deliberate in order to assess the delocalization between the rings. Synthetic accessibility of such a system is not impossible, but would be challenging.

- Semiempirical methods are models of necessity for these large systems, but zero-frequency finite-field is not, and the consequent absence of frequency dependence makes these results more tenuous. Development of a sufficient SOS program is under way.
- These systems have been calculated as singlets, which tends to impose a closed shell upon optimization, which then forces the distortion that is observed. A biradical or triplet structure is not impossible, and may be thermodynamically favored. We have not calculated such yet due to our choice of initial system type to investigate and present computational equipment limitations, though such calculations are strongly warranted to complete the picture.

These caveats outline further investigations that must be done. Our present computational resource capability precludes resolving these issues without considerable further computation time.

Conclusions:

AMPAC AM1 calculations offer a prediction of extremely large, gigantic, third order optical susceptibilities, γ, in through-space three-dimensionally delocalized systems. A companion unusual result is that the ratio of γ/α is increasing, though this cannot be properly interpreted without frequency dependent calculations. A number of significant caveats have been outlined, and this system has primarily been pursued as a simplified model system. Stacked benzene systems are thus not presented here as a best candidate for a potential real system. The real significance of this result is that using real molecules, but imposing extreme constraints and conditions, one appears to be able to enhance γ. The questions are whether the computational method is too limited, and if not so, whether synthetic accessibility could ever be feasible to attain a real system that would display the predicted effects. The main next steps are frequency dependence investigation and inclusion of configuration interaction. The investigation of other spin states is also necessary. The gist of this presentation is higher dimensionality of delocalization, and it is thus also necessary to extend the system not only in length, but in width. This may also stabilize some of the observed instabilities. Finally, real experimental analogues are currently under preparation.

ACKNOWLEDGMENTS

We wish to thank the Robert Welch Foundation, the Ballistic Missile Defense Organization, the Texas Higher Education Coordinating Board, and the Air Force Office of Scientific Research for support.

REFERENCES

(1) Green, B. I.; Orentstein, J.; Schmitt-Rink, S. *Science* **1990**, *247*, 679.

(2) Spangler, C. W.; Liu, P.-K. *Synthetic Metals* **1991**, *44*, 259.

(3) Spangler, C. W.; Havelka, K. O. ; The Society of Photo Optical Instrumentation Engineers: San Diego, 1991; Vol. 1560, p 66.

(4) Spangler, C. W.; Bryson, P.; Liu, P.-K.; Dalton, L. R. *Journal of the Chemical Society, Chemical Communications* **1992**, 253-254.

(5) Spangler, C. W.; Picchiotti, L.; Bryson, P.; Havelka, K. O.; Dalton, L. R. *Journal of the Chemical Society. Chemical Communications* **1992**, 145-146.

(6) Sapochak, L. S.; Strohkendl, F.; Dalton, L. R.; Tang, N.; Dartanen, J. P.; Hellworth, R. W.; Chang, T. Y.; Spangler, C. W.; Lin, Q. In *Organic Materials for Non-Linear Optics III*; Ashwell, G., Bloor, D., Eds.; Royal Society of Chemistry: Cambridge, 1993, p 283-288.

(7) Lögdlund, M.; Dannetun, P.; Strafsrom, S.; Salanek, W. R.; Ramsey, M. G., Fredrickson, C.; Bredas, J. L.; Spangler, C. W. *Physical Review Letters* **1993**, *79*, 970.

(8) Spangler, C. W.; Nickel, E. G.; Tang, N.; Hellworth, R.; Dalton, L. *Nonlinear Optics* **1993**, *6*, 135.

(9) Swiatiewicz, J.; Orczyk, M. E.; Prasad, P. N.; SPangler, C. W.; He, M. ; The Society for Photo-Optical Instrumentation Engineers: San Diego, 1993; Vol. 2025.

(10) Dannetun, P.; Logdlund, M.; Bredas, J. L.; Salanek, W. R.; Spangler, C. W. *Journal of Physical Chemistry* **1994**, *98*, 2853.

(11) Tang, N.; Partanen, J.; Hellworth, R.; Laguindanum, J.; Dalton, L.; Spangler, C. W.; He, M. ; The Society for Photo-Optical Instrumentation Engineers: San Diego, 1994; Vol. 2285, p 186.

(12) Spangler, C. W.; He, M. In *Handbook of Organic Conductive Molecules and Polymers*; Nalwa, H. S., Ed.; John Wiley & Sons, Ltd.: Chichester, 1997; Vol. 2, p 389-414.

(13) Dirk, C. W.; Bao, J.; Kuzyk, M.; Poga, C. In *Nonlinear Optical Properties of Organic Materials VII*; Mohlmann, G. R., Ed.; The International Society for Optical Egineering: San Diego, 1994; Vol. 2285, p 32-40.

(14) Casstevens, M. K.; Samoc, M.; Pleger, J.; Prasad, P. N. *Journal of Chemical Physics* **1990**, *92*, 2019.

(15) Ho, Z. Z.; Ju, C. Y.; III, W. M. H. *Journal of Applied Physics* **1987**, *62*, 716

(16) Wada, T.; Hosoda, H.; Garito, A. f.; Sasabe, H.; Terasaki, A.; Kobayashi, T., Tada, H.; Koma, A. In *Nonlinear Optical Properties of Organic Materials IV*; The International Society of Optical Engineering: San Diego, 1991; Vol. 1560, p 162-171.

(17) Suda, Y.; Shighara, K.; Yamada, A.; Matsuda, H.; Okado, S.; Masaki, A.; Nakanishi, H. In *Nonlinear Optical Properties of Organic Materials IV*; Singer, K. D., Ed., The International Society of Optical Engineering: San Diego, 1991; Vol. 1560, p 75-83

(18) Misumi, S. In *Cyclophanes*; Keehn, P. M., Rosenfeld, S. M., Eds.; Academic Press: New York, 1983; Vol. II, p 573.

(19) Vögtle, F. *Cyclophane Chemistry*; John Wiley & Sons Ltd.: Chichester, 1993.

(20) Dirk, C. W.; Xie, O. In *Nonlinear Optical Properties of Organic Materials IX*; Möhlmann, G. R., Ed.; The International Society for Optical Engineering: Denver, Colorado, 1996; Vol. 2852, p 162-169.

(21) Dirk, C. W.; Cheng, L.-T.; Kuzyk, M. G. *International Journal of Quantum Chemistry* **1992**, *45*, 27-36.

(22) Dirk, C. W.; Herndon, W. C.; Cervantes-Lee, F.; Selnau, H.; Martinez, S.; Kalamegham, P.; Tan, A.; Campos, G.; Velez, M.; Zyss, J.; Ledoux, I.; Cheng, L.-T. *Journal of the American Chemical Society* **1995**, *117*, 2214-2225.

(23) Kuzyk, M. G.; Dirk, C. W. *Physical Review A* **1990**, *41*, 5098-5109.

(24) Dirk, C. W.; Kuzyk, M. G. In *Materials for Nonlinear Optics: Chemical Perspectives*; Marder, S. R., Sohn, J. E., Stucky, G. D., Eds.; American Chemical Society: 1991; Vol. 455.

(25) Mathis, K. S.; Kuzyk, M. G.; Dirk, C. W.; Martinez, S.; Selnau, H.; Craig, P.; Green, L. In *The International Society for Optical Engineering*; Möhlmann, G., Ed.; The Society of Photo-Optical Instrumentation Engineers: San Diego, 1995; Vol. 2527, p 240-249.

(26) Mathis, K. S.; Kuzyk, M. G.; Dirk, C. W.; Martinez, S.; Selnau, H.; Craig, P.; Green, L. In *ICONO 3* Marco Island, FLorida, 1996, p in press.

system size, number of rings	symmetry	IP (ev)	ΔHf	α (E4)	α (DIP)	γ (E4)	γ (DIP)
1	D2H	21.6	589.6	15.11	15.11	1.14E+00	1.15E+00
2	D2H	18.2	570.9	50.34	50.34	-4.09E+01	-4.11E+01
3	D2H	15.89	579.6	110.75	110.75	-4.44E+02	-4.46E+02
4	D2H	14.52	597.9	119.22	119.21	-1.96E+03	-1.99E+03
5	D2H	13.6	620.9	317.55	317.57	-6.00E+03	-6.13E+03
6	C2H	12.93	646.6	468.01	468.1	-1.50E+04	-1.54E+04
7	D2H	12.43	674.1	653.88	654.18	-3.47E+04	-3.46E+04
8	C2H	12.03	702.8	876.28	875.11	-6.52E+04	-6.32E+04
9	D2H	11.71	732.4	1137.85	1138.66	-1.12E+05	-1.15E+05
10	D2H	11.45	762.7	1440.58	1420.38	-1.81E+05	-1.58E+05
11	C2H	11.22	793.5	1782.5	1732.3	-2.72E+05	-2.20E+05
12	C2H	11.03	824.7	2192.76	2200.33	-4.81E+05	-5.05E+05
13	C2H	10.87	856.3	2643.88	2654.89	-7.36E+05	-7.63E+05
14	C2H	10.72	888.2	3149.28	3160	-1.09E+06	-1.09E+06

TABLE 1: AM1 results for Charge = +2 stacked benzene systems. Heats of formation are in kcal/mole. Polarizabilities (10^{-24} esu) and second hyperpolarizabilities (10^{-36} esu) are reported for the energy (E4) and dipole (DIP) expansions of the finite field.

system size, number of rings	symmetry	IP (ev)	ΔHf	α (E4)	α (DIP)	γ (E4)	γ (DIP)
1	D6H	9.65	22	14.45	14.45	7.48E-01	7.49E-01
2	D6H	9.01	56	25.7	25.7	1.05E+00	1.05E+00
3	D6H	8.71	90.1	36.68	36.69	1.39E+00	1.39E+00
4	D6H	8.55	124.2	47.57	47.57	1.71E+00	1.73E+00
5	D6H	8.46	158.3	58.41	58.4	2.07E+00	2.04E+00
6	D6H	8.4	192.5	69.22	69.21	2.37E+00	2.39E+00
7	D6H	8.36	226.6	80.01	80	2.75E+00	2.71E+00
8	D6H	8.33	260.7	90.79	90.79	3.06E+00	3.05E+00
9	D6H	8.31	294.9	101.57	101.56	3.32E+00	3.40E+00
10	D6H	8.295	328.98	112.33	112.33	3.84E+00	3.78E+00
11	D6H	8.283	363.11	123.1	123.09	4.04E+00	3.94E+00
12	D6H	8.27	397.2	133.86	133.85	4.37E+00	4.55E+00
13	D6H	8.266	431.37	144.62	144.61	4.71E+00	5.47E+00

TABLE 2: AM1 results for Charge = 0 (neutral) stacked benzene systems. Heats of formation are in kcal/mole. Polarizabilities (10^{-24} esu) and second hyperpolarizabilities (10^{-36} esu) are reported for the energy (E4) and dipole (DIP) expansions of the finite field.

FIGURE CAPTIONS

Figure 1: Plot of bond length alternation (BLA; as defined in the text) versus ring position in any given charge=+2 stacked benzene system. The +2 benzene 'monomer is represented by a single point, while all other groups of data are connected by lines. Note that BLA is defined within each ring, so that the plot is of each ring's BLA as a function of the position of that ring within the stack.

Figure 2: An expansion of Figure 1, more clearly showing the variation of BLA versus ring position in any given charge=+2 stacked benzene system.

Figure 3: Bar graph illustrating the BLA alternation averaged over all rings for any given system.

Figure 4: The AM1 calculated ionization potential (IP) for both charge=0 (neutral) and charge=+2 (dication) stacked benzene systems.

Figure 5: The AM1 calculated heat of formation (ΔH_f) for both charge=0 (neutral) and charge=+2 (dication) stacked benzene systems.

Figure 6: The heat of formation for reaction of a (n-1) size dication system with a neutral benzene to make a n size dication system, based on the AM1 calculated results presented here.

Figure 7: The AM1 finite field $\gamma(0)$ calculated using the DIP (dipole expansion; squares) and E4 (energy expansion; circles), as a function of the size of the system, for neutral systems. The esu untis are cm^7esu^{-2}.

Figure 8. The ratio γ/α as a function of the size of the system for neutral systems. The DIP (dipole expansion) is the dotted line while the solid line is the E4 (energy expansion). The units are 10^{-12} cm^4esu^{-2}. Note that both α and γ are solely real quantities.

Figure 9. The AM1 finite field $\gamma(0)$ calculated using the DIP (dipole expansion; squares) and E4 (energy expansion; circles), as a function of the size of the system, for charge =+2 systems. The esu untis are cm^7esu^{-2}.

Figure 10: The ratio γ/α as a function of the size of the system for charge=+2 systems. The DIP (dipole expansion) is the dotted line while the solid line is the E4 (energy expansion). The units are 10^{-12} cm^4esu^{-2}. Note that both α and γ are solely real quantities.

Figure 11: The improvement of (γ/α) for the charge=+2 systems relative to neutral systems as a function of system size. Note that both α and γ are solely real quantities.

Figure 1

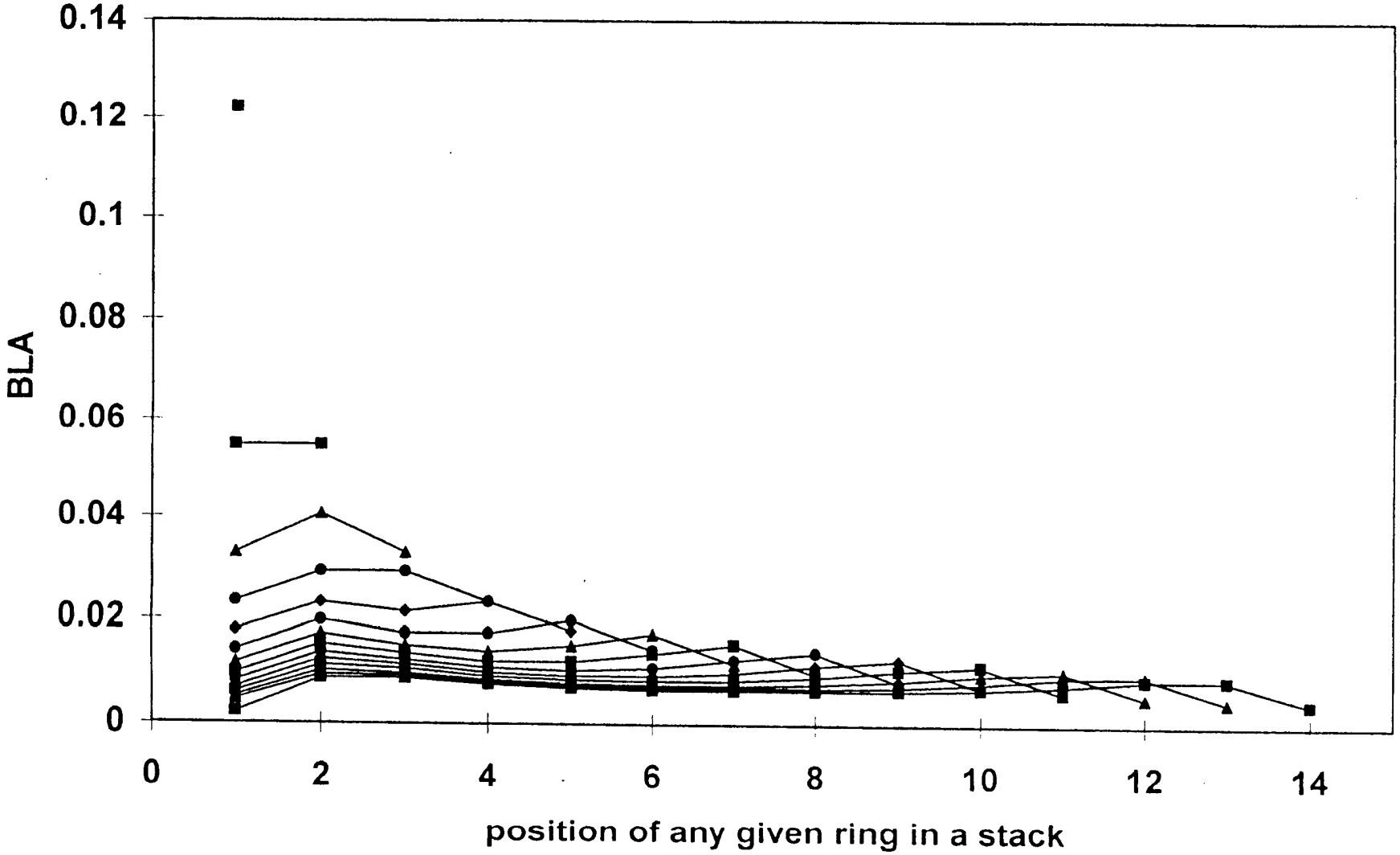
0.14
0.12
0.1
0.08
0.06
0.04
0.02
0
BLA
0
2
4
6
8
10
12
14
position of any given ring in a stack

Figure 2

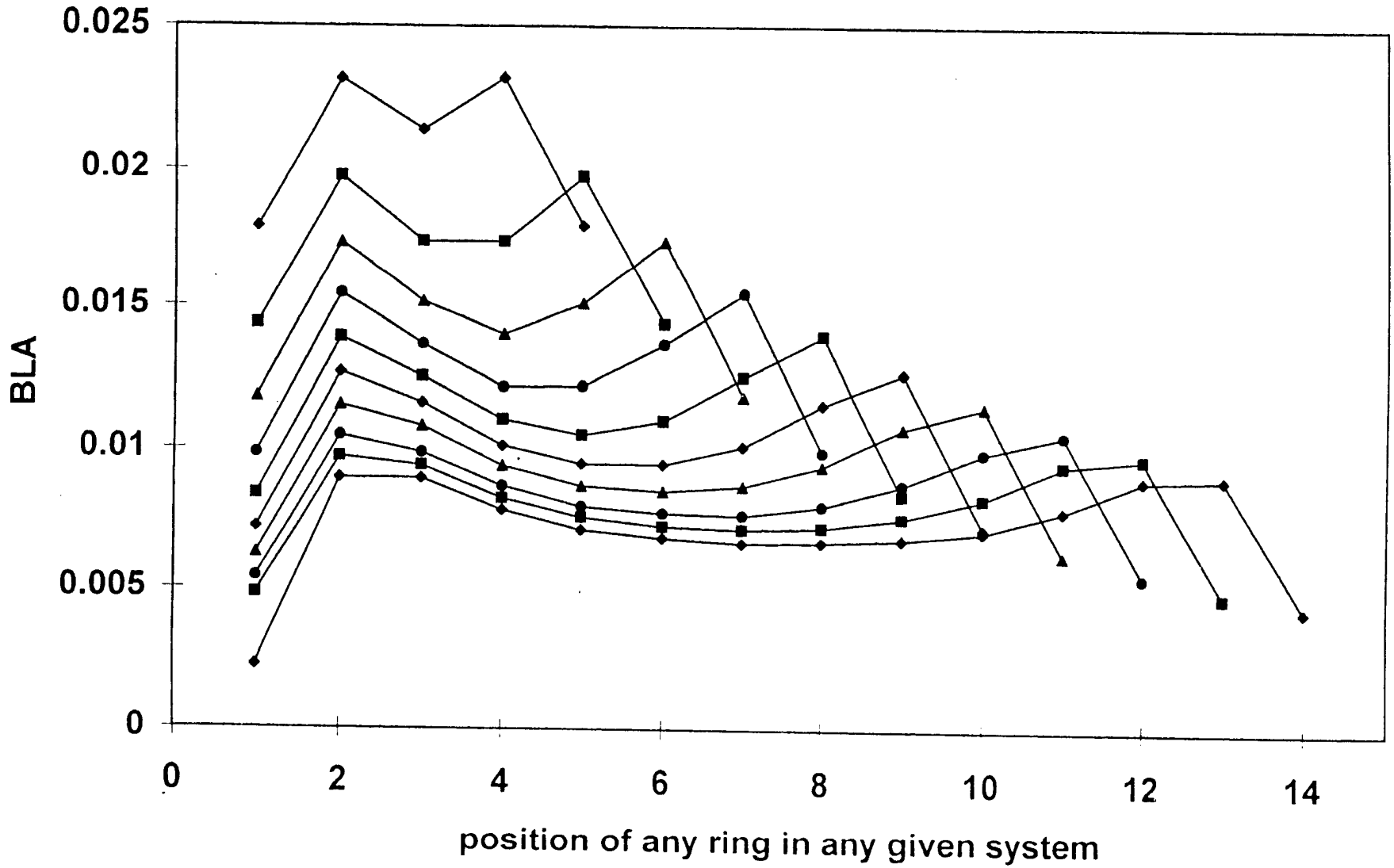
0.025
0.02
0.015
0.01
0.005
0
BLA
0
2
4
6
8
10
12
14
position of any ring in any given system

Figure 3

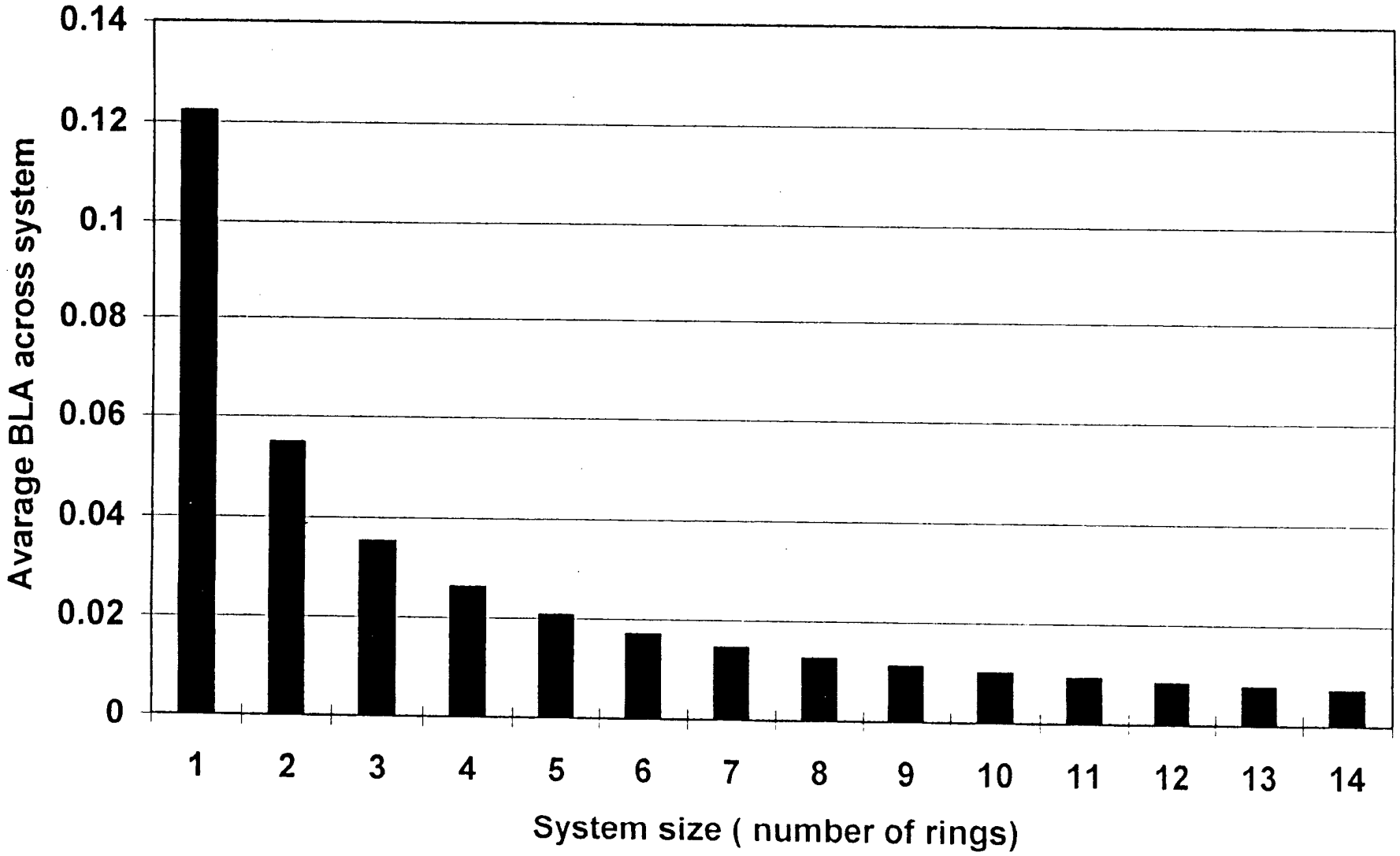
0.14
0.12
0.1
0.08
0.06
0.04
0.02
0
Avarage BLA across system
1
2
3
4
5
6
7
8
9
10
11
12
13
14
System size (number of rings)

Figure 4

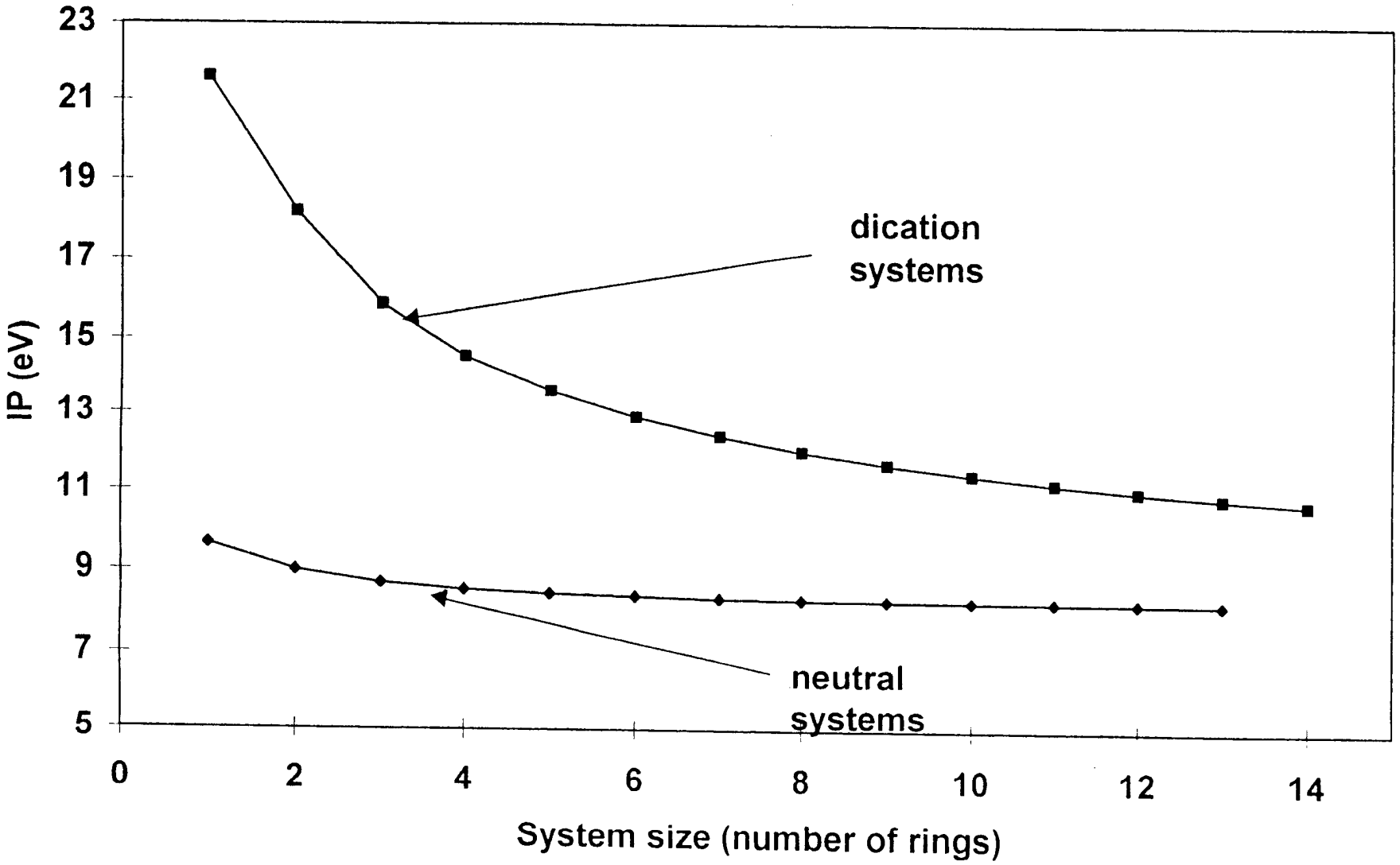
23
21
19
17
15
13
11
9
7
5
IP (eV)
dication
systems
neutral
systems
0
2
4
6
8
10
12
14
System size (number of rings)

Figure 5

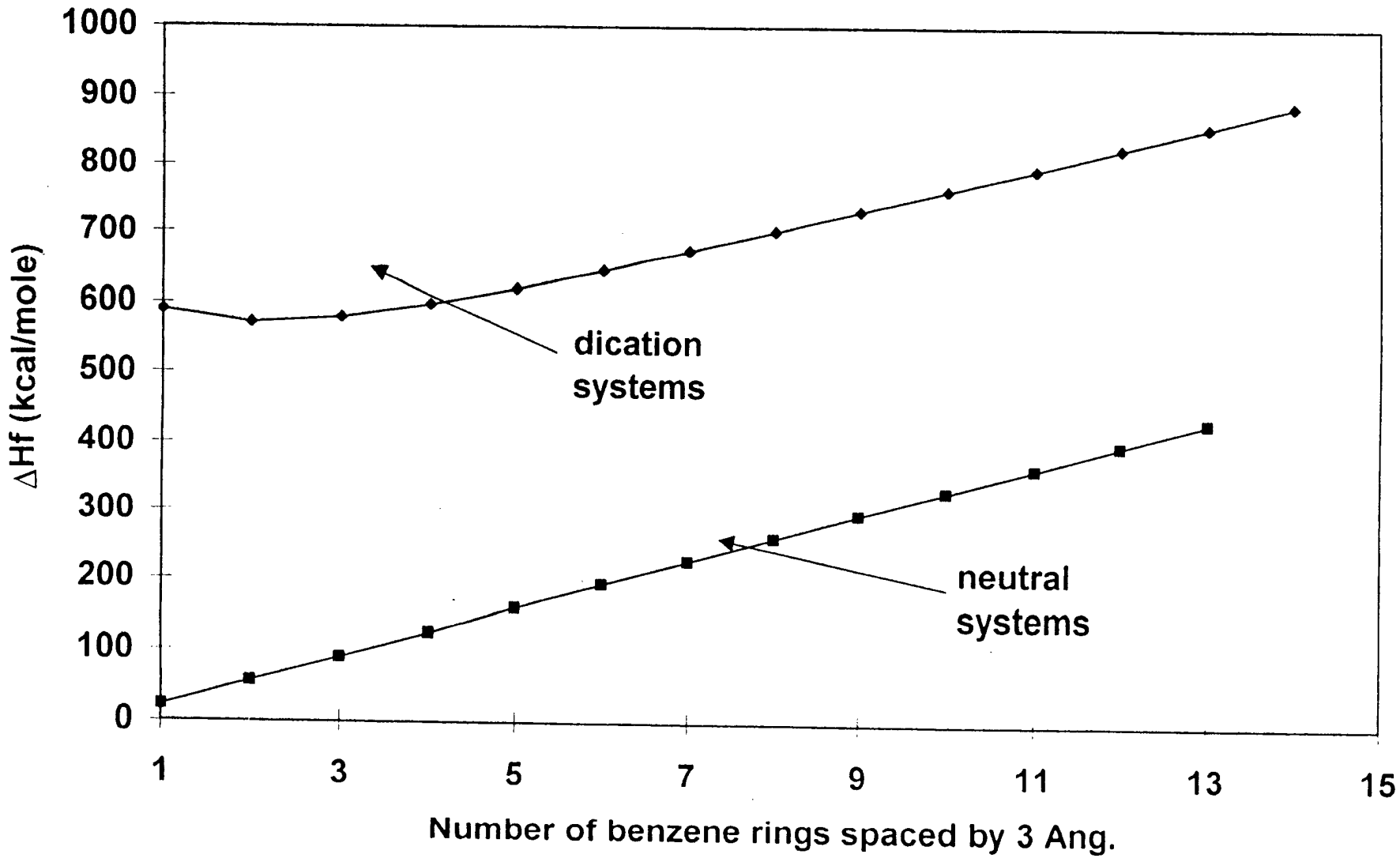
1000
900
800
700
600
500
400
300
200
100
0
ΔHf (kcal/mole)
dication systems
neutral systems
1
3
5
7
9
11
13
15
Number of benzene rings spaced by 3 Ang.

Figure 6

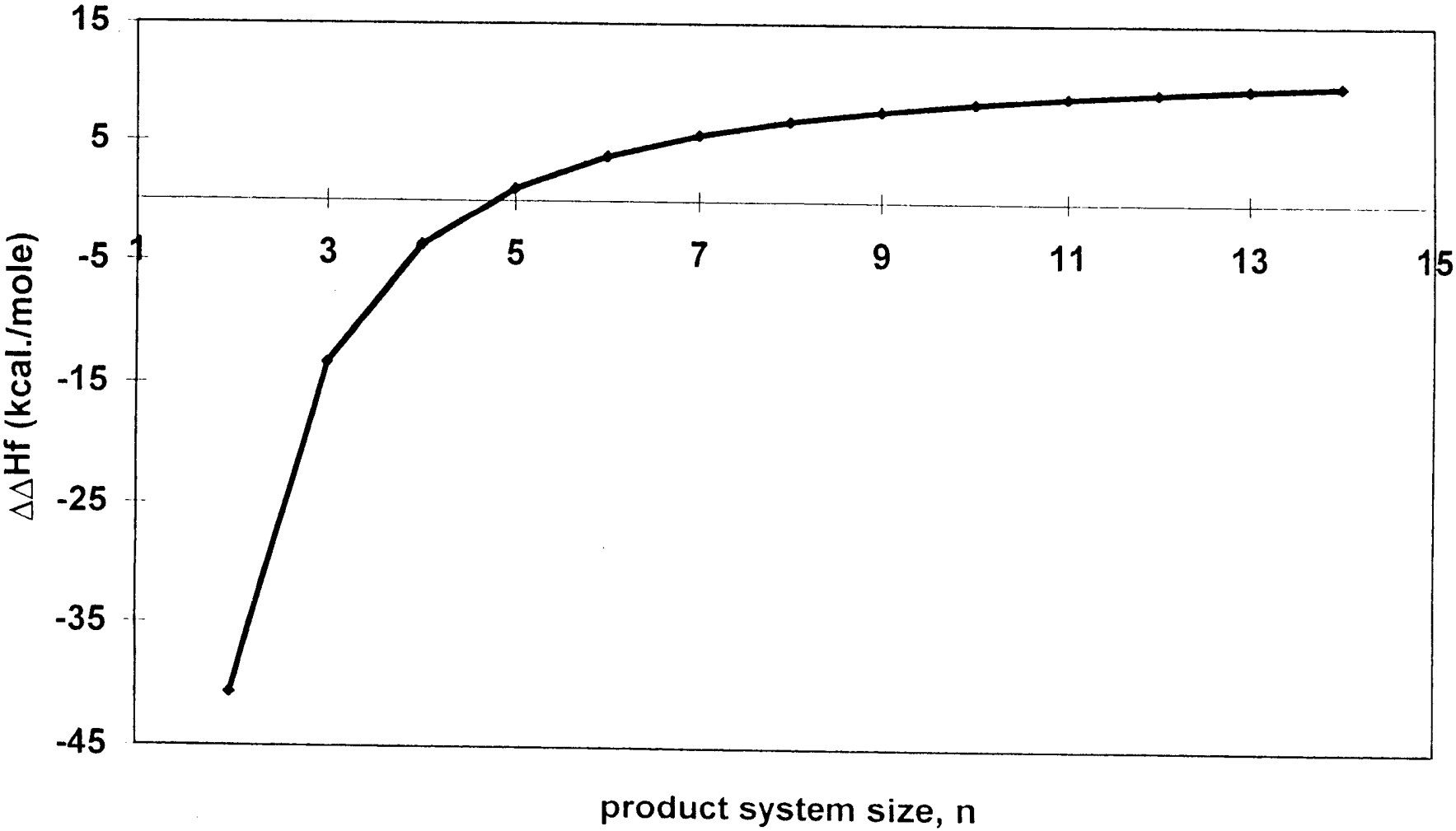
15
5
-5
-15
-25
-35
-45
1
3
5
7
9
11
13
15
ΔΔHf (kcal./mole)
product system size, n

Figure 7

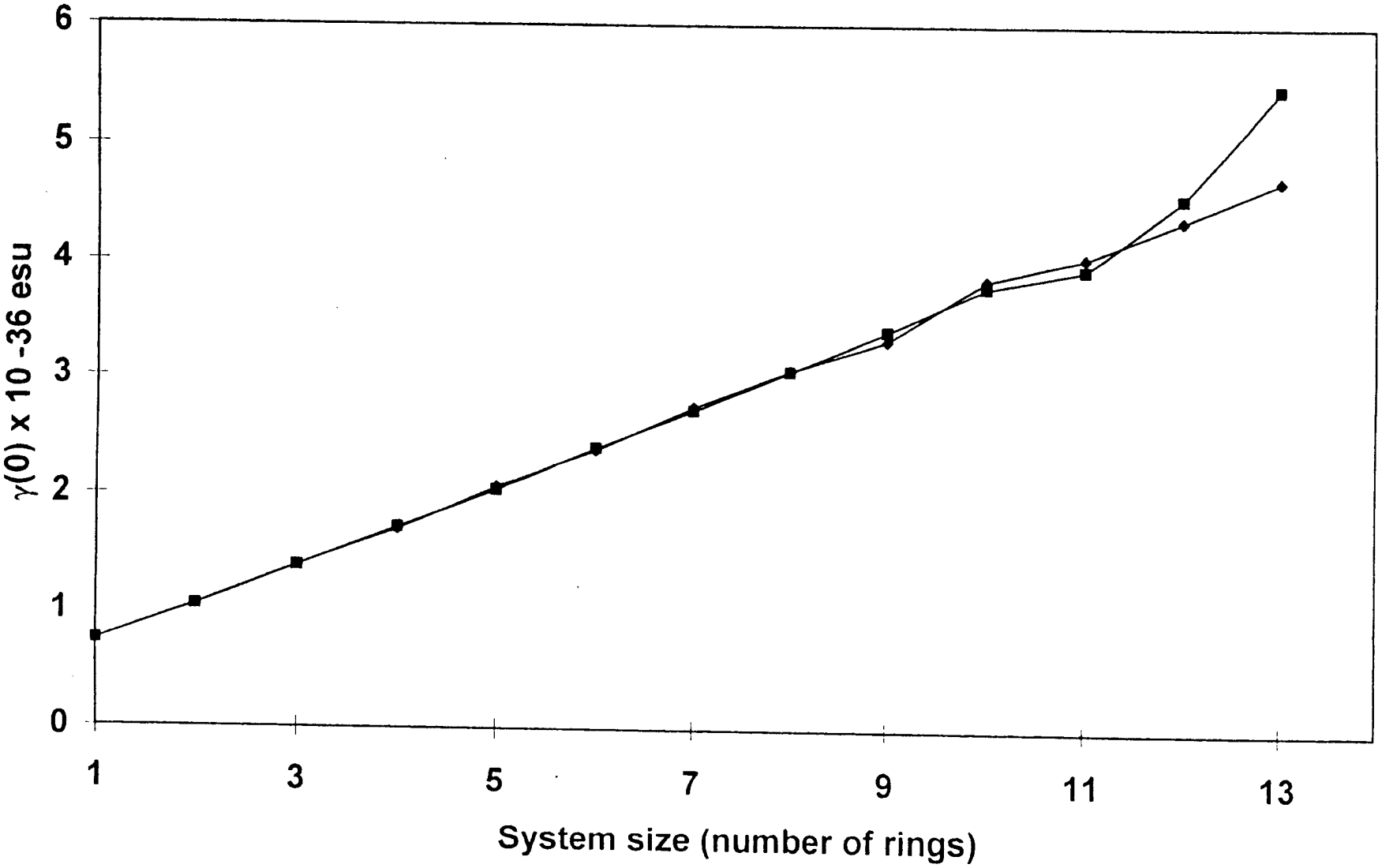

Figure 8

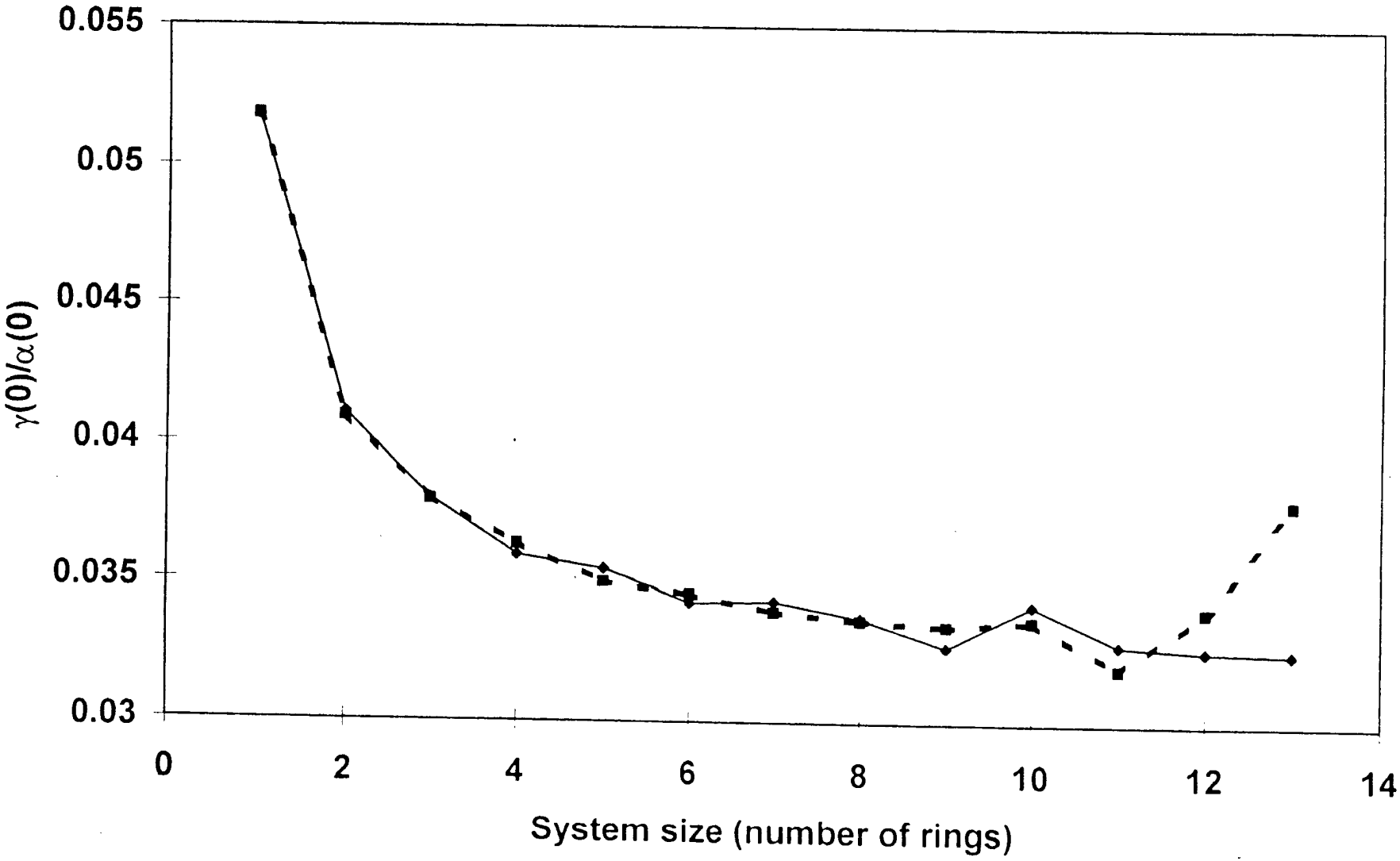
0.055
0.05
0.045
0.04
0.035
0.03
γ(0)/α(0)
0
2
4
6
8
10
12
14
System size (number of rings)

Figure 9

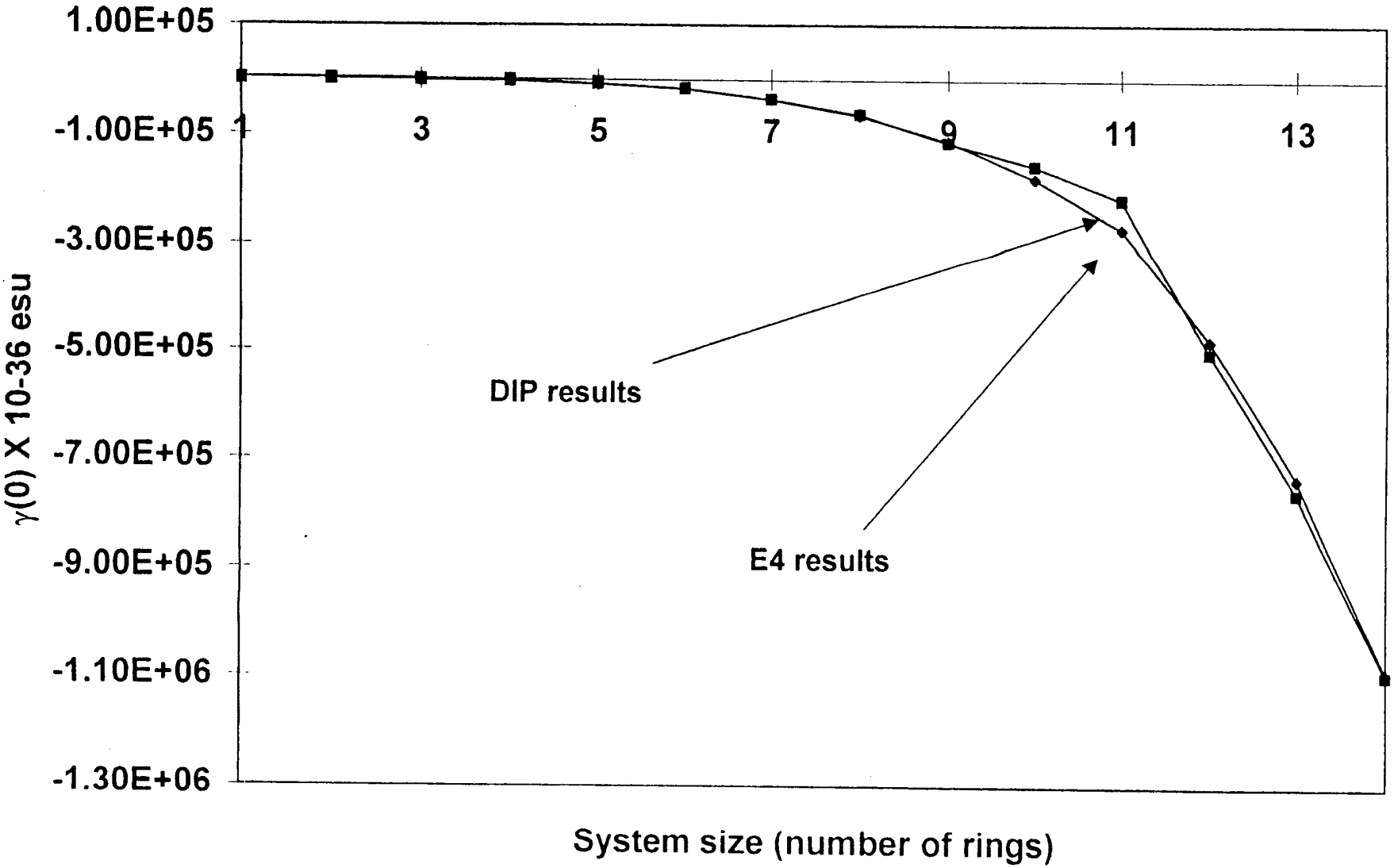
1.00E+05
-1.00E+05
-3.00E+05
-5.00E+05
-7.00E+05
-9.00E+05
-1.10E+06
-1.30E+06
1
3
5
7
9
11
13
γ(0) X 10-36 esu
DIP results
E4 results
System size (number of rings)

Figure 10

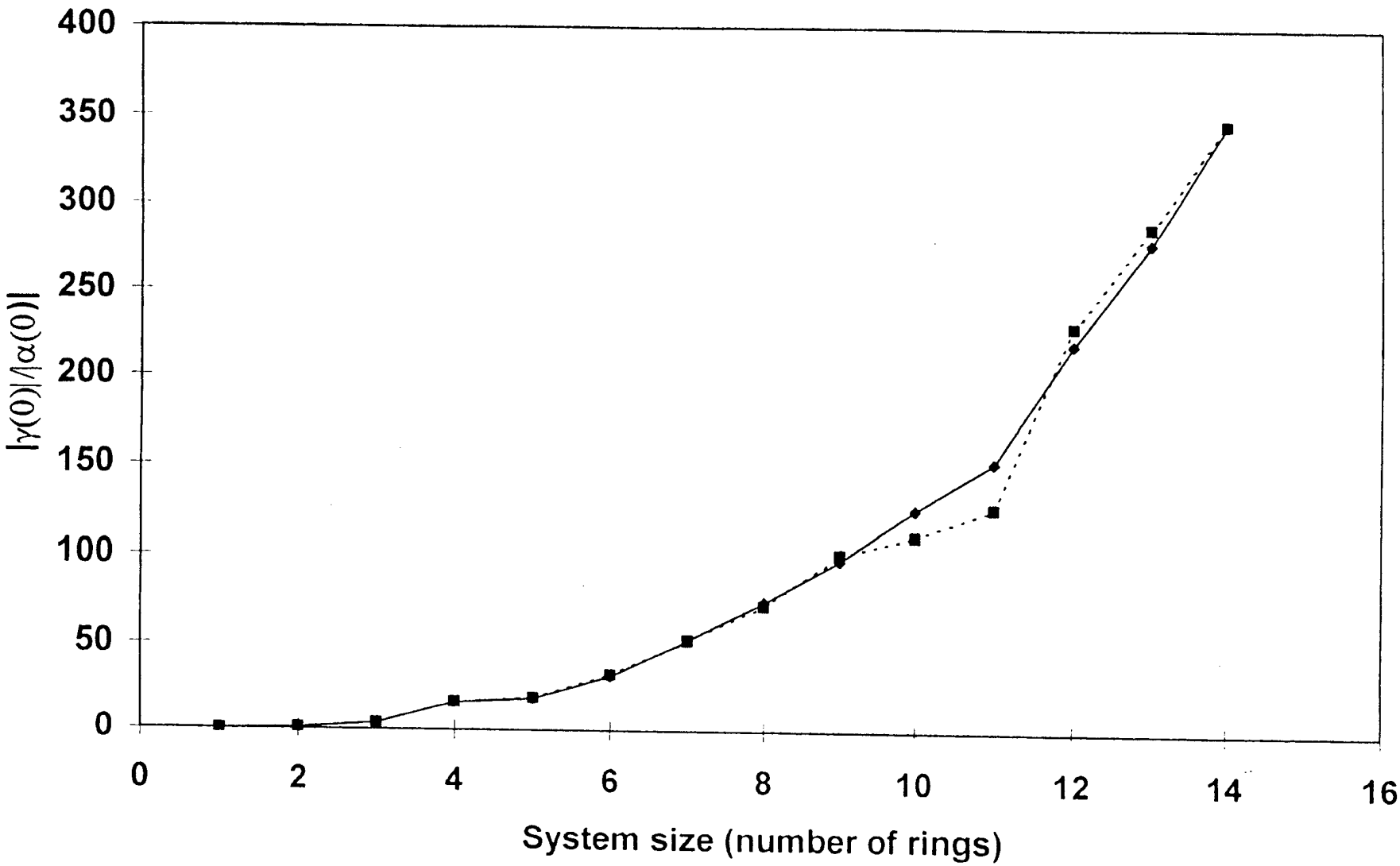
400
350
300
250
200
150
100
50
0
|γ(0)|/|α(0)|
0
2
4
6
8
10
12
14
16
System size (number of rings)

Figure 11

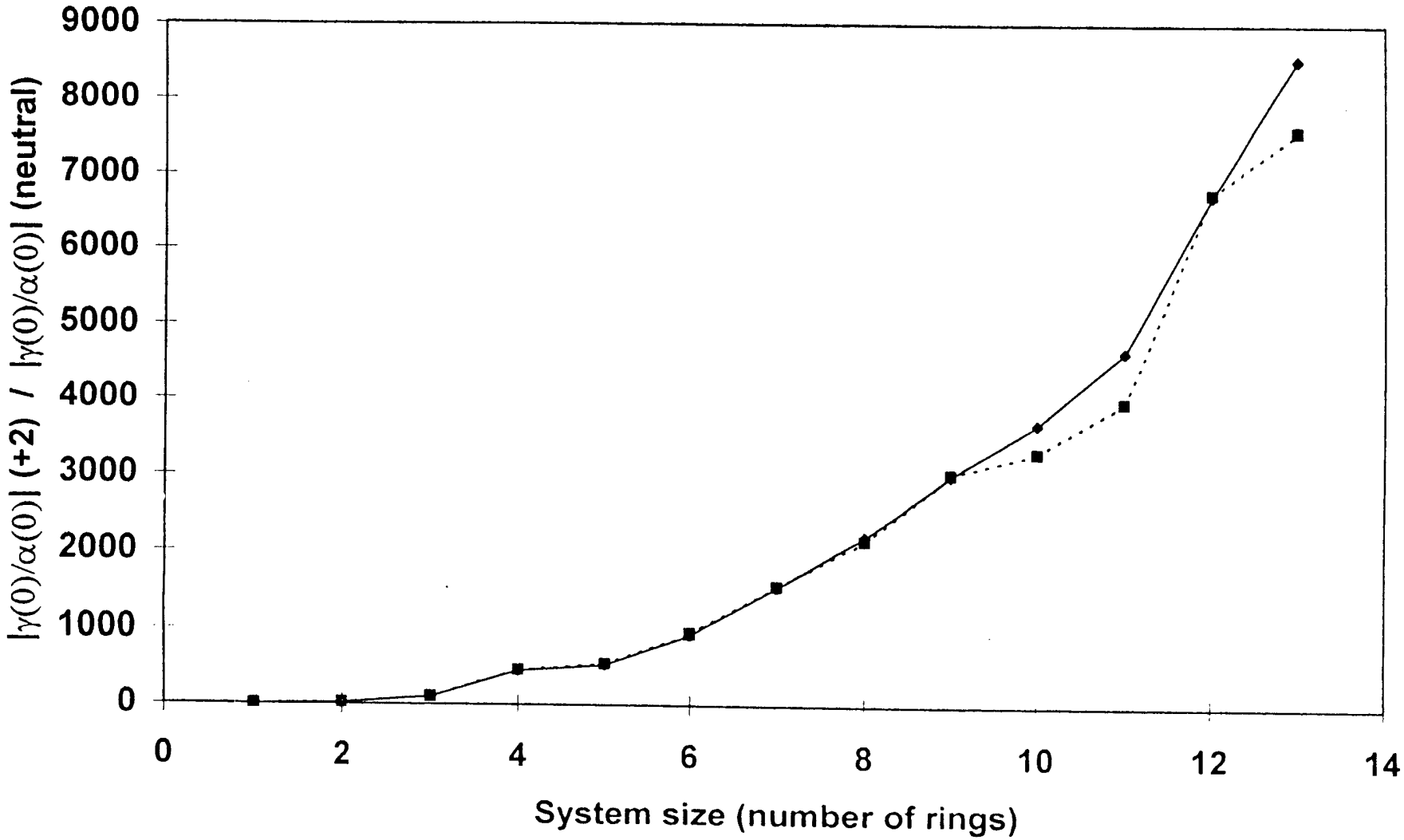
9000
8000
7000
6000
5000
4000
3000
2000
1000
0
|γ(0)/α(0)| (+2) / |γ(0)/α(0)| (neutral)
0
2
4
6
8
10
12
14
System size (number of rings)

ELSEVIER

Chemical Physics 245 (1999) 99–106

Chemical Physics

www.elsevier.nl/locate/chemphys

Thermal stability and rate order dependence for the thermal decomposition of electro-optic dyes

Lixia Zhang, Praya Kalamegham, Margarita Romero, Carl W. Dirk *

Materials Research Institute and Department of Chemistry, The University of Texas at El Paso, El Paso, TX 79968, USA

Received 7 October 1998

Abstract

A variety of electro-optic dyes have been measured by sealed capillary DSC. Thermal decomposition is most often accompanied by an exotherm, sometimes of great thermal intensity. The exotherm is characterized by an onset temperature, as well as a peak temperature. Upon dilution of the dyes in biphenyl or naphthalene solutions, the exotherm onset and peak typically shift to much higher temperatures. Quantitative fits to trial rate expressions suggest that the rate shifts from higher order to a first order decomposition mechanism upon dilution. This kinetic shift suggests strongly that matrices of electro-optic dyes can be best stabilized thermally by isolating the dyes chemically from one to another. Success at such may improve the device thermal stability by as much as 100–150°C. © 1999 Elsevier Science B.V. All rights reserved.

1. Introduction

Optical communication is currently restricted to relatively low-frequency transmission of voice and data structures [1]. Over the past ten to fifteen years, nonlinear optical organic materials have attracted significant attention as potentially fast and efficient components of optical communication and computing systems. There has been an intensive amount of work in increasing the optical communication speed. But one of the urgent problems that must be solved prior to the practical application of these organic materials is the thermal stability of the electro-optic (EO) materials. These EO devices are based on EO dyes. EO devices may operate continually at the temperatures above 80°C, and the EO dyes also need to survive the device manufacture processing condition which approximately ranges from 250 to 300°C for a period as long as 2 h [2–4]. Thus the thermal stability of these materials is of interest.

There are two fundamental thermal stability issues. One is the thermal stability of the polar order of the material. This is the order that establishes and maintains the second-order polarizability process. The other major issue deals with the chemical thermal stability of both the dyes and the polymer matrix surrounding the dyes. High temperature polymers are already well known and well characterized. However, dyes are typically much more reactive because of their extensive π-electron structure and available excited states that often involve significant π-electron re-organization. Our study will focus on dye thermal stability.

* Corresponding author. E-mail: cdirk@utep.edu

0301-0104/99/$ - see front matter © 1999 Elsevier Science B.V. All rights reserved.
PII: S0301-0104(99)00051-8

2. Objective

Our research project is to systematically study the thermal stability of a large group of varied electro-optic organic dyes and look for ways of increasing their thermal stability.

3. Method

We will use differential scanning calorimetry (DSC) to measure the thermal stability. DSC is a commonly used method for thermal analysis studies especially in the case of the thermal stability studies of electro-optic dyes [5–7]. It records the phase transition temperatures of the materials versus the heat flow. To prevent the evaporation or sublimation of the materials, we use a sealed capsule as a holder of the materials [8]. In this case, the decomposition temperatures of the dyes are used as the measure of their thermal stability.

In order to assure that the thermal transition temperatures of the samples are closely related to the instrument temperature, we attempt to scan across temperature at a slow rate but fast enough to finish a run in a reasonable length of time. The smaller the heating ramp, the closer the measured temperatures are to the real values. But a slower heating speed means a longer time of thermal analysis. In this case, a heating ramp of 5°C/min has been implemented.

Since reaction rate is usually expressed as a function of concentration of one of the participating substances — reactants or products — in the case of single reacting species, the rate and reaction order are connected by an equation, for instance:

$$r = -\mathrm{d}C/\mathrm{d}t = kC^n \tag{1}$$

where r is reaction rate, k rate constant, C concentration of reactant and n reaction order. Here, the rate is the total reaction rate − the total amount of reactant disappeared during the time $\mathrm{d}t$. k is also a temperature dependent factor. The relation of k with temperature is defined by the Arrhenius equation:

$$k = A\mathrm{e}^{-E_a/RT} \tag{2}$$

where A is pre-exponential factor, constant; E_a activation energy; R ideal gas constant; T absolute temperature.

A is a constant independent of temperature and concentration and sometimes is called the pre-exponential factor. Combining Eq. (1) and Eq. (2), we get:

$$r = A\mathrm{e}^{-E_a/RT}C^n \tag{3}$$

The DSC instrument only records the values for these parameters such as temperature, time and heat flow. Among these, only the temperature shows up in the above equation. According to Eq. (3), we also need the reaction rate in order to get the other kinetic properties such as reaction order. Hence the needed information has to be calculated from the recorded DSC plots. To calculate the concentration, we have to make an assumption. Assumption (1): the concentration is strictly proportional to the heat effect of the reaction system. Then we have:

$$\mathrm{d}C \propto \mathrm{d}(\Delta H) \propto \mathrm{d}A \tag{4}$$

where A stands for the area under the DSC curve. Many reactions may take place in the reaction cell, in addition to the main reaction that we are interested in for the kinetic investigation. Those reactions possibly include secondary reactions of the products of the first-step reaction, and the further reaction (or decomposition) of the products of the secondary reaction because the reaction cell is in an environment that the temperature is constantly increasing. At a temperature that is several hundred degrees, the overall reactions could be more complicated than we could imagine, so that it is impossible to know the true concentration of the original reactant. What we can do is to make a second assumption. Assumption (2): there are no post first-step reactions for the system. This excludes the complication by the secondary reactions. This assumption is often and mostly not valid, however under the extreme of high dilution, or at a stage early in the initial decomposition, it likely can be valid. At any other times, it can contribute to the uncertainty of the data, but mostly only at high concentrations, or later in the reaction. Thus, some portion of the data may adhere to assumption (2), while another portion may be less so.

For Eq. (3), we have the reaction rate r, the concentration C and the reaction temperature T, which are known or can be obtained from assumptions (1) and (2). For the other three parameters: pre-exponential factor A, activation energy E_a and

reaction order n, we can use a nonlinear least squares fitting method to find their values.

4. Results and discussion

We have tested more than 300 electro-optic (EO) dyes. The dyes display a broad range of thermal stability. From the analysis of all DSC curves, it is clear that there also exist different shapes of DSC plots for the decomposition peaks. Some are symmetric while some are not; some peaks begin with a small slope but drop very fast at the end of decomposition while some others are vice versa.

From the observation of the thermal behaviour of many compounds [9–11], intuition suggested that the thermal decomposition mechanism might be different for different samples. It is possible that the decomposition of the neat samples may be very complicated for some systems because of the high concentration of the materials as well as the high temperature and high pressure that resulted from the sealed vessel.

We start from a very simple system, *para*-nitroaniline. This is a good nonlinear optical (NLO) dye with a simple molecular structure. The nitro-group is a good electron acceptor while the amino-group is a good electron donor. The recorded onset decomposition temperature T_{di} is 328°C and the peak decomposition temperature T_{dm} is 356°C. The shape of its decomposition peak, is not completely centrally symmetric (Fig. 1). It drops abruptly at the higher temperature side. This means that the beginning part of the decomposition gives out heat relatively slower than the last part of the peak. This can mean at least two things. (a) Reaction rate changes: the beginning part of decomposition is relatively slower than the last part. If this is true, one can assume that as more and more decomposition products arise, the reaction becomes faster. In other words, the products may be speeding up the decomposition reaction of the original dye. This is typical of an auto-catalyzed reaction [12]. (b) Secondary reaction or decomposition: the decomposition product(s) of the original dye may undergo secondary reactions. These secondary reactions can either be general chemical reactions among the ingredients or further decomposition of the decomposition products. In this case, the original decomposition may have a relatively smaller heat effect. As the reaction goes on and the temperature continues to increase, secondary reactions also give off heat and hence results in this kind of peak shape.

We will use the following general kinetic mechanisms to test the real mechanism of the decomposition peak of the dyes.

(1) First-order mechanism:

$$A \rightarrow \text{products}$$

$$r = Ae^{-E_a/RT}C$$

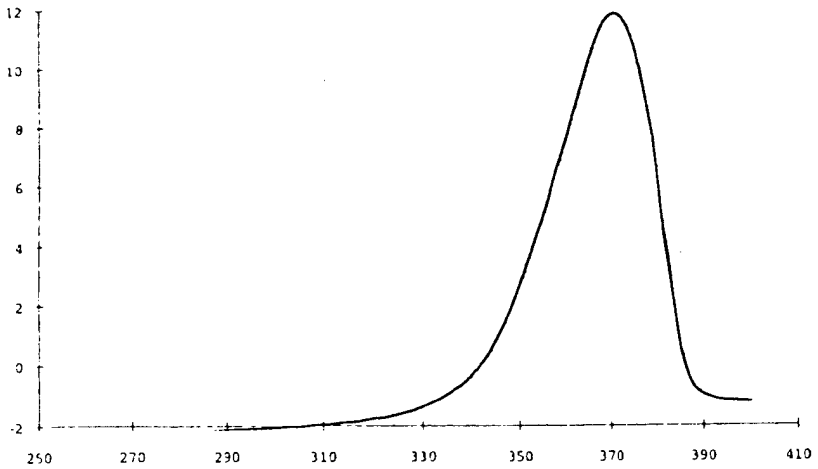

Fig. 1. DSC plot of *p*-nitroaniline.

(2) Second-order mechanism:

$2A \rightarrow$ products

$r = Ae^{-E_a/RT}C^2$

(3) nth-order mechanism:

$nA \rightarrow$ products

$r = Ae^{-E_a/RT}C^n$

(4) Parallel reactions of first and second orders:

$r = Ae^{-E_a/RT}C + Be^{-E'_a/RT}C^2$

(5) Auto-catalysis:

$A \rightarrow B +$ products

$A + B \rightarrow$ products

$r = Ae^{-E_a/RT}C \cdot (C_0 - C)$

where C_0 is the starting concentration of reactant, while r, A, E_a, C, T and R are the same as stated earlier.

The decomposition peak of *para*-nitroaniline (PNA) does not fit at all with the first-order or second-order mechanisms. But it is well fitted with an auto-catalysis mechanism (Fig. 2). The real decomposition rate calculated from the DSC measurement is depicted as the dashed line in the plot and the simulated rate using the best fit auto-catalysis rate expression is drawn as the solid line.

It is well known that nonlinear optical dyes are organic compounds that typically have an electron donor at one end of the molecular structure and an electron acceptor at the other end of the structure. Because of the existence of the electron donor and acceptor in the dye molecule, there can be some interactions between these two groups on adjacent molecules in a neat environment. To weaken this interaction, we mix the dye with an inert material and then measure the decomposition temperature of the dye. The inert material is selected so that it is thermally stable and chemically nonreactive in the temperature range of the measurement. DSC analyses of these diluted dye solutions show that the decomposition temperature of the dye molecules shifts to higher temperature relative to the neat dye. Fig. 3 is a representative result of this investigation. The sample is PNA diluted in naphthalene in different concentrations. Naphthalene is the inert solid solvent in order to separate the dye molecules.

The peak position for neat PNA is 356°C. As the ratio of PNA to naphthalene decreases, the peak up-shifts to higher temperature, so that larger amounts of naphthalene in the system make the decomposition position of PNA shift higher. The total shift is 49°C for the lowest concentration relative to the neat sample. This is quite significant since it suggests an approach to stabilize a matrix of EO dyes.

A question may be raised with this mixed system. Is the peak shifting purely as a result of the concen-

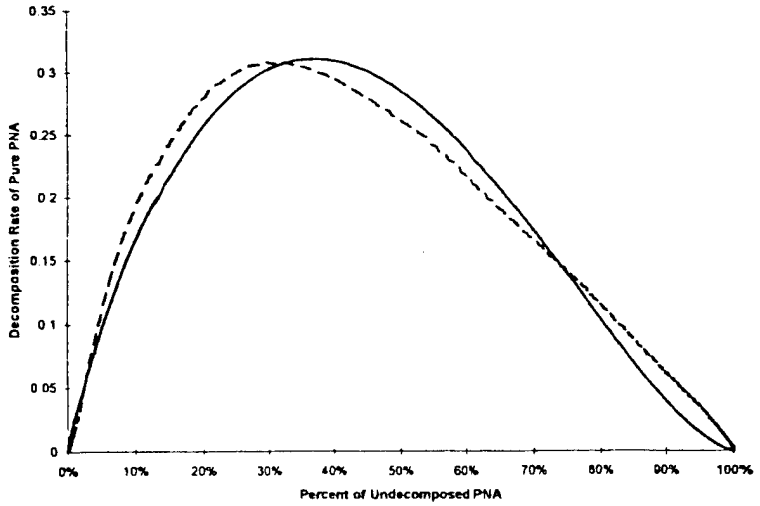

Fig. 2. Decomposition rate curve of neat *p*-nitroaniline (solid line is the simulation by auto-catalysis mechanism).

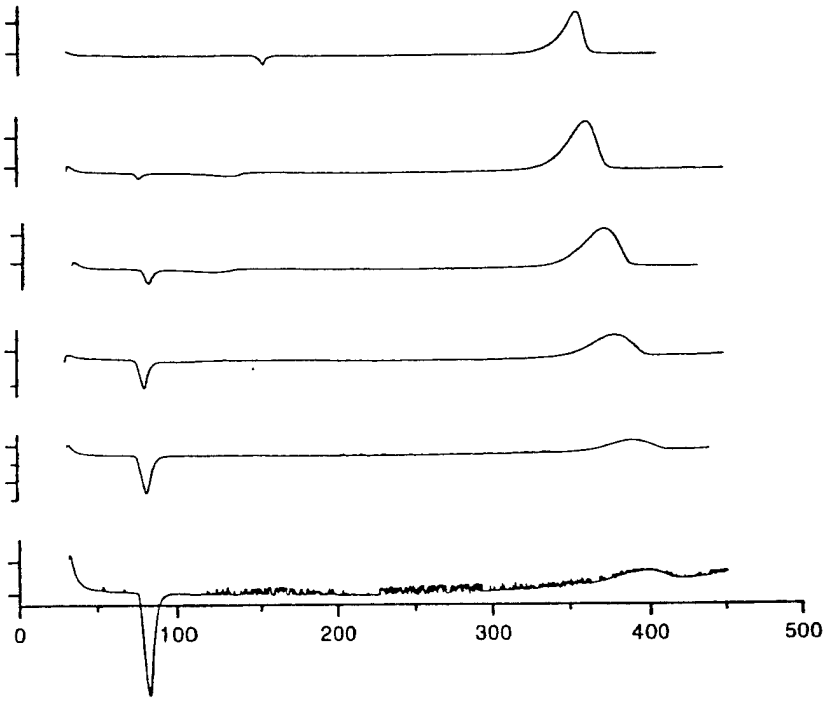

Fig. 3. DSC plots of *p*-nitroaniline in naphthalene with different concentrations (from top to bottom: 100, 71.4, 55.6, 18.5, 6.4 and 2.5 mole% of PNA)

tration change, or is it due to the lag response of the instrument signal on a smaller sample? To answer this question, a series of DSC analyses has been done. We have used different solvents to investigate this dilution problem. It is found out that the peak shifts about the same amount whether the inert solvent is biphenyl, naphthalene, phenylcarbazole, *p*-terphenyl and *o*-terphenyl when the dye has the

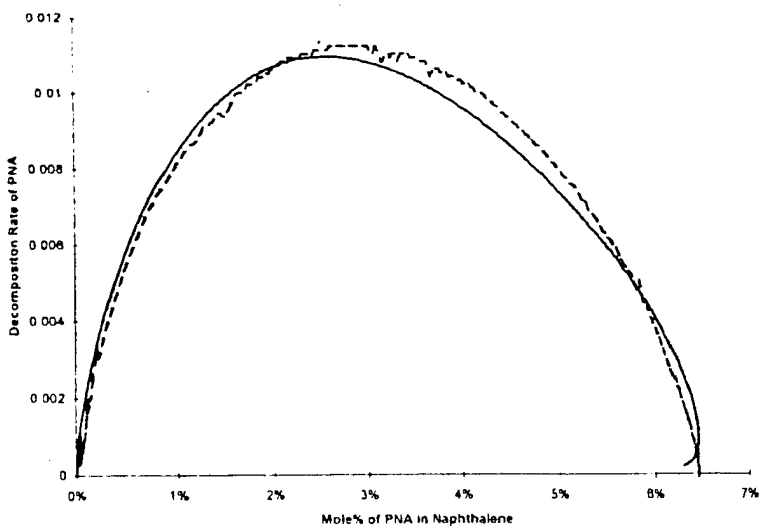

Fig. 4. Kinetic simulation of diluted PNA system in naphthalene (solid line is the simulation using first-order mechanism).

Table 1
Comparison of the decomposition temperatures of neat and diluted samples

Name	Mole%	Enhancement (°C)	e^- Acceptor
PNA	5.7	39	Nitro-
N2	4.8	58	Nitro-
N3	4.5	52	Nitro-
N19	4.6	30	Nitro-
N100	4.5	58	Nitro-
N20	4.8	95	Dicyanovinyl
N21	4.7	101	Dicyanovinyl
N85	10.4	92	Dicyanovinyl
M111	4.9	101	Dicyanovinyl
M123	5.2	101	Dicyanovinyl
N5	4.1	95	Tricyanovinyl
N6	2.2	102	Tricyanovinyl
N11	3.7	103	Tricyanovinyl
N13	5.9	106	Tricyanovinyl

same concentration in the mixture. Since these solvents possess different heat capacities, we would expect a heat lag effect to vary with each. This is not observed, suggesting that a thermal lag is not occurring. For reference, the standard heat capacity for biphenyl is 198.4, naphthalene is 165.7 and PNA is 167.0 J/K mol [13]. The main role of the solid solvent in the mixture is only to separate the dye molecules and hence reduce the interaction between the donor and the acceptor of the dye. A sample size test is also carried out for this purpose. It is proved that the sample size does not have much influence on the shifting of the decomposition peak.

One of the kinetic studies of the solution systems we have investigated is a very dilute system: PNA in naphthalene with a 6.4% molar concentration. Fig. 4 is the kinetic result. It turns out that PNA tends towards an unimolecular path when diluted. The best fit first order line (solid) fits very well with the real kinetic line (dotted).

With no exception to date, other EO dyes display the same behaviour as we have just described for

Table 2
Molecular structures of the EO dyes in Table 1

Name	Structure	Name	Structure
PNA	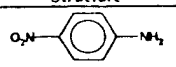	N85	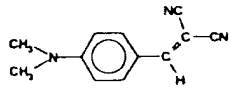
N2	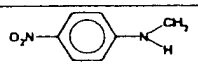	M111	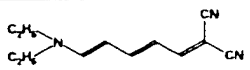
N3	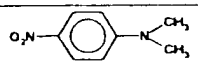	M123	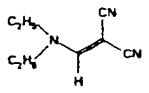
N19	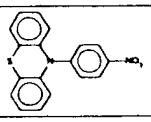	N5	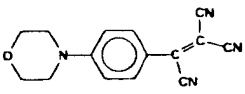
N100	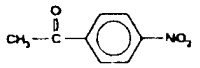	N6	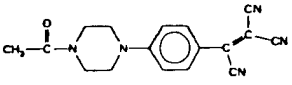
N20	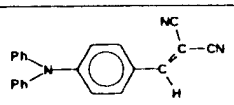	N11	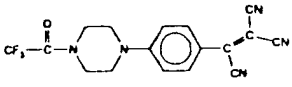
N21	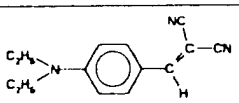	N13	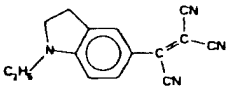

para-nitroaniline. This includes up to 50 different dyes for which dilution studies have been performed. When diluted, their decomposition peak up-shifts to higher temperature and decomposition mechanism shifts to unimolecular. This shift indicates the enhancement of the thermal stability of these EO dyes by the decrease of the interaction between the electron donor and electron acceptor in different dye molecules. But, as it is true that different dyes have different thermal stability, different dyes also exhibit a different amount of stability enhancement when diluted by an inert solvent. Table 1 lists some of the results of the dilution measurements. The molecular structures of the dyes are listed in Table 2.

Looking at the table, it is very interesting to notice that dye molecules containing nitro group as the electron acceptor have the tendency toward a stability enhancement of 40 to 50°C. Dyes with the cyanovinyl group (including bicyanovinyl and tricyanovinyl groups) as electron acceptor generally display a stability enhancement of 70 to 100°C.

It has been pointed out that [14], neat cyanovinyl NLO dyes are more thermally stable than neat nitro NLO dyes. From this dilution analysis, it is also known that when diluted, cyanovinyl dyes increase their thermal stability by 70 to 100°C, much higher than that of nitro dyes. We may conclude that from the point of thermal stability, cyanovinyl dyes are more promising than nitro dyes.

5. Conclusions

It is concluded from our kinetic studies of neat NLO dyes that the neat dyes undergo non-unimolecular decomposition. This is probably due to the strong intermolecular interaction between the electron donor and acceptor. When the dye is mixed with a nonactive component, there becomes less opportunity to react with itself and hence decomposes at a higher temperature, since the inert solvent separates the dye molecules and reduces the interaction between donor and acceptor. It is presumed that this donor–acceptor interaction is the primary mechanism of the decomposition of the dyes when neat. As the dye concentration in the system decreases, this intermolecular interaction is weakened and eventually the dyes take a unimolecular decomposition path.

Although it is a general phenomenon that the decomposition occurs at a higher temperature when the dyes are diluted in an inert environment, the extent of the stability enhancement is different for different kinds of dyes. For a dye concentration of about 5 mole%, nitro dyes have a trend of 40 to 50°C enhancement relative to the neat samples while cyanovinyl dyes tend to be 70 to 100°C more stable than their neat samples. This makes cyanovinyl dyes more desirable than nitro dyes in term of thermal stability and stability enhancement upon dilution.

The observation of a concentration dependence for the decomposition of the NLO dyes is not only intriguing but very practical, since we are expecting the possibility to improve the thermal stability of the EO dyes especially when the dyes are to be implemented into a real electro-optic device. With the typical polymer matrices used in EO devices, the dye molecules are expected to be more stable than expected relative to the neat dyes because in this case the matrix serves as the inactive media which separates the dye molecules from interacting with each other. Significant dilution of the dye within the matrix can likely always improve its thermal stability.

Acknowledgements

We would like to express our appreciation to the Office of Naval Research (CAMP-University of Arizona), Air Force of Scientific Research, the Texas Higher Education Coordinating Board, the Robert Welch Foundation and the Ballistic Missile Defense Organization. We would also like to thank Dr. Robert Twieg for helpful comments and advice, and Dr. Twieg, S. Ermer (Lockheed–Martin), Alex Jen (Northeastern University) and S. Marder (University of Arizona) for generously providing EO dye samples.

References

[1] C.R. Moylan, Proc. SPIE Int. Soc. Opt. Eng. 17 (1994) 2285.
[2] R.B. Prime, J. Therm. Anal. 46 (1996) 1133.
[3] R. Lytel, Polymers for Lightwave and Integrated Optics:, Technology and Applications, New York, 1992.

[4] D.S. Chemla, Nonlinear Optical Properties of Organic Molecules and Crystals, Vol. 1, Academic Press, New York, 1987.
[5] D.M. Burland, R.G. Devoe, M.C. Jurich, V.Y. Lee, R.D. Miller, C.R. Moylan, J.I. Thackara, R.J. Twieg, T. Verbiest, W. Volksen, Proc. OSA 21 (1995) 289.
[6] A.K.-Y. Jen, V.P. Rao, T.-A. Chen, Y. Cai, K.J. Drost, Y.-J. Liu, J.T. Kenney, R.M. Mininni, P.V. Bedworth, S.R. Marder, L. Dalton, Proc. OSA 21 (1995) 251.
[7] C.C. Henderson, P.A. Cahill, T.C. Kowalczyk, K.D. Singer, Chem. Mater. 5 (1993) 1059.
[8] L.F. Whiting, M.S. Labean, S.S. Eadie, Thermochim. Acta 136 (1988) 231.
[9] C. Dirk, L. Zhang, P. Kalamegham, S. Ermer, S. Lovejoy, D. Leung, R. Twieg, S. Marder, A.K.-Y. Jen, OSA-ACS Meeting, Orlando, FL, 1996.
[10] C. Dirk, L. Zhang, P. Kalamegham, S. Ermer, S. Lovejoy, D. Leung, R. Twieg, S. Marder, A.K.-Y. Jen, Polym. Mater. Sci. Eng. 75 (1996) 375.
[11] L. Zhang, P. Kalamegham, C. Dirk, S. Ermer, R.J. Twieg, OSA Meeting, Portland, OR, September 21, 1995, p. 166.
[12] S. Berkman, J.C. Morrell, G. Egloff, Catalysis, Reinhold Publishing, 1940.
[13] CRC Handbook of Chemistry and Physics, 75th ed., 1995, pp. 5–36, pp. 5–44, pp. 5–46.
[14] L. Zhang, Dissertation, The University of Texas at El Paso, in preparation.

Squarylium Dyes: Structural Factors Pertaining to the Negative Third-Order Nonlinear Optical Response

Carl W. Dirk,*,† William C. Herndon,† Francisco Cervantes-Lee,† Henry Selnau,† Sergio Martinez,† Priya Kalamegham,† Alarice Tan,† Gabriel Campos,† Mayra Velez,† Josef Zyss,‡ I. Ledoux,‡ and Lap-Tak Cheng§

Contribution from the Department of Chemistry, University of Texas at El Paso, El Paso, Texas 79968-0513, Centre National D'etudes des Telecommunications, Laboratoire de Bagneux, 196 Avenue Henri Ravera, BP 107, 92225 Bagneux Cedex, France, and Central Research & Development, E. I. DuPont de Nemours & Company, Experimental Station, Wilmington, Delaware 19880-0356

Received June 27, 1994[⊗]

Abstract: Off-resonant electric field induced second harmonic generation (EFISH) and resonant third harmonic generation (THG) measurements of two squarylium dyes are reported. The magnitude of γ is large for both processes. The EFISH measurement clearly shows that the off-resonant third-order polarizability is negative, a consequence of the dominance of a non-two-photon mechanism. This unusual result is in agreement with our earlier reports on two other squarylium dyes. Resonant THG measurements strongly suggest that the two-photon contribution, while smaller than the one-photon contribution, is not negligible and cannot be entirely ignored when defining the overall third-order optical susceptibility. Consequently, the squaryliums are best qualitatively described by a three-level model that truncates to two dominant perturbation terms. Also reported is the isomeric distribution of squaryliums. Proton NMR results are interpreted by way of molecular mechanics to show that the squaryliums can readily exist as a mixture of isomers. The possible effects on nonlinear optical (NLO) measurements via an orientational contribution to the EFISH γ are discussed. An X-ray structure for the squarylium dye TSQ is presented and interpreted. The X-ray structure clearly suggests that the squarylium dyes are extensively bond delocalized with relatively little bond length alternation.

Introduction

Negative third-order polarizabilities (γ for the molecular property and $\chi^{(3)}$ for the bulk) are relatively uncommon. Such all-optical nonlinearities are self-defocusing, rather than self-focusing, eliminating the concern of the nonlinear optical auto-optical annihilation of a potential all-optical device. Negative γs have recently also been instrumental in helping define the family of microscopic electronic mechanisms which can contribute to γ.[1,2] Additionally, the few negative γs that have been measured are relatively large in absolute magnitude compared to molecules with positive γ. These large magnitudes have been the consequence of relatively small contributions from two-photon states and have led to the hope of increasing the magnitude of γ considerably beyond those reported in the past. We report here some new measurements on squarylium dyes, as well as verify the presence of a non-negligible two-photon state. We report linear-optical and proton NMR spectral details suggesting that the dyes ISQ and BSQ exist as a mixture of isomers and provide some interpretation of the impact of this on the optical properties.

Structural concerns such as relative bond length alternation[3] are becoming important in optimizing structures for nonlinear optics. We have determined the crystal structure of the squarylium dye TSQ and show, by way of analysis of its crystal structure and calculated structures, that this dye shows significant bond delocalization, as evidenced by its reduced bond length alternation.

Theory

Defining the mechanisms which contribute to the electronic γ has been a nontrivial undertaking. Early work in the field identified two-photon contributions as being an important element.[4] This has required the implementation of models which require at least three states, one of which must be a two-photon state. In addition, in the absence of relatively sophisticated nonlinear spectroscopy or calculations, the two-photon state remains a mysterious unknown contribution for the materials chemists who have been undertaking the optimization of molecules for all-optical applications. The consequent frustratingly slow development of new molecules has prompted a pessimistic prediction for all-optical organic devices.[5]

With the experimental problems and theoretical restrictions in mind, we[1] and others[6,7] attempted to define a limited model which should provide the necessary qualitative and semiquantitative behaviors. Such a model would be useful in providing materials chemists with the structure−property guidelines to systematically enhance γ. The development of this model involved starting with the relatively complex one-dimensional

† University of Texas at El Paso.
‡ Laboratoire de Bagneux.
§ E. I. DuPont de Nemours & Co.
⊗ Abstract published in *Advance ACS Abstracts*, February 1, 1995.

(1) (a) Dirk, C. W.; Cheng, L.-T.; Kuzyk, M. G. *Int. J. Quant. Chem.* **1992**, *43*, 27. (b) Dirk, C. W.; Cheng, L.-T.; Kuzyk, M. G. *Mater. Res Soc. Symp. Proc.* **1992**, *247*, 73.

(2) Gorman, C. B.; Marder, S. R. *Proc. Natl. Acad. Sci. U.S.A.* **1993**, *90*, 11297.

(3) Marder, S. R.; Cheng, L.-T.; Tiemann, B. G.; Friedli, A. C.; Blanchard-Desce, M.; Perry, J. W.; Skindhøj, J. *Science* **1994**, *263*, 511. For the foundation of the bond length alternation concept, see also ref 7

(4) Bredas, J. L.; Adant, C.; Tackx, P.; Persoons, A.; Pierce, B. M. *Chem. Rev.* **1994**, *94*, 243.

(5) Green, B. I.; Orenstein, J.; Schmitt-Rink, S. *Science* **1990**, *247*, 679.

(6) Garito, A. F.; Heflin, J. R.; Wong, K. Y.; Zamani-Khamiri, O. In *Organic Materials for Nonlinear Optics*; Hann, R. A., Bloor, D., Eds.; Royal Society Chemistry: London, 1989; p 16.

(7) Pierce, B. M. *Proc. SPIE Int. Soc. Opt. Eng.* **1991**, *1560*, 148.

nine-term three-level model[8] and choosing an approximation path that reduced it to a simpler and more intuitive one-dimensional three-term three-level model

$$\gamma \approx \gamma_c + \gamma_n + \gamma_{tp} \quad (1)$$

where $\gamma_c = -K\mu_{01}^4 D_{111}$, $\gamma_n = K\mu_{01}^2(\Delta\mu 01)^2 D_{111}$, $\gamma_{tp} = K\mu_{01}^2\mu_{12}^2 D_{121}$, μ_{01} is the transition moment to the significant[9] one-photon state, μ_{12} is the transition moment between the one-photon and significant two-photon state, $\Delta\mu_{01}$ is defined as $\mu_{11} - \mu_{00}$, D_{lm} and D_{lmn} are dispersion terms which have been defined earlier,[8] and K is a constant defined by the optical process. The constant K is always positive, as are D_{lm} and D_{lmn} when all resonant interactions contributing to the process $\gamma(\omega_4;\omega_1,\omega_2,\omega_3)$ are off resonance and to low energy of the electronic excitation manifold. In the notation used by Garito,[6] γ_c is a type I term, γ_{tp} is a type II term, and γ_n is a type III term. In Pierce's notation,[7] γ_c is identified as "G", γ_{tp} is identified as "X", and γ_n is identified as "D".

Under the circumstances defined above, there are three optimization approaches to eq 1. The simplest optimization is to consider centrosymmetry, requiring that γ_n. This reduces the model to

$$\gamma \approx \gamma_c + \gamma_{tp} \quad (2)$$

Note here that γ_c and γ_{tp} are opposite in sign but contain a cross term, μ_{01}, that makes them compete. Thus, if the magnitude of μ_{01} is greater than μ_{12}, γ is negative, while if it is smaller, γ is positive. This will always be true under the resonant conditions defined above as long as the two-photon state is higher in energy than the one-photon state (i.e., $D_{111} \geq D_{121}$). In general, as a presumption, the magnitude of μ_{12} has commonly been larger than μ_{01}, which may have been influenced by the one-photon and two-photon energy difference, E_{12}, which is commonly smaller than the ground and one-photon energy difference, E_{01}. This latter realization about E_{01} and E_{12} has recently[10] been used to reveal excited state optical nonlinearities of large magnitude. The condition of $|\mu_{12}| > |\mu_{01}|$ typically is more significant than $D_{111} \geq D_{121}$ (or $D_{11} \geq D_{121}$) so that most third-order optical nonlinearities are dominated by the two-photon state and are positive. Normally, the condition $|\mu_{12}| > |\mu_{01}|$ can be so dominant that even great differences in energy (increasing the ratio $D_{11} \geq D_{121}$) between the one- and two-photon states cannot allow for negative γs. This, in combination with an experimental habit of two-photon *resonant* measurements means that most molecules will only reveal themselves as positive optical nonlinearities, γ. Thus, finding negative γ required us to specifically look for it. The important main search criteria were centrosymmetry, a molecule with its oscillator strength concentrated in one significant μ_{01}, as well as perhaps a measurement process that did not bias two-photon resonances over one-photon or three-photon resonances. The earlier reported work of Stevenson et al. showed that free-electron structures could display negative γs, even in the absence of strict centrosymmetry, though some structures also displayed positive γs.[11] At the time, in the absence of Marder's bond length alternation studies, which work toward rationalizing such behavior, it was necessary for us to apply strict centrosymmetry criteria to optimize for a negative nonlinearity.

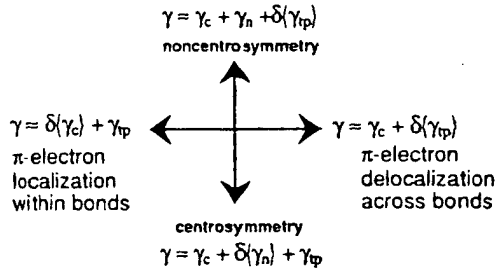

Figure 1. Optimization neumonic for the third-order nonlinear optical response. Note that $\delta\{\}$ signifies a less important contributing term.

The choice[12] of the free-electron-delocalized squaryliums with their narrow intense isolated low-energy transitions and the creation[13] of a specialized quadratic electro-optic measurement follow from the previous arguments. The QEO process involves an optical frequency probe ω modulated by a much lower frequency Ω. The contributions from one- ($\omega_{01}-\omega$) and three-photon resonances ($\omega_{01}-\omega-2\Omega$) are large, being close to the significant transition frequency (ω_{01}), while two-photon resonance ($\omega_{01}-2\Omega$) contributions are always minimized. This permitted the comparison of the measured electro-optic γ_{QEO} to that obtained by calculating γ_c from linear spectroscopic results. As it may be, the squarylium dye we first investigated possessed a significant negative nonlinearity so that biasing the measurement with the QEO process was unnecessary.

Given the above discussion, it is also relevant to examine the theoretical consequence of noncentrosymmetry. Under this restriction, one can argue that molecules with large dipole changes could lead to a situation where the magnitude of γ_n is much greater than the magnitude of γ_c. Since the moments contribution to the two-level model for β is embedded in γ_n, it is clear that optimization of γ_n can proceed by way of optimization of β, though with some possible deviation from maximum due to the extra $\Delta\mu$ factor. Further, the shift in state symmetries upon moving from a centrosymmetric to an extreme noncentrosymmetric system should lead to a decline in the magnitude of γ_{tp}. We have recently shown that the QEO γ for molecules with large hyperpolarizabilities, β, can be rationalized in just this manner.[14] A similar conclusion has been reached by Garito et al.[15] Thus, γ reduces to

$$\gamma \approx \gamma_c + \gamma_n \quad (3)$$

The above arguments define an optimization mnemonic (Figure 1) which involves either shifting symmetry or electron localization. In this context, shifting symmetry involves modifying the structural atomic positions, while shifting electron localization involves adjusting the relative donor and accepting capabilities of substituents. It is important to recognize that, in the discussion of symmetry, we strictly are referring to nuclear coordinate symmetry, though, in principle, a molecule which is nuclear coordinate acentric could be electronically nearly symmetric. Marder's recent results[2] thus can be interpreted and made to suggest that negative γ nonlinearities could be obtained in a polar molecule by reducing the electronic asymmetry and increasing the electron delocalization (reducing bond length alternation). This is important because it could represent a

(8) Kuzyk, M. G.; Dirk, C. W. *Phys. Rev. A* **1990**, *41*, 5098.

(9) In this regard, states 1 and 2 are relative, and not absolute. In other words, there may be nonessential states between 0 (ground) and 1 or between 1 and 2 which may be unimportant for the four-wave mixing scattering process.

(10) Zhou, Q. L.; Heflin, J. R.; Wong, K. Y.; Zamani-Khamiri, O.; Garito, A. F. *Phys. Rev. A* **1991**, *43*, 1673.

(11) Stevenson, S. H.; Donald, D. S.; Meredith, G. R. *MRS Proc.* **1988**, *109*, 103.

(12) Dirk, C. W.; Kuzyk, M. G. *Chem. Mater.* **1990**, *2*, 4.

(13) Kuzyk, M. G.; Dirk, C. W. *Appl. Phys. Lett.* **1989**, *54*, 1628.

(14) Dirk, C. W.; Caballero, N.; Kuzyk, M. G. *Chem. Mater.* **1993**, *5*, 733.

(15) Garito, A. F.; Heflin, J. R.; Wong, K. Y.; Zamani-Khamiri, O. *SPIE Proc.* **1989**, *971*, 9.

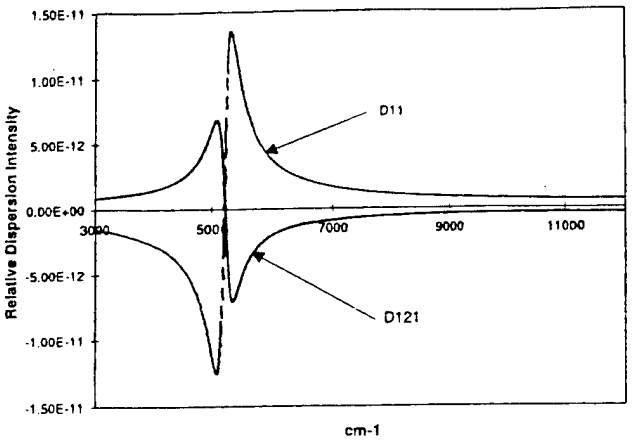

Figure 2. Plot of the calculation of the dispersion terms D_{11} and D_{121} for the THG process as a function of the THG fundamental frequency presuming λ_{max} of 640 nm for the one-photon state and 333 nm for the two-photon state and approximating the theoretical Lorentzian damping as the experimental peak width $2\Gamma_G$ of 704 cm^{-1} of TSQ. The presumed two-photon energy comes from the work of Garito et al.[16]

systematic path to negative γ nonlinearities which do not require nuclear coordinate centrosymmetry. It is important to recognize that Marder's bond length alternation results approach provides the mechanics to generate the details for the smooth transition between two positive γ optimized structures (one corresponding to positive β and the other negative β) and the one negative optimized structure. We had earlier suggested that such a smooth transition must exist, as well as correctly predicted the nature of the maxima (positive γ) and minima (negative γ).

Our past work[1] implied that the two-photon contribution was small for the squaryliums, though we were not able to determine the true magnitude of γ_{tp}. Garito and co-workers have investigated the mechanisms that determine the sign and the magnitude of γ in the squaryliums and have suggested that a two-photon contribution is significant.[16] Consequently we chose to undertake a third harmonic generation measurement of BSQ

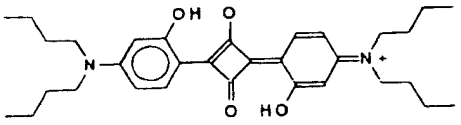

and another dye, TSQ (n = 3)

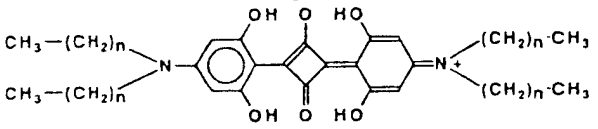

This measurement was chosen to yield a third harmonic embedded in the absorption spectrum of the dye near where a two-photon state might be expected to exist. Under such circumstances, a positive third-order nonlinearity would suggest that γ is being mostly influenced by γ_e, and that the nearest relevant two-photon state was very high in energy relative to the significant singlet ground state. A negative nonlinearity would suggest a significant two-photon contribution. This is obvious if one examines Figure 2, where the one-photon and two-photon dispersions terms, D_{11} and D_{121}, of γ_e and γ_{tp} respectively, are illustrated as a function of THG fundamental frequency. It can be seen that, in the absence of a γ_{tp} (D_{121}) contribution, the off-resonant negative nonlinearity should become positive as the three-photon resonance passes through the one-photon state excitation energy. The presence of a significant γ_{tp} contribution can lead to a significant negative nonlinearity under the same circumstances. The negative and positive contributions compete, though depending on the relative magnitudes of the transition moments, μ_{01} and μ_{12}, a γ_{tp} contribution is necessary for the observation of a negative γ above the one-photon transition, when a negative γ is observed below the one-photon transition.

Comparisons are also made to ISQ:

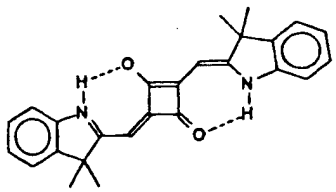

Both ISQ and BSQ can exist as sets of cis−trans isomers. We explore this possibility, and show how this isomerization can affect and complicate the interpretation of third-order nonlinear optical polarizations.

Experimental Section

Reagent chemicals and solvents were used as purchased without further purification. Calculations were performed with PCMODEL V4.0 (Serena Software) or HYPERCHEM (Autodesk Software) on an Intel 80486 based machine or using SPARTAN (Wavefunction Software) and SYBYL (Tripos) on a Silicon Graphics Indigo or Indigo-2 workstation. CNDO singly and doubly excited configuration electronic spectral calculations were performed with an adaptation of the QCPE program CNDUV99 (QCMP062) on an Intel 80486 based personal computer.

To make calculations computationally more manageable for the sometimes limited hardware, we eliminated methyl groups (CNDO calculation of ISQ isomers) or shortened longer alkyl chains to methyl groups (AM1 and PM3 calculations of TSQ, BSQ, and HSQ: N-alkyls → N-methyls). All AM1 and PM3 calculations were performed by utilizing the default SCF conditions and parameters inherent to MOPAC.

Finite field calculations of γ were performed using AM1 MOPAC 5.0 by utilizing the "POLAR" option following full SCF AM1 single configuration geometry optimization. Calculations of γ were performed using the induced dipole approximation[17] on both the single configuration calculations of this optimized geometry and the configuration interaction calculations based on this geometry. Configuration interaction calculations were performed using the 100 lowest energy configurations derived from all excitations from the seven highest occupied orbitals to the seven lowest unoccupied orbitals (MOPAC keyword "C.I. = 7").

The preparation of the squarylium dye ISQ follows the procedure outlined for indoliniums.[18] BSQ is a known dye whose preparation is outlined in the literature.[19] Dyes such as TSQ and HSQ (n = 5) were prepared using the general procedure outlined below:

TSQ. To a 250 mL round bottomed flask containing 150 mL of benzene and 15 mL of n-butanol is added 3.7 g (0.0286 mol) of dibutylamine and 5.10 g (0.0314 mol of 1,3,5-trihydroxybenzene dihydrate. A Dean−Stark trap, water cooled condenser, and nitrogen bubbler inlet are affixed, and the reaction is refluxed for 48−72 h with azeotropic distillation of water. The solution is cooled briefly, and 1.63 g (0.0143 mol) of 1,2-dihydroxy-1-cyclobutene-3,4-dione is added. Refluxing is resumed and continued for 5−6 days, during which period water is azeotropically removed. The resulting blue solution is reduced in volume, removing the benzene. Butanol is removed by azeotropic

(16) Zhou, Q. L.; Shi, R. F.; Zamani-Khamiri, O.; Garito, A. F. *Nonlinear Opt.* **1993**, *6*, 145.

(17) Kurtz, H. A.; Stewart, J. J. P.; Dieter, K. M. *J. Comput. Chem.* **1990**, *11*, 82.

(18) Sprenger, H.-E.; Ziegenbein, W. *Angew Chem., Int. Ed. Engl.* **1967**, *6*, 553.

(19) Kazmaier, P. M.; Hamer, G. K.; Burt, R. A. *Can. J. Chem.* **1990**, *68*, 530.

Scheme 1

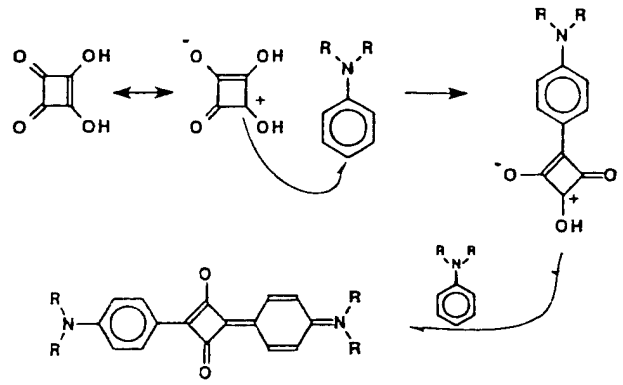

distillation with cyclohexane, at which point the final cyclohexane solution of 15–20 mL is allowed to cool to promote crystallization. After the solution is cooled, the crystalline product is filtered and washed with cold 5:95 ethyl ether/hexane, yield 4.33 g (36%). By NMR, the product is typically >99% pure. Further purification of small quantities can be achieved by low-pressure liquid chromatography on silica gel (eluent: ethyl acetate mixtures with hexane).

We also prepared TSQ by another procedure:

TSQ. To a 250 mL round bottomed flask containing 140 mL of benzene and 7 mL of *n*-butanol is added 6.43 g (0.0397 mol) of 1,3,5-trihydroxybenzene dihydrate and 2.26 g (0.0198 mol) of 1,2-dihydroxy-1-cyclobutene-3,4-dione. A Dean–Stark trap, water cooled condenser, and nitrogen bubbler inlet are affixed, and the reaction is refluxed for 48 h with azeotropic distillation of water. The solution was cooled, followed by addition of 5.23 g (0.0397 mol) of dibutylamine. Refluxing and azeotropic distillation is continued for 4–7 days, yielding a dark blue solution. Benzene is removed by distillation followed by removal of *n*-butanol by azeotropic distillation using cyclohexane. The volume is reduced to 20 mL, then cooled to promote crystallization of the product. The product is filtered and washed with hexane or a 5:95 mixture of ethyl ether/hexane, yield 2.2 g (20%).

This second procedure worked well once, but was not generally reproducible to give high yields, and so was not further pursued.

Dyes were verified by elemental analyses,[20] NMR and/or UV–visible spectroscopy. A typical proton NMR spectrum of TSQ and relevant proton NMR spectral regions of ISQ are provided in the supplementary material.

It is possible to purify the long alkyl chain anilinium squarylium dyes by low-pressure liquid chromatography on silica gel (eluent: mixtures of ethyl acetate and hexane). Nonforced gravity columns typically lead to some decomposition, possibly due to slow hydrolysis. Because TSQ traveled relatively slowly down the low-pressure column, using the same synthetic procedures outlined above, we lengthened the alkyl chains to six carbons (using dihexylamine) to give the molecule HSQ. HSQ proved relatively easy to obtain pure by chromatography in larger quantities than TSQ, so that quantitative electronic absorption measurements were made on this molecule (*vide infra*). Nonquantitative (unspecified concentration) measurements were performed on TSQ (as well as BSQ and ISQ) to obtain λ_{max}s and peak width data as a function of solvent.

Synthesis

The synthesis of squarylium dyes is relatively straightforward, involving a double electrophillic attack by squaric acid on the electron-rich substrates. Preparation of the TSQ family of dyes, possessing four hydroxys ortho to the squarate, is facilitated by recognition of the tautomerization of phloroglucinol to permit nucleophillic attack by a secondary amine.[21] The resulting

(20) BSQ. Calcd: C, 73.80; H, 8.53. Found: C, 73.86, H: 8.50. TSQ. Calcd: C, 69.53; H, 8.04. Found: C, 69.60; H, 8.07. ISQ. Calcd: C, 78.75; H, 6.11. Found: C, 78.80; H, 6.13. HSQ. Calcd: C, 72.24; H, 9.11. Found: C, 71.97; H, 9.12. Further characterization by sealed quartz capillary DSC provided melting points: ISQ, 148 °C; BSQ, 188 °C; TSQ, 233 °C; HSQ, 204 °C.

(21) Effenberger, F.; Niess, R. *Chem. Ber.* **1968**, *101*, 3787.

Scheme 2

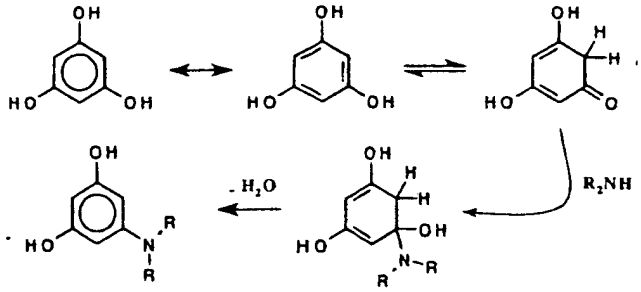

aminoresorcinol reacts readily with squaric acid to yield the TSQ family of dyes. HSQ was synthesized by substituting dihexylamine for dibutylamine. These latter dyes were prepared because the longer alkyl groups improved the ability to purify the dyes by low-pressure liquid chromatography. The dyes TSQ and HSQ display no apparent differences in their linear absorption spectra. Nonlinear optical measurements were initially performed on purified samples of TSQ, though subsequent quantitative linear optical measurements were made on HSQ.

Linear and Nonlinear Optical Results. An EFISH measurement (Table 1) of TSQ in methylene chloride at 1.907 μm supplied a value of -9.5×10^{-34} cm^7/esu^2 for γ. This is the largest magnitude negative nonlinearity measured to date for a squarylium dye. For molecules possessing γs dominated by γ_c, γ is expected to be proportional to the square of the integrated absorption of the main electronic transition. TSQ possesses an EFISH γ that is 1.27 times that of the EFISH γ for BSQ. This implies that the integrated absorptions would differ by 13%. This prompts a quantitative comparison of the linear electronic spectra of the two dyes.

We have prepared another dye HSQ (*n*-hexyls substituted on the nitrogens), which only differs in the lengths of the alkyl chains relative to those of TSQ (*n*-butyls substituted on the nitrogens). This dye was carefully purified by low-pressure liquid chromatography, and its electronic absorption spectrum was measured quantitatively in methylene chloride, supplying an extinction coefficient, ϵ, of 284 000 L M^{-1} cm^{-1}. Given the anticipated negligible effect of the alkyls on the electronic structure of the molecule, TSQ would be expected to possess a similar absorption coefficient. Thus, the nonquantitative electronic absorption spectrum for TSQ, otherwise identical to that of HSQ, was renormalized by the HSQ extinction magnitude for the purposes of further analysis presented here.

Comparison of the spectra of BSQ and TSQ (HSQ) shows that TSQ possesses approximately 19% greater integrated absorption. CNDO-SCI-DCI calculations predict an opposite effect, with the TSQ transition intensity predicted to be slightly lower in intensity.

For the CNDO calculation of TSQ, the main transition is at 484.1 nm, which is considerably different than the pentane spectrum λ_{max} of 635 nm, though one must recall that even the pentane environment is different than a "gas phase" calculation. A solvatochromism extrapolated gas phase value (*vide infra*) is close to the CNDO calculated value. There is another CNDO calculated singlet transition located at 419.2 nm with an isotropic dipole transition intensity of 0.9 D, which could conceivably contribute to the γ_c term, which might contribute to the observed difference in nonlinearities. The electronic absorption spectrum of TSQ does reveal a significant shoulder to higher energy of the main peak. Neither isomer (*vide infra*) of BSQ shows a similar significant calculated transition near the lowest singlet, though the experimental spectrum of BSQ shows (supplementary material) a weak (weaker than in TSQ) shoulder. Possibly some

Table 1. Experimental and Calculated Nonlinear Optical Coefficients[a]

molecules measd	EFISH γ[b]	THG γ[c]	molecules calcd	$\gamma(0)$[d,e]	$\gamma(0)$[d,f] (CI)
ISQ	-3.5×10^{-34} [g]		ISQ4	-11.3×10^{-34}	-27.3×10^{-34}
			ISQ6	-17.1×10^{-34}	-53.9×10^{-34}
BSQ	-7.5×10^{-34} [g]	-8.98×10^{-34}	BSQ-T	-7.12×10^{-34}	-33.2×10^{-34}
			BSQ-C	-7.41×10^{-34}	-37.7×10^{-34}
TSQ	-9.5×10^{-34}	-37.45×10^{-34}	TSQ	-7.69×10^{-34}	-20.6×10^{-34}

[a] Units of esu. [b] Fundamental of 1907 nm, in methylene chloride. [c] Fundamental of 1390 nm, in chloroform. [d] Zero-frequency MOPAC AM1 finite field calculation from MOPAC AM1 optimized structures. Note that the 1/6 permutation correction has not been applied. [e] Based on single configuration AM1 finite field calculations. [f] Based on AM1 CI finite field calculations. [g] From ref 1.

Table 2. Calculated Transition Wavelengths and Oscillator Strengths versus Experimental Extinction Coefficients

	λ_{max}(exptl) nm, CH_2Cl_2	λ_{max}(exptl) nm, pentane	AM1-CI[a] γ (nm)[b]	CNDO SCI+DCI[c] γ (nm)	CNDO isotropic[d] transition moment, D	ϵ(exptl),[e] L M^{-1} cm^{-1}	CNDO based calcuation of ϵ_{CNDO}, L M^{-1} cm^{-1}; pure isomers	CNDO based calculation of ϵ_{CNDO}, L M^{-1} cm^{-1}; isomer mixtures
ISQ4			537.1	472.6[f]	6.8[f]	177 000	226 000[g]	187 000[h,i]
ISQ6	655	658	529.3	502.0[f]	7.4[f]		253 000[g]	168 000[h,i]
BSQ-C			552.3	515.8	7.5	232,000	273 000[k]	289 000[h,l]
BSQ-T	649	640	552.5	514.8	7.5		274 000[k]	289 000[h,h]
TSQ[m]	650	635	543.8	484.1	7.0		274 000[h]	
HSQ[m]						284,000		

[a] This calculation was used to calculate the AM1-CI finite field $\gamma_{(0)}$s presented in Table 1; MOPAC 5.0 within the TRIPOS program SYBYL; keyword "C I. = 7". [b] This calculated extinction coefficient presumes 79% BSQ-T and 21% BSQ-C and is shown in Figure 4. [c] Includes singly excited and doubly excited configurations; starting structures based on PCMODEL mmx/SCF π-electron optimized structures. [d] Transition moment vectors were isotropically averaged to represent the true relative intensity seen experimentally in solution. Recall that the electronic absorption area is proportional to the square of this value. [e] Determined in dichloromethane. [f] These molecules were calculated with the methyl groups removed since the size of these molecules exceeded the capabilities of the computer presently being used for the CNDO calculation. [g] Calculated using Gaussian peaks and a 1/e peak width of 794 cm^{-1} taken from the experimental determination of ISQ in dichloromethane. [h] Calculated using Gaussian peaks and a 1/e peak width of 704 cm^{-1} taken from the experimental determination of TSQ in dichloromethane. [i] This calculated extinction coefficient presumes 64% ISQ6 and 36% ISQ4 and is shown in Figure 6. [j] This calculated extinction coefficient presumes 36% ISQ6 and 64% ISQ4 and is shown in Figure 6. [k] Calculated using Gaussian peaks and a 1/e peak width of 744 cm^{-1} taken from the experimental determination of BSQ in dichloromethane. [l] This calculated extinction coefficient presumes 21% BSQ-T and 79% BSQ-C and is shown in Figure 4. [m] Note that TSQ and HSQ differ only in the length of alkyl groups attached to the nitrogens.

of the shouldering in BSQ (as well as TSQ) is vibronic in origin. However, in a relative sense, the differences in calculated transition intensity, as well as in the EFISH NLO behavior can probably not be considered significant.

Third harmonic generation (THG) measurements on both BSQ (-8.98×10^{-34} esu) and TSQ (-37.45×10^{-34} esu) were performed in $CHCl_3$ at 1.39 μm. This places the third harmonic at 463 nm, well below the main absorptions near 640 nm. Both results are large negative nonlinearities, indicating, as suggested above, that a significant two-photon state is likely to be present. Thus, at least for measurements for which one resonant frequency is embedded in the excitation spectrum, one must model the nonlinearity as

$$\gamma \approx \gamma_c + \gamma_{tp}$$

The calculations of Garito et al. support this.[16] This might help put into the perspective the observed difference between the γ_c determined from linear optical quantities and the quadratic electro-optic γ measured at 799 nm.[1]

The similarity between the EFISH results and the dissimilarity between the THG results is problematic. Our own finite field calculations (Table 1) verify the negative nonlinearity behavior in all of the squaryliums and agree well (single configuration AM1 MOPAC finite field γ) with EFISH measurements which could be considered nearly off-resonant. On-resonant measurements, such as the THG measurement reported here, might be expected to show more significant differences if the relative two-photon contribution varies or if higher excited states contribute (i.e., not a three-level system).

Interestingly, nonlinear optical calculations (Table 1) suggest that ISQ should possess a significantly larger γ than either BSQ or TSQ in contradiction with the experimental results. These discrepancies are dealt with further below.

Table 3. X-ray Crystallographic Atomic Coordinates ($\times 10^4$) and Equivalent Isotropic Displacement Coefficients ($Å^2 \times 10^3$) for the TSQ molecule[a]

	x	y	z	U(eq)
O(1)	11074(4)	11816(2)	4054(1)	54(1)
O(2)	6812(4)	13285(2)	4788(1)	54(1)
O(3)	4402(4)	9355(2)	6785(1)	54(1)
N	−1075(5)	13329(2)	7033(2)	44(1)
C(1)	10468(6)	10809(3)	4583(2)	40(1)
C(2)	8260(6)	10525(2)	5312(2)	36(1)
C(3)	5912(5)	11230(2)	5735(2)	37(1)
C(4)	5241(6)	12593(3)	5467(2)	38(1)
C(5)	2976(6)	13274(3)	5884(2)	41(1)
C(6)	1177(6)	12670(3)	6609(2)	39(1)
C(7)	1822(6)	11324(3)	6888(2)	42(1)
C(8)	4068(6)	10634(2)	6469(2)	38(1)
C(9)	−2055(6)	14697(3)	6699(2)	53(1)
C(10)	−2360(7)	15482(3)	7509(2)	59(1)
C(11)	170(7)	15484(3)	7865(3)	74(2)
C(12)	−219(10)	16279(3)	8661(4)	137(3)
C(13)	−2880(6)	12679(3)	7799(2)	47(1)
C(14)	−2062(6)	12339(3)	8850(2)	53(1)
C(15)	−3875(8)	11611(4)	9599(3)	86(2)
C(16)	−3162(9)	11277(4)	10639(3)	102(2)

[a] Space group $P\bar{1}$, a = 5.2600(10) Å, b = 10.965(3) Å, c = 13.786(4) Å, α = 77.14(2)°, β = 80.08(2)°, γ = 77.15(2)°.

Crystallographic Results

Atomic coordinates for TSQ are supplied in Table 3, with additional data available in the the supplementary material.

Prior to this work, there were four previously known crystallographic structures of squarylium dyes: one phenolinium

(Cambridge Crystallographic Data Base REFCODE: MXPBUQ)[22]

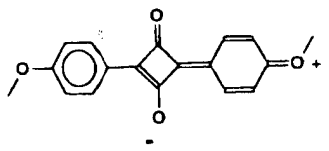

one indolinium (CCD REFCODE: DONXEJ)[23]

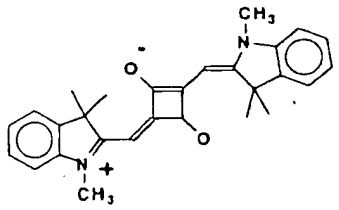

and two crystal morphs of an anilinium squarylium dye (CCD REFCODES: VAYSET and VAYSET01)[24]

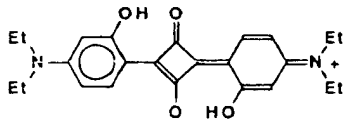

Structures VAYSET and VAYSET01 are analogous to molecule BSQ, allowing us, with the present determination of TSQ, to make a comparison between two significant squarylium dyes. Further comparison to MXPBUQ, DONXEJ, and other 1,3-cyclobutanedione structures, two of which can be considered fairly localized (CCD REFCODE: BERGAG)[25]

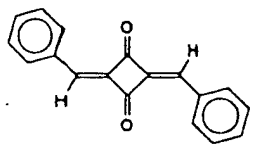

and (CCD REFCODE: BERGEK)[26]

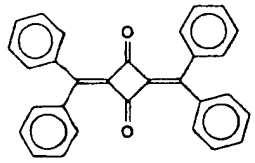

and the delocalized structure (CCD REFCODE: DEDSEK)[27]

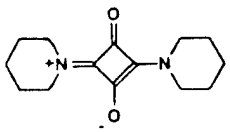

reveals (Table 4) relevant structural features pertaining to the electronic properties of TSQ.

The present structure (Figure 3) of TSQ is centric and essentially planar. Structures MXPBUQ, VAYSET, and VAYSET01 are centrosymmetric and essentially planar, while structure DONXEJ is significantly twisted out of planarity and is noncentric. We have usually formulated and considered our squarylium structures as cross conjugated fully delocalized cyanine and oxonol-type structures. Such a polymethine-type formulation presumes these molecules to be free-electron like. A typical characteristic of such structures is the relatively even

Table 4. Comparison of X-ray and Calculated Structural Parameters of Squarylium Dyes and Related Structures[a]

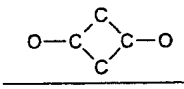

	mean squarate C–O length (Å)	mean squarate C–C length (Å)	conjugated carbon chain: conjugation path[b]	conjugated carbon chain: mean C–C length (Å)	conjugated carbon chain: std dev (Å)
TSQ X-ray[c]	1.253	1.447		1.414	0.029
TSQ AM1	1.241	1.477		1.426	0.031
TSQ PM3	1.235	1.472		1.422	0.031
VAYSET	1.249	1.461	a	1.407	0.036
			b	1.401	0.045
VAYSET01	1.248	1.462	a	1.414	0.031
			b	1.417	0.036
BSQ-T AM1	1.235	1.476	a	1.422	0.028
			b	1.421	0.037
BSQ-T PM3	1.226	1.474	a	1.420	0.029
			b	1.418	0.036
BSQ-C AM1	1.242[d]	1.466[d]	a	1.421	0.026
	1.229[e]	1.485[f]	b	1.423	0.037
BSQ-C PM3	1.243[d]	1.457[d]	a	1.417	0.023
	1.211[e]	1.492[e]	b	1.421	0.042
MXPBUQ	1.230	1.482		1.411	0.043
DONXEJ	1.224	1.471		1.413	0.046
BERGAG	1.213	1.492		1.409	0.051
BERGEK	1.208	1.501		1.419	0.054
DEDSEK	1.240	1.456			

[a] The conjugation path, a or b, is a defined in the text. BSQ structures that are "*trans*" are indicated by the letter "T", while "C" indicates "*cis*". PM3 and AM1 optimized structures are from SPARTAN. [b] Defined in the text. [c] See Figure 3. [d] The carbonyl syn with both OH. [e] The carbonyl anti with both OH.

bond lengths between conjugated carbons. Thus, the average bond length should be between that of a single bonded C—C and a double bonded C=C. The average CC length in the TSQ structure is 1.414 Å with a standard deviation of 0.029 Å. Other squarylium dyes as well as calculated structures (to be discussed, *vide infra*) illustrate similar average lengths, suggesting there is extensive delocalization throughout the molecule. A considerable amount of double bond character evidently exists between all conjugated carbons. As expected, a quinone contraction exists between carbons C(7) and C(8) (1.365 Å) or carbons C(4) and C(5) (1.366 Å), implying the contribution of the quinone resonance form inherent to the squarylium polymethine resonance structures. The most significant deviation toward single bond character exists in the squarate ring itself. Thus, while the net molecular carbon–carbon bond order lends itself toward equilibrating delocalized cross conjugated cyanine/oxonol structures

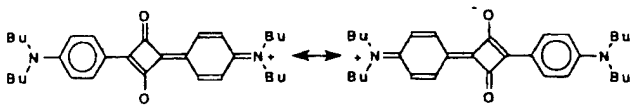

the squarate still possesses cyclobutadienylium dication character

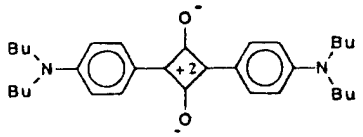

Thus, the true resonance structure must be a complex mixture of these two basic resonance forms. The cyclobutadienylium ring is most contracted in the TSQ squarylium structure. This may be occurring due to the hydrogen bonding stabilizing the anionic oxygen. Either structure should display long carbonyl

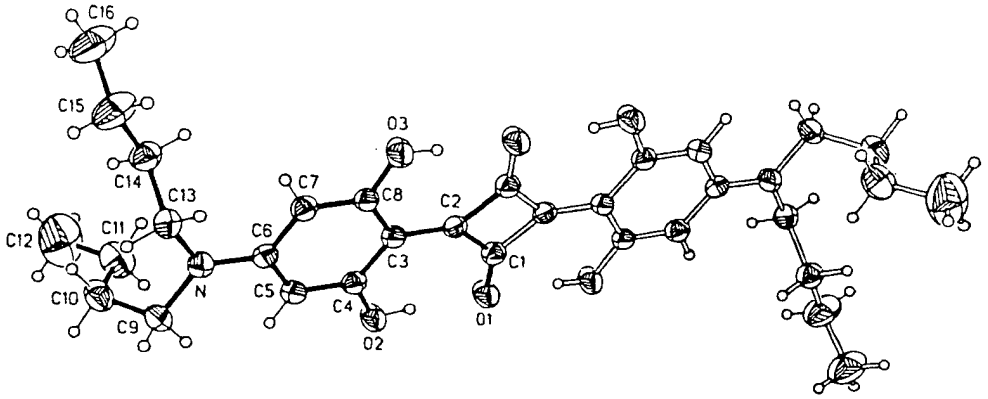

Figure 3. Molecular structure of TSQ from X-ray crystal structure determination. Atomic coordinates are provided in Table 3.

Table 5. Comparison of Calculated and NMR-Derived Experimental Isomer Ratios for ISQ and BSQ

	ISQ6/ ISQ4	ISQ6: ISQ4	BSQ-C/ BSQ-T	BSQ-C: BSQ-T
PCMODEL				
based on *mmx*	0.680	40:60	0.455	31:69
based on $\Delta H°_f$	0.095	9:91	0.538	35:65
PM3				
based on $\Delta H°_f$	0.446	31:69	1.328	57:43
AM1				
based on $\Delta H°_f$	0.832	45:55	0.548	35:65
expt, ref 19				24:76[a]
expt, this work	0.57[b,c]	36:64[b,c]	0.27[c]	21:79[c,d]
	0.52[a,b]	34:66[a,b]		
	0.69[a,e]	41:59[a,e]		

[a] $CDCl_3$. [b] Based on integration of N-H protons. [c] CD_2Cl_2. [d] Based on integration of the aromatic protons ortho to the squarate. [e] Based on integration of olefinic protons.

carbon−oxygen bonds. All of the zwitterionic squaryliums display long carbonyl bonds, with TSQ possessing the longest of any reported to date. By contrast, the localized cyclobutadiones (BERGAG and BERGEK) display considerably shorter carbonyl bonds. The delocalized DEDSEK displays a long carbonyl bond.

The effect of the ortho hydroxys is of interest since these moieties may be influencing the overall bond delocalization. We compare two distinct conjugation paths (Table 4)

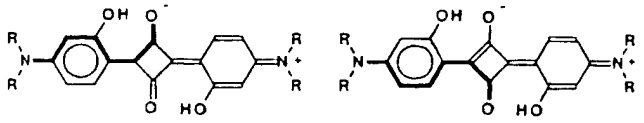

one involving conjugation on the side with the hydroxy and the other on the side without the hydroxy. Standard deviations for the averages of these conjugation paths are significantly different with the standard deviation along the hydroxy side being comparable to that for TSQ. This is seen in the crystal structures of the VAYSET and VAYSET01, as well as in calculations (both AM1 and PM3) of BSQ. The hydroxy evidently helps further polarize the squarate carbonyl, and it is clear that this is enhanced in TSQ relative to BSQ (or VAYSET and VAYSET01). Under this influence, the squaryliums in some sense could also be viewed as an antiparallel system of two donor−acceptor substructures within the molecule.

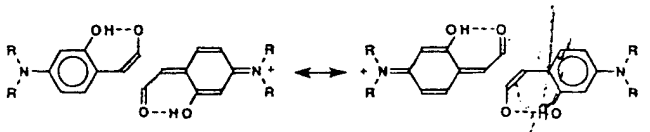

This assessment is similar to that reached by Garito and coworkers.[16]

Isomeric Squarylium Dyes

There is a report in the literature on the NMR analysis of BSQ.[19] Proton NMR distinctly suggests that BSQ exists as a mixture of two isomers, in the proportion of 24:76 in favor of the centrosymmetric structure:

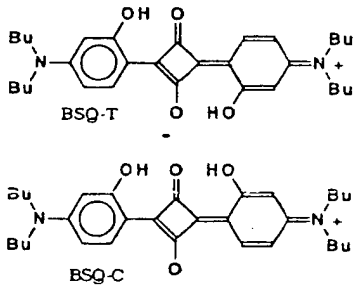

We had suspected the presence of an isomer mixture for ISQ when attempts at deconvolution of the electronic spectra consistently suggested the presence of at least two distinct vibronic absorption manifolds. The presence of a polar isomer has some implications with regard to the third-order optical polarization. It could possibly lead to contributions of a significant γ_n term and could also greatly perturb the EFISH γ due to an orientational contribution via the hyperpolarizability, β, projected on the dipole moment. Presuming a positive orientational contribution, this would reduce the negative nonlinearity further beyond the cancellation due to the γ_{tp} term. In order to further clarify this isomerism issue, we have investigated the proton NMR of ISQ, BSQ, and TSQ.

Investigation of BSQ primarily consisted of verifying the earlier study of Kazmaier et al.[19] Proton NMR spectra collected in CD_2Cl_2 reveal ortho (to the squarate) aromatic doublets at 7.92 and 7.81 ppm (^3J = 9.2 Hz) with relative intensities in good agreement (Table 5) with the $CDCl_3$ spectrum of Kazmaier et al. The meta protons, more distant from the squarate, appear at 6.10 ppm (^4J = 2.3 Hz) and 6.36 ppm (^3J = 9.2 Hz, ^4J = 2.3 Hz)

(22) Farnum, D. G.; Neuman, M. A.; Suggs, W. T., Jr. *J. Cryst. Mol. Struct.* **1974**, *4*, 199.
(23) Kobayashi, Y.; Goto, M.; Kurahashi, M. *Bull. Chem. Soc. Jpn.* **1986**, *59*, 311.
(24) Bernstein, J.; Goldstein, E. *Mol. Cryst. Liq. Cryst* **1988**, *164*, 213.
(25) Gatehouse, B. M. *Cryst. Struct. Commun.* **1982**, *11*, 365.
(26) Gatehouse, B. M. *Cryst. Struct. Commun.* **1982**, *11*, 369.
(27) Budzelaar, P. H. M.; Dietrich, H.; Macheleid, J.; Weiss, R.; Schleyer, P. v. R. *Chem. Ber.* **1985**, *118*, 2118.

Table 6. Calculated Heats of Formation, Strain Energies, and Dipole Moments for the Isomers of ISQ and BSQ[a]

	PC MODEL			PM3		AM1	
	mmx strain, kcal/mol	$\Delta H°_f$ kcal/mol	$\lvert\bar{\mu}_0\rvert$, D	$\Delta H°_f$ kcal/mol	$\lvert\bar{\mu}_0\rvert$, D	$\Delta H°_f$ kcal/mol	$\lvert\bar{\mu}_0\rvert$, D
ISQ1	93.58	185.20	1.24				
ISQ2	93.08	184.85	0.22				
ISQ3	76.26	168.76	3.14				
ISQ4	60.12	153.28	5.69	54.780	4.149	95.126[b]	3.666[b]
ISQ5	76.57	168.85	4.41				
ISQ6	60.35	153.31	0.01	55.298	0.020	95.236[b]	0.020[b]
BSQ-T	49.13	128.54	0.74	−45.544	1.760	−12.758[c]	2.842[c]
BSQ-C	48.66	128.17	0.17	−45.375	0.029	−13.117[c]	0.003[c]

[a] Not included in this table is the CNDO-SCI-DCI dipole moment for BSQ-C (1.67D). [b] Optimized under the AM1 version of SPARTAN. [c] Optimized under the AM1 version of HYPERCHEM.

Proton NMR spectra of TSQ were obtained in CD_2Cl_2 and $CDCl_3$. TSQ is symmetric, with meta aromatic protons appearing at 5.76 ppm (CD_2Cl_2) or 5.74 ppm ($CDCl_3$) as a singlet. The hydroxy protons were observed at 10.84 ppm (CD_2Cl_2) or 10.95 ppm ($CDCl_3$) as singlets. The hydroxy proton resonance is noticeably broader in CD_2Cl_2 than in $CDCl_3$. The presence of singlets for either resonance in either solvent verifies the presence of this molecule as a single isomer.

Proton NMR spectra of ISQ reveal two sets of amine protons (CD_2Cl_2, 12.82 and 12.57 ppm; $CDCl_3$, 12.81 and 12.52 ppm) and two sets of olefinic protons ($CDCl_3$, 5.50 and 5.43 ppm; CD_2Cl_2, solvent residual proton signal obscures signals). This suggests the presence of two different isomers. The molecule ISQ can exist as six obvious cis−trans isomers:

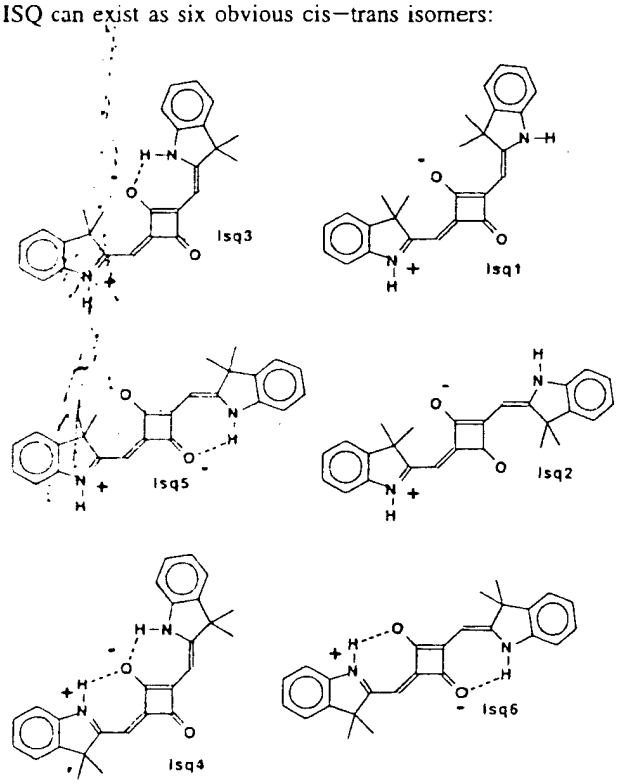

In order to determine which isomers are present, we have conducted a molecular mechanics investigation of BSQ and ISQ (Table 6). This first involved calculations based on the PCMODEL mmx force field augmented by a PPP type π-electron calculation inherent to the PCMODEL program. This permitted a first-order ranking of the possible isomeric structures. More time consuming PM3 and AM1 structure optimization calculations were then performed on each of the subsequent most likely structures. Each of these calculations provided free energies of formation or strain energies for each of the possible isomers. On the basis of these calculations, it was concluded that there are two most likely isomers each for either BSQ or ISQ.

NMR ratios of the two BSQ isomers are compared to thermodynamic predictions based on the molecular mechanics calculations (Table 5). If one presumes that the minor NMR isomer is the cis isomer, then the AM1 and PCMODEL based predictions are reasonably close to the experimental results. The PM3 calculations predict a close equilibrium though biased against the trans isomer. We have examined the carbon atom charges in both optimized AM1 and optimized PM3 calculations in the hope of determining which NMR resonances can be assigned to either isomer. The more positively charged the carbon, presumably the more down-field would be the protons attached to the carbons. Both AM1 and PM3 calculations predict slightly more positively charged ortho carbons in the cis form (charges AM1: −0.012, PM3: 0.018) than in the trans form (charges AM1: −0.024, PM3: 0.017). This suggests that the more downfield protons may be assigned to the cis form, making it the minor isomer.

Proton NMR data collected for ISQ suggest the presence of two isomers, in agreement with the PCMODEL mmx force field calculations. All calculations suggest that the minor isomer should be ISQ6, the centrosymmetric structure, while the major isomer would be the very polar ISQ4. The major isomer N-H protons are shifted further downfield. Both PM3 and AM1 calculations resulted in identical nitrogen atom charges, precluding proton NMR assignments of the N-H protons based on atom charge differentials between the two isomers. The vinylic protons display an opposite chemical shift dependence with the minor isomer being shifted downfield. Calculations predict vinylic carbon atom charges: cis isomer—AM1 (−0.224), PM3 (−0.187); trans isomer—AM1 (−0.225), PM3 (−0.188). The vinyl carbons of the cis isomer are slightly more positive than those of the trans isomer, suggesting that the cis isomer vinyl protons would be shifted further downfield, making this the minor isomer. This contradicts all of the calculations. Because of the proximity of these protons to the squarate ring and its own ring current and polarization effects, it is probably safer to assume that the proton NMR resonances cannot be so trivially assigned. In any case, whichever is the major or minor isomer, the ratio inferred from NMR integration suggests that both isomer molecules exist as significant mole fractions. Finally, the most stable structures for ISQ are ISQ4 and ISQ6, though note that the crystal structure of DONXEJ would be comparable to the highest energy ISQ structure, ISQ2. While the most likely structures for ISQ are ISQ4 and ISQ6, simply substituting ISQ with an *N*-methyl group permitted isolation of a related high-energy form, albeit nonplanar. Thus, substituting ISQ with *N*-alkyl to improve solubility potentially creates yet another isomer distribution.

Solvatochromism and Spectral Simulation

Solvatochromism studies have been performed on TSQ and the isomeric mixtures of BSQ and ISQ (Table 7). Calculations (AM1, PM3, and CNDO) suggest that the two isomers of BSQ share resonance frequencies that differ little, at least in the gas phase, while the two ISQ isomers should possess significantly different γ_{max}s. Curiously, experimental spectra show that ISQ is most red-shifted relative to TSQ and BSQ, while CNDO calculations suggest that it is the most blue shifted. Solvatochromism gas phase extrapolated values, $\bar{\nu}_g$, agree well with the CNDO trend, though one must remember that both the BSQ and ISQ solvatochromism results are due to a mixture of

Table 7. Electronic Spectral and Solvatochromism Analysis Results for the Squarylium Dyes ISQ, BSQ, and TSQ, with λ_{max} and Peak Half-Widths (Γ_G) at $1/e$ Assigned by Fits of the Low Energy Side of the Peak to a Gaussian Profile with the Indicated Standard Deviations, $\sigma_{\bar{\lambda}}$[a]

	ISQ			BSQ			TSQ		
	λ_{max} (nm)	$\sigma_{\bar{\lambda}}$	Γ_G (cm^{-1})	λ_{max}(nm)	$\sigma_{\bar{\lambda}}$	Γ_G (cm^{-1})	λ_{max}(nm)	$\sigma_{\bar{\lambda}}$	Γ_G (cm^{-1})
Electronic Spectral Results									
acetonitrile	650	0.016	417	645	0.014	437	644	0.014	421
pentane	658	0.020	350	640	0.017	282	635	0.043	277
dichloromethane	655	0.009	397	649	0.019	372	650	0.025	352
cyclohexane	662	0.020	351	637	0.016	290	640	0.042	288
isooctane	659	0.019	361	634	0.033	296	637	0.046	267
methylcyclohexane	661	0.007	364	636	0.011	308	639	0.010	291
chloroform	654	0.008	418	649	0.041	383	649	0.016	343
benzene	663	0.014	372	647	0.007	356	648	0.020	340
ethyl acetate	654	0.018	402	643	na	363	643	na	na
DMF	658	0.010	406	660	0.039	373	651	0.013	439
Solvatochromism Results									
A (cm^{-1})			−2540			−7880			−7150
B (cm^{-1})			207			−628			−437
$\bar{\nu}_g$ (cm^{-1})			15700			17300			17100

[a] The constants A, B, and $\bar{\nu}_g$ (the extrapolated "gas phase" transition frequency) have been previously defined (see ref 14). Note that the Gaussian fits are good in contrast to our earlier[1b] incorrect assignment of these peaks as Lorentzian.

isomers. TSQ typically displays the narrowest resonances, as might be expected for a single isomer. Thus, ISQ should show the broadest spectra with BSQ possessing spectra slightly broader than for TSQ. Generally, this is what is observed in most solvents. The solvatochromatic parameter B reveals the amount of dipolar character in both the excited and ground states, relative to the dipolar or induced dipolar nature of the environment. For all samples, the magnitude of this number is relatively small compared with that expected for a very polar dye[14] with large hyperpolarizability β. It is noteworthy that the ISQ-B solvatochromism parameter is positive, which implies negative solvatochromism, or red shifting with decreasing polarity. This is unexpected and is best explained if one considers two possibilities: (1) The polar isomer may be blue shifting with decreasing polarity, while the centrosymmetric isomer remains essentially unchanged. It is then likely that the weighted average of the two peaks might appear to red shift since this centrosymmetric isomer peak would not be shouldering as much of the polar isomer peak. BSQ displays a smaller B parameter than TSQ, which might suggest that a similar effect is operable with this isomeric mixture, though slight enough so as to not lead to negative solvatochromism. (2) The other possibility is that the polar isomers of ISQ and BSQ display negative changes in dipole moment upon excitation from the ground to the excited state. This would lead to negative solvatochromism. The molecular hyperpolarizability, β, would then be negative, which would contribute to the negative γ as an orientational contribution to the EFISH γ. If this is occurring, then the true electronic γ would be somewhat smaller in magnitude than originally reported, for ISQ and possibly for BSQ. The significant difference in the THG γs between BSQ and TSQ might support this contention, though it is more likely that the THG differences between BSQ and TSQ are due to differences in two-photon behavior.

Because of the isomer mixtures, short of complete vibronic deconvolution, it is not possible to use solvatochromism to assign excited state dipole moments to either ISQ4 or BSQ-C. Such an assignment would be useful since the magnitude and sign of the EFISH γ_n and orientational contributions could be estimated. Without such a correction, comparing calculated and measured γs for either BSQ or ISQ could be treacherous (*vide infra*). Full vibronic deconvolutions are difficult and are presently being attempted.

As a further effort to characterize the isomeric behavior, the electronic spectra of ISQ, BSQ, and "TSQ" (HSQ) were

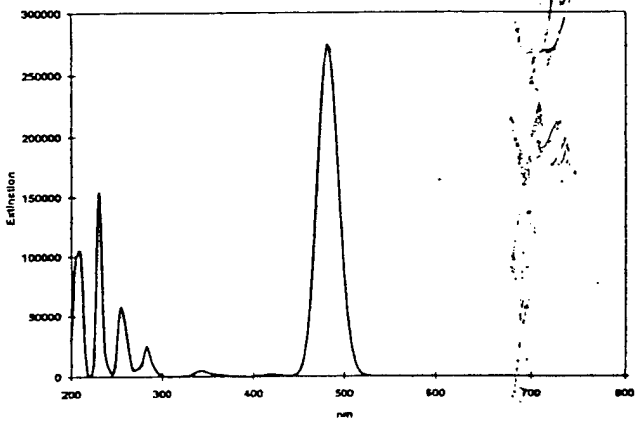

Figure 4. Calculated quantitative gas phase UV−visible electronic absorption spectrum of HSQ (TSQ). Structures actually calculated were slightly modified as detailed in the Experimental Section. Note that the experimental peak width of 704 cm^{-1} (TSQ) of the maximum intensity resonance was assumed for all resonances. See Table 2.

simulated by calculating the spectral transitions by CNDO-SCI-DCI, fitting Gaussian peaks to each transition, and then in the case of the isomeric mixtures, linearly combining calculated spectra of the isomers using the weighting suggested by NMR. Electronic peak widths, which define the extinction maximum were set on the basis of the experimental peak widths. All peaks were defined to have the same peak width as the maximum absorption peak, though this is almost certainly not correct for all peaks and will likely lead to poorer quantitative fits for the higher frequency transitions. For the isomeric mixtures, the peak width of TSQ was used to generate each of the calculated spectra for the BSQ and ISQ isomers. This was done because TSQ, which is presumably not a mixture of isomers, would possess the only spectra where the peak width represents a system unperturbed by isomeric mixtures. Isomeric mixtures would normally possess wider peaks merely due to the combination of spectra of two or more compounds with different peak maxima. By examining Table 2 and Figures 4−7, one can easily see that extinction coefficients are predicted well, though transition wavelengths are blue-shifted as would be expected for "gas-phase" calculations. For ISQ, it is apparent that the smaller extinction coefficient is due to the mixture of two isomers, each of which individually would possess extinction coefficients comparable to TSQ or BSQ. The spectrum of ISQ is best reproduced when ISQ6 is calculated as the major

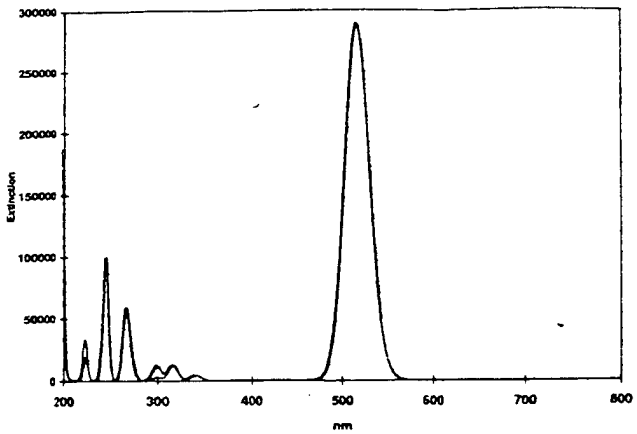

Figure 5. Calculated quantitative gas phase UV−visible electronic absorption spectrum of BSQ. Solid line: 21% BSQ-T and 79% BSQ-C. Dotted line: 79% BSQ-T and 21% BSQ-C. Structures actually calculated were slightly modified as detailed in the experimental section. Note that the experimental peak width of 704 cm^{-1} for TSQ was assumed. See text for details. See Table 2.

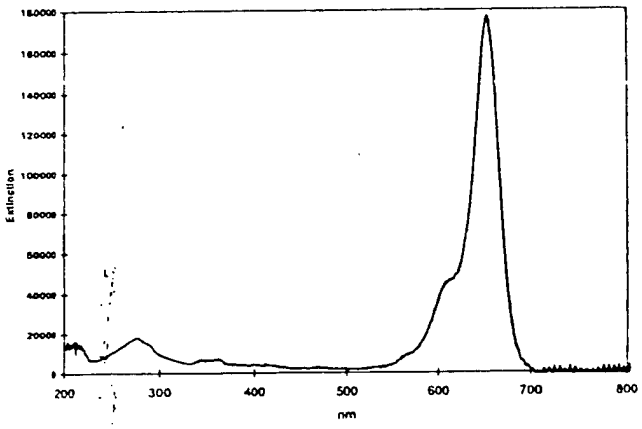

Figure 6. Experimental quantitative UV−visible electronic absorption spectrum of ISQ in methylene chloride. See Tables 2 and 7.

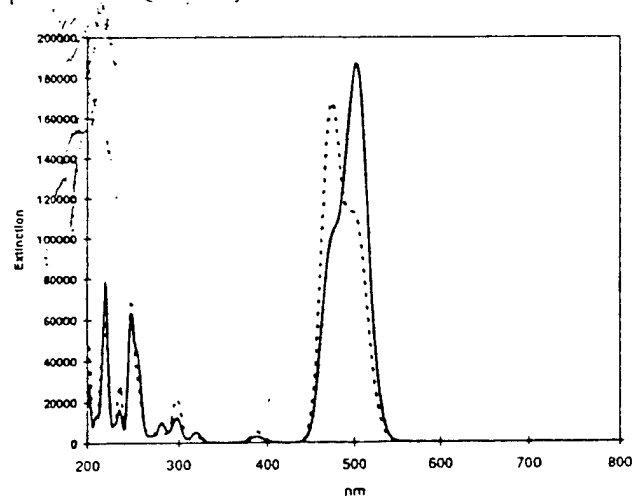

Figure 7. Calculated quantitative gas phase UV−visible electronic absorption spectrum of ISQ. Solid line: 64% ISQ6 and 36% ISQ4. Dotted line: 36% ISQ6 and 64% ISQ4. Structures actually calculated were slightly modified as detailed in the Experimental Section. Note that the experimental peak width of 704 cm^{-1} for TSQ was assumed. See text for details. See Table 2.

component, in contradiction to molecular mechanics and semiempirical quantum mechanical calculations.

The calculated spectrum (Figure 5) of BSQ is insensitive to the definition of the isomer mixture. Additionally, the calculated extinction coefficient of BSQ appears too large. These two latter calculated observations suggest that BSQ may naturally possess broader peaks than TSQ and that isomerism does not seriously affect the electronic linear-optical properties of BSQ. Finite field calculations (Table 1) evidently suggest that the nonlinear optical properties also will differ little between BSQ-C and BSQ-T.

The calculated linear spectra of ISQ4 and ISQ6 are significantly different. The ISQ4 isomer also displays a significantly smaller (less negative) calculated γ, as might be expected due to the presence of a γ_n contribution. Additionally, the calculated γs for both ISQ isomers suggest that both are expected to possess γs bigger than or at least comparable to those for BSQ and TSQ. However, the opposite is observed experimentally. A reasonable explanation is that ISQ4 possesses a significant β which is negating the electronic γ of the isomeric mixture of ISQ4 and ISQ6 via a significant canceling positive γ_n contribution. The finite field calculations suggest that this alone is not enough cancellation since the ISQ4 isomer is still expected to possess a larger magnitude γ than either BSQ or TSQ. The discrepancy between the calculated (single configuration) and experimental EFISH trends of nonlinearities suggests that ISQ4 is likely also contributing a significant positive $\mu\beta$ orientational contribution. Finite field calculations for ISQ4 suggest that $\mu\beta_0$ is weakly positive ($+6.4 \times 10^{-30}$ D cm^5 esu^{-1}). However, even this small magnitude of $\mu\beta_0$ would correspond to an orientational γ_0^{or} of approximately $+1.5 \times 10^{-34}$ cm^7 esu^{-2}. Though this appears to be relatively small compared to the static electronic value of $\gamma_0 = -11.3 \times 10^{-34}$ (ISQ4) or $\gamma_0 = -17.1 \times 10^{-34}$ (ISQ6), one must keep in mind that β increases faster than γ as one approaches resonance. Thus it is likely the orientational γ_0^{or} would possess a larger canceling effect at the EFISH measurement frequency of 1907 μm. The calculated $\mu\beta_0$ for BSQC of 50.7×10^{-30} D cm^5 esu^{-1} corresponds to an orientational γ_0^{or} of $+12.3 \times 10^{-34}$. Here the zero frequency canceling effect of the orientational contribution is predicted to be 65% greater than the electronic effect. The orientational contributions are estimates based on the presumption of

$$\gamma_0^{or} \approx \frac{\mu\beta_0}{5kT}$$

Given calculational uncertainties, the canceling effects for either ISQ4 or BSQC should be viewed as approximate. It is clear, however, that the canceling orientational effects could be significant.

Note that the predicted positive β suggests that the solvatochromism shifts must be positive (or red shifting with increasing solvent polarity).

Note that configuration interaction finite field calculations show some additional variation that the single configuration calculations did not display. With CI, BSQ is suggested to possess a larger γ than TSQ, while ISQ's γ, should be bigger yet, even as a mixture of isomers, both in contradiction to experiment. If the CI calculations are given more weight than the single configuration calculations, this supplies more credence for a canceling orientational γ_0^{or} for BSQC.

Conclusion

We have demonstrated that the molecules BSQ and ISQ can exist as a mixture of isomers. Our results are in good agreement with those of Kazmaier et al. for BSQ and with quantum mechanical and molecular mechanical calculations of the relative molecular strain energies or heats of formation. The squaryliums are clearly π-bond delocalized, as demonstrated by the

X-ray structure results and by optimization of structures by semiempirical calculations. Comparison to other structures indicates that the main role of the hydroxys is to stabilize the charge transfer from the amine nitrogens to the squarate oxygens.

We have also demonstrated again that the squaryliums generally appear to display large off-resonant *negative* third-order polarizabilities. Resonant third harmonic generation results clearly suggest the significant contribution of a two-photon state as predicted by Garito et al. Linear and nonlinear optical calculations suggest that γ should not differ significantly between BSQ and TSQ, at least far off resonance. Near resonance, the experimental resonant THG measurements suggest that the location of the two-photon state may differ significantly between BSQ and TSQ or that the three-level model effectively breaks down when in such a resonant interaction. Garito and co-workers have suggested the contribution of two or three significant two-photon states, which could contribute differently for BSQ and TSQ.[16] Alternatively, there could be a significant positive γ_n contribution from the BSQ-C isomer. Such a contribution would be orthogonal to the main γ_c and γ_{tp} components. However, the isotropic CI finite field γ is larger (in negative magnitude) for BSQ-C than for BSQ-T, suggesting that such a contribution is not significant. It is more likely that BSQ-C possesses a canceling orientational contribution which cancels via a positive $\mu\beta$ contribution. This mechanism should be operative for the EFISH results and could rationalize the difference in trends between EFISH γ and the CI finite field trends. However, the orientational contribution cannot be used to explain the differences in THG γ, suggesting that the location of the two-photon states may be different between BSQ and TSQ.

Calculations of linear optical spectra clearly suggest that ISQ possesses an integrated absorption comparable to BSQ or TSQ, at least for the theoretical pure isomers. Calculated nonlinear optical results suggest that either isomer of ISQ should be superior to TSQ or BSQ. The noncentrosymmetric ISQ4 isomer component is significant in its mole fraction, and it probably possesses a significant dipole moment. There may be a significant orientation contribution to the EFISH γ, as well as a significant γ_n contribution which would contribute to the electronic γ in a positive sense. Quadratic electroabsorption studies suggest that ISQ in a PMMA matrix can be explained well by a three-level model, requiring only the contributions γ_c and γ_{tp} to explain the dispersion, which itself independently supports the presence of a significant two-photon state.[28] This might be thought to suggest that γ_n and EFISH orientational contributions would not be significant. However, the results presented here hint at a significant positive orientational contribution as well as perhaps a significant positive γ_n contribution from the noncentrosymmetric isomer ISQ4. This may not be incompatible with the electroabsorption results when considering that the electroabsorption studies have been conducted under conditions of a viscous polymer matrix which would impede motional contributions to γ. Also, the contributing quadratic electroabsorption dispersion of the γ_n term would probably be convolved with the quadratic electroabsorption dispersion of a γ_{tp} term. Due to the isomer complication, the story with regard to ISQ will remain complicated. Further work is necessary.

Overall, we arrive at a curious inference. The compound (TSQ) with apparently the largest experimental γ may actually possess the smallest γ when correcting either BSQ or ISQ for orientational contributions.

It is possible, in light of Marder's bond length alternation results, that the observed contradictory variation in experimental and theoretical nonlinear optical behavior is due to solvent effects. In this regard, Law has suggested that in chlorinated hydrocarbons anilinium squaryliums with no stabilizing hydroxys can be considered essentially planar, though may be less so in other solvents.[29] The measurements reported here were made only in either chloroform or methylene chloride, and comparisons were confined largely within either of these solvents. Also, the presence of the hydroxys should lead to even more stability. Given their similar structures, it is unlikely that the molecules investigated here would have behaved significantly differently relative to one another with regard to their solvent interactions.

The experimental inference of a two-photon contribution to the squaryliums is significant. This observation rounds out and better defines a three-level model description for most molecules:

(1) Electron-localized molecules such as carotenes which display large positive nonlinearities. In the extreme of centrosymmetry, the model reduces to two terms

$$\gamma \approx \gamma_c + \gamma_{tp}$$

with γ_{tp} dominating.

(2) The extreme of noncentrosymmetry is represented by molecules with large β. Under these circumstances, γ_n, is dominant, and the model is represented by

$$\gamma \approx \gamma_c + \gamma_n$$

The sign of β is irrelevant with regard to γ_n, so that molecules with either large positive or negative βs can produce large positive γ_n.

(3) The squarylium dyes, while displaying large negative γs, evidently possess non-negligible γ_{tp} two-photon contributions. The model is then represented by

$$\gamma \approx \gamma_c + \gamma_{tp}$$

though with γ_{tp} being less significant. Optimization here tends toward molecules with free-electron character which are characterized by bond orders which do not deviate significantly along the backbone chain. Crystallographic evidence presented here supports this. However, bond orders alone are merely a symptom of an effect. The factor which evidently evened out the bond orders of TSQ relative to BSQ was the substitution of another pair of hydroxys.

Recent results of Mazumdar and co-workers[30] on polydiacetylene suggest that some molecules may require more than a three-level model to adequately quantitatively explain the third-order NLO behavior. However, the basic symmetry considerations should still hold for all terms, so that the NLO behavior mostly needs only to be considered in terms of additional higher order γ_c, γ_n, and γ_{tp} components (as also suggested by Garito and co-workers for the squarates),[16] which should behave qualitatively the same as the first-order three-level components.

It must be recognized that the motivation for developing a restricted model such as the three-level model is not to improve quantitative fits, which by definition it can not accomplish, but to provide a simple structure/property tool to guide materials development. It has never been argued that the two-level model

(28) Poga, C.; Brown, T. M.; Kuzyk, M. G.; Dirk, C. W. Characterization of the Excited States of a Squaraine Molecule with Quadratic Electroabsorption Spectroscopy. Submitted to *J. Opt. Soc. Am.*

(29) Law, K. Y. *J. Phys. Chem.* **1989**, *93*, 5925–5930.

(30) Kawabe, Y.; Peygambarian, N.; Guo, D.; Mazumdar, S.; Dixit, S. N.; Kajzar, F. *Phys. Rev. B* **1991**, *44*, 6530.

for β is quantitatively accurate. It is not, though it is inarguable that the two-level model for β has lead to systematic enhancement of β by allowing materials chemists to impose on it their intuitive insight regarding molecular electronic structure. It must further be recognized, as discussed here, that there are different mechanisms (electronic, orientational, etc., which each contribute *both* positive and negative components)[31] contributing significant components to γ, especially for molecules with large γ. The *electronic* three-level model for γ helps categorize and distinguish the electronic positive and negative components—which are operating on a completely different temporal scale—from the orientational contributions, which also possess positive and negative components.

With regard to the isomer problem, more studies and some caution in interpreting past results are necessary. In particular, because of the centrosymmetry restriction on γ_n and the EFISH orientational contribution, molecules which naively may be presumed centrosymmetric, but which can possess other isomeric structures, must be dealt with carefully when interpreting third-order optical polarization results. For instance, variations in magnitude and sign of γ with varying environment may reflect, in some cases at least, a shift in conformational isomer structure and distribution. Also, unanticipated deviations from the three-level model may occur when failing to consider a γ_n contribution in a supposed centrosymmetric dye which may contain a noncentrosymmetric component.

(31) Poga, C.; Kuzyk, M. G.; Dirk, C. W. *J. Opt. Soc. Am. B* **1994**, *11*, 80.

Acknowledgment. The authors gratefully acknowledge support from the following agencies or institutions: Texas Higher Education Coordinating Board, The National Science Foundation, The University of Texas at El Paso, The Air Force Office of Scientific Research, and The Robert A. Welch Foundation. C.W.D. would like to thank Dr. Robert Twieg of IBM and Dr. Paul Cahill of Sandia National Laboratories for helpful discussions that led to the investigation of the squarylium dye structures and for invaluable advice on synthetic details.

Supplementary Material Available: Tables listing complete X-ray crystallographic data and figures showing UV−visible electronic absorption spectra of HSQ and BSQ, the proton NMR spectrum and electron absorption spectrum of TSQ, and proton NMR spectra for isomeric mixtures of ISQ (22 pages); observed and calculated structure factors for TSQ (8 pages). This material is contained in many libraries on microfiche, immediately follows this article in the microfilm version of the journal, can be ordered from the ACS, and can be downloaded from the Internet access instructions.

JA942052S

ELSEVIER

Thin Solid Films 315 (1998) 294–300

thin solid films

Stability and superstructure of squarylium dye TSQ Langmuir–Blodgett films

Tom X. Zhong [a,1], Richard K. Workman [a], Xiaowei Yao [a], Ghassan E. Jabbour [a], Charles A. Peterson [a], Dror Sarid [a,*], Carl W. Dirk [b], David de la Cruz [b], Aruna Nagarur [b]

[a] *Optical Science Center, University of Arizona, Tucson, AZ 85721, USA*
[b] *Department of Chemistry, University of Texas at El Paso, El Paso, TX 79968, USA*

Received 14 April 1997; accepted 16 September 1997

Abstract

The stability of monolayer Squarylium Dye TSQ in air-subphase interface was studied. Langmuir–Blodgett films of this dye were deposited on mica and on hydrophobic silicon (100) wafers and a contact mode atomic force microscope (AFM) was used to characterize the structures of these films. It was found that the stability of a TSQ monolayer in the air-subphase interface was increased substantially when cadmium chloride was added to the subphase. Although TSQ dye does not have a long alkyl tail typically required to form a LB film, AFM images of these films and their 2D Fourier Transform analyses show that TSQ LB films possess a triclinic superstructure. Based on the analyses of pressure-area (π-A) isotherms and AFM images of these films, models of TSQ molecules packing on the subphase were developed. © 1998 Published by Elsevier Science S.A.

Keywords: Squarylium dye TSQ; Langmuir–Blodgett film; Isotherm; Superstructure; Atomic force microscopy

1. Introduction

Squarylium dyes possess many optical characteristics such as nonlinearity and photoconductivity. These properties make them very attractive for some industrial applications, e.g., xerographic, photoreceptors, organic solar cells, optical recording, etc. [1,2]. TSQ (see Fig. 1) has the largest negative nonlinearity measured to date for a squarylium dye [3]. This dye has a centric and essentially planar molecular structure with relatively little bond length alternation which is important in optimizing structures for nonlinear optics [3]. The maximum non-linear optical effects in organic materials can be expected from specially designed dye molecules situation in a non-centrosymmetric structure. The LB technique is a well known method to create this type of structure [4]. Because photogeneration efficiency of squarylium dyes is directly related to the dye aggregation structures, studying their structures as LB films using AFM carries commercial value [5].

Unlike any previous materials used to make LB films, the material (TSQ) used in this study does not have a relative long alkyl tail which is generally required for LB films. A molecule of TSQ has four short tails each with only four single carbon–carbon bonds. The length of a hydrophobic tail (or multiple tails) for LB films should be long enough to prevent the deposited materials from dissolving into subphase and, on the other hand, short enough to keep sufficient flexibility for subsequent deposition from subphase to substrate. The typical length of the tails for most LB films reported has 16 to 22 single carbon–carbon bonds. The short tails of a TSQ make the monolayer formed in the air-subphase interface unstable due to the relatively small contact area between molecules. Nevertheless, short tails may also provide the necessary flexibility to form different valuable structures which long-tail materials cannot form.

A common practice to improve the deposition characteristics of monolayer films is to deliberately add divalent ions, such as Cd^{2+} and Zn^{2+}, to the subphase to form a salt monolayer. The formation of the salt monolayer ap-

* Corresponding author. Fax: +1-520-6219665; e-mail: sarid@sarid.opt-sci.arizona.edu.
[1] Permanent address: Silicon Valley Group, 541 E. Trimble Road, San Jose, CA 95131, USA.

0040-6090/98/$19.00 © 1998 Published by Elsevier Science S.A. All rights reserved.
PII S0040-6090(97)00780-3

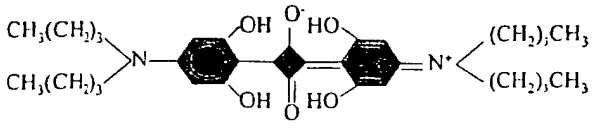

Fig. 1. Molecular structure of squarylium dye TSQ.

pears to convert the floating monolayer into a more condensed solid as the head groups are drawn closer together and the tails move closer to the vertical [6]. This study was aimed at finding whether the stability of TSQ monolayer in the air-subphase interface can be improved by adding cadmium to the subphase.

Most reports [1,2,7–9] on the aggregation structures of squarylium dyes were determined by π-A isotherms which is a common technique used to determine the limiting area each molecule occupies. Knowing the limiting area of each molecule in a monolayer film determines the orientation of the molecule in the film because the area taken by each molecule depends on the direction which the molecule orients itself in the monolayer. The drawback of this technique, however, is that sometimes it cannot guarantee that a monolayer will indeed form. Some studies [1,8] suggest that squarylium dye molecules start to tilt and stack on each other before they form a stable monolayer in air-subphase interface. However, another possibility of squarylium dyes transforming into multilayer films may also exist [10]. The π-A isotherm method by itself cannot differentiate between these two possibilities. In contrast, AFM has been proven to be an excellent tool to image LB films with molecular resolution in recent years [11–18]. Molecular resolution images by AFM can not only be used to identify the aggregation structures of deposited films but also to determine the limiting area each molecule occupies in a periodical molecular arrangement. Hence, in this study, besides π-A isotherms, we also utilize an atomic force microscopy to identify the aggregation structures of TSQ in LB films.

2. Experiment

Squarylium dye TSQ was dissolved in chloroform to form a solution with a concentration of 0.1 kg/m^3. A computer controlled NIMA 2000 model LB though was used to deposit the films at room temperature. The pH value of the subphase (de-ionized water or de-ionized water with 0.5 mol/m^3 cadmium, 99.99%, Alderich) was adjusted to about 7.0 with sodium bicarbonate (> 99.5%, E. Merk). The TSQ dye was spread on the subphase very slowly (droplet by droplet). After the chloroform was allowed to evaporate for several minutes, the film was compressed at speed of 8.3×10^{-7} m^3/s. The deposition pressure was 2.5 N/m and the dipping speed was 8.3×10^{-5} m/s. One monolayer of TSQ film was deposited on hydrophillic mica and one bimonolayer TSQ film on a hydrophobic silicon (100) wafer. Mica substrates were cleaved and silicon substrates etched by HF solution to remove oxide layers right before deposition.

The deposited films were examined soon after preparation with a commercial AFM (NanoScope III, Digital Instruments, Santa Barbara, CA). A 12 μm by 12 μm scanner and a silicon nitride tip on a cantilever with a spring constant of 0.08 N/m were used for measurements. In order to assess the overall periodicity contained within each AFM image, two-dimensional fast Fourier transform (FFT) analysis was carried out. All measurements taken in air at room temperature were reproducible and stable under the experimental conditions.

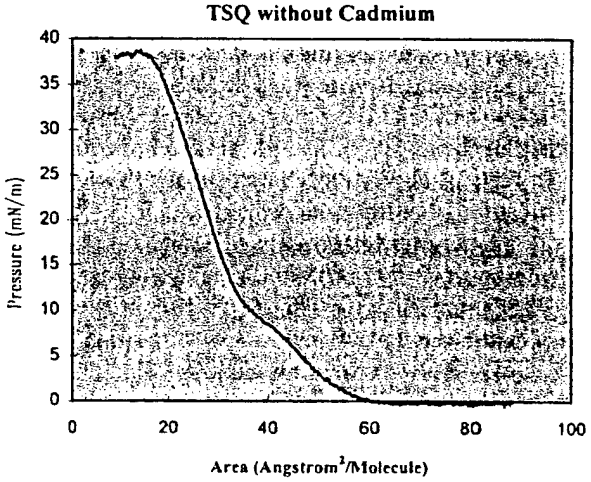

(A)

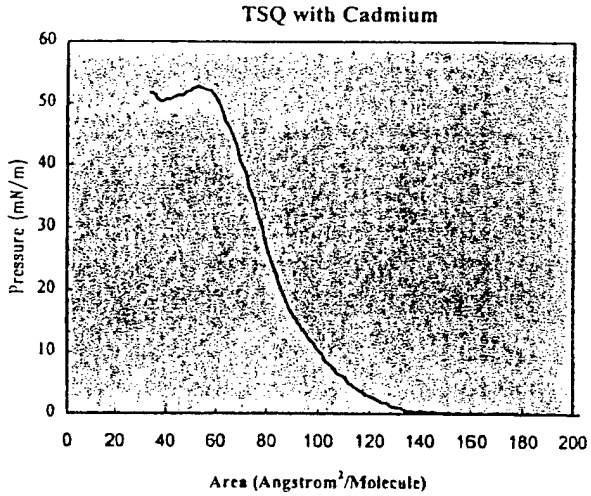

(B)

Fig. 2. (A) Isotherm for TSQ monolayer formed without cadmium. (B) Isotherm for TSQ monolayer formed with cadmium in subphase.

3. Results and discussion

3.1. π-A Isotherm

Fig. 2A and B show the π-A curves for TSQ monolayers formed with and without cadmium, respectively, in the air-subphase interface. As shown in these figures, the collapse pressures of the monolayers increase from 3.8×10^{-2} N/m without cadmium to 5.2×10^{-2} N/m with cadmium. There are two limiting areas in the π-A curve shown in Fig. 2A for a monolayer formed without cadmium: one is 0.58 nm^2/molecule and the second is 0.39 nm^2/molecule. The limiting area shown in Fig. 2B for the TSQ on the subphase with cadmium is 0.95 nm^2/molecule.

To interpret the information of the π-A curves properly, the molecular structure of TSQ has to first be analyzed. A simplified structure of the TSQ molecule is shown in Fig. 3A where the rectangular box represents the squaraine chromophore (excluding the alkyl chains) and each alkyl chain is represented by a wave-shaped line. The dimensions of the box and the length of each tails are approximated using bond length data determined by X-ray methods [3]. Fig. 3B shows the views of a TSQ molecule after simplification from different directions.

Two types of close-packing arrangements of TSQ molecules are possible. The first type is an arrangement in which TSQ molecules first lie down flat on the subphase surface with four tails bending away from the subphase surface. As the compressing pressure increases, some molecules from the monolayer are squeezed out forming a second layer (multilayers). In this type of arrangement, the angle between the subphase surface and the tail pointing direction will determine the limiting area of each molecule. The second type is an arrangement in which the TSQ molecules lie down flat on the subphase first and then start to tilt and stack on each other as the compressing pressure increases. In this type of arrangement, both the angle between the subphase surface and molecule faces (*ab*, *ac* or *bc* in Fig. 3) and the angle between the subphase surface and the tail pointing direction will determine the limiting area of each molecule. The calculated limiting areas for the first type of arrangement range from 0.80 nm^2/molecule when the tail is perpendicular to the subphase surface to 1.72 nm^2/molecule when the tail is lying flat on the subphase. The calculated limiting areas for the second type of arrangement range from 0.09 nm^2/molecule when both the molecule face (*ab*, shown in Fig. 3) and tails are perpendicular to 1.72 nm^2/molecule.

The first limiting area measured for TSQ film formed without cadmium is smaller than the minimum calculated limiting area for the first type of arrangement described in the previous paragraph. This indicates that there is a certain degree of molecular tilting before the first limiting area. After the first limiting area, we were able to vividly see multilayer films (purple streaks) forming. These start from the areas next to both the compressing bars right after the first limiting area appeared in the π-A curve and can be observed due to the strong fluorescence of TSQ dye. More and more purple streaks were formed as the pressure increased till the second limiting area was reached. After the second limiting area, the film became stable and the pressure in π-A curve rose steadily with little area change till the film totally broke down. This phenomenon partially confirmed Kawabata et al. [10] assumption that multilayer films might form after the first limiting area. However, this

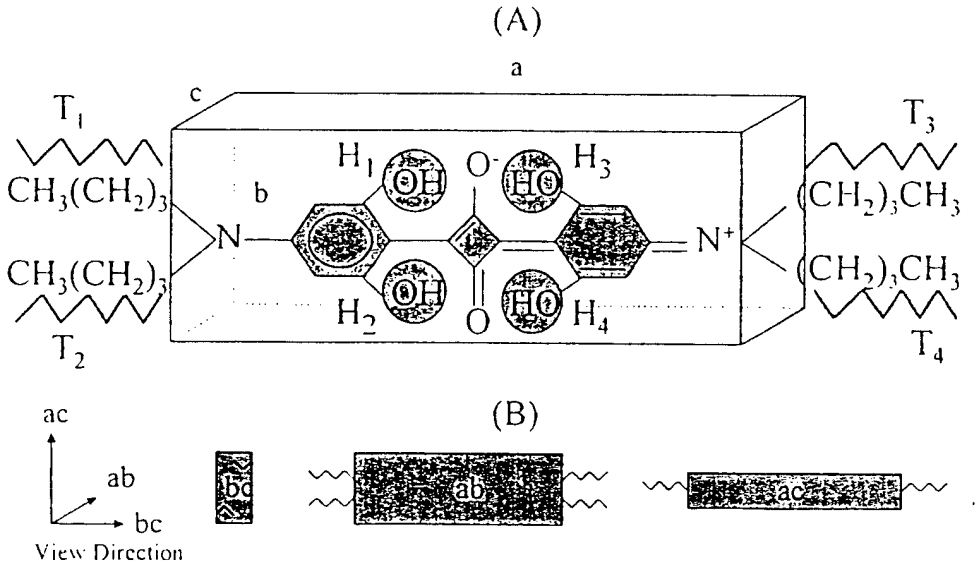

Fig. 3. (A) The rectangular box is the calculated maximum volume that a TSQ molecule occupies (excluding alkyl tails) where *a*, *b*, *c* are 1.3, 0.60, 0.14 nm, respectively. H_1, H_2, H_3, and H_4 represent heads 1 through 4 and T_1, T_2, T_3, and T_4 represent tails 1 through 4. The length of each tail is approximately 0.53 nm (B) Simplified molecule views from different directions. The calculated areas (excluding the tails) are 0.09, 0.8, 0.19 nm^2/molecule for *bc*, *ab*, and *ac* respectively.

phenomenon could not prove whether or not a superstructure exists, as suggested by Kawabata et al.

Law and Chen [1] also observed a double limiting area in a π-A curve with TSSQ (bis(4-(distearylamino)phenyl) squaraine). The major differences between TSQ and TSSQ are that the later has four longer (18 C–C bond alkyl chain) tails and no (–OH) groups. They believe that the first limiting area is due to the formation of a monolayer with each TSSQ molecule lying flat and each tail standing up straight perpendicular to subphase surface because their measured first limiting area is slightly larger than the calculated one. After the first limiting area, they believe that TSSQ molecules start to tilt and stack on each other. The difference of aggregation structures before the first limiting area between our results and Law and Chen's could be due to the difference in the tails length between TSQ and TSSQ.

The purple streaks described earlier have not been observed in the case of films prepared with cadmium. The disappearance of the purple streaks and the increase of collapsing pressure are indications of increased stability for films formed with cadmium in subphase. The role of cadmium played here should be similar to that played when forming cadmium arachidic films, that is, to link two or more molecules together and make it more difficult to be squeezed out or tilt the molecules. Because there is a negative charge ($-O^-$) in TSQ molecule, the following reaction may have happened:

$$TSQ(-O^-) + TSQ(-O^-) + Cd^{2+} \rightarrow TSQ(-O\text{-}Cd\text{-}O-)TSQ \quad (1)$$

The positive charge existing in a TSQ molecule ($=N^+<$) could have been balanced by other negative charge ions in subphase such as OH^- and Cl^-. The second possibility could be that the polar head groups (–OH) have been ionized. As the pH increases to a certain value, the hydrogen associated with the head group will be ionized to form hydrogen ions and four oxygen ions for each TSQ molecule. The cadmium ions then react with the ionized TSQ molecules and form a closely packed monolayer. The question of which of the above stated reactions contribute to the increase of stability of the TSQ films remains unanswered in this point.

The measured limiting area (0.95 nm^2/molecule) for a monolayer formed with cadmium is in reasonable agreement with the calculated limiting area when the molecule is lying down flat with four tails perpendicular to subphase surface. The fact that a Y-type bimonolayer LB film was successfully deposited further suggests that TSQ molecules lie down flat on the subphase. That the measured limiting area is slightly larger than the calculated area could be due to either the angle between the subphase surface and the tail being less than 90° or a systematic error. Accordingly, we propose an aggregation structure of TSQ monolayer formed with cadmium in air-subphase interface as shown in Fig. 4.

To further confirm that the type of arrangement in Fig. 4 indeed represents the actual aggregation structure of TSQ molecules in air-subphase interface, we imaged the films with molecular resolution, the alternative approach (AFM characterization) to study the arrangements of TSQ molecules.

3.2. Atomic force microscopy analysis

Atomic resolution images of mica and molecular resolution images of cadmium arachidic LB films were taken and used as standards for calibration of later images. We have obtained the first images of ordered structures of TSQ films. Two types of periodical structures were observed by AFM analysis for bimonolayer TSQ films formed with cadmium on silicon (100) wafers. The most common structure is shown in Fig. 5A where the molecular rows in the film are clearly visible. FFT analysis of Fig. 5A shows a triclinic structure from which, by cross-sectional analysis, a periodical molecule row distance of 1.1 nm with surface corrugations of 0.15 nm could be extracted. The molecule row distance is in good agreement with the calculated molecule length excluding the tails (*a* in Fig. 3A). Provided TSQ molecules indeed lie down flat on subphase, the limiting area per molecule is approximately 0.7 nm^2 which is also in good agreement with the calculated limiting area. Hence, we believe that each row in Fig. 5A is indeed TSQ molecules lying down flat next to each other, as proposed in Fig. 4.

Another type of superstructure observed is shown in Fig. 6A. This type of superstructure accounts for only a small portion of the periodical structures observed. The two-dimensional Fourier spectrum in Fig. 6B also shows

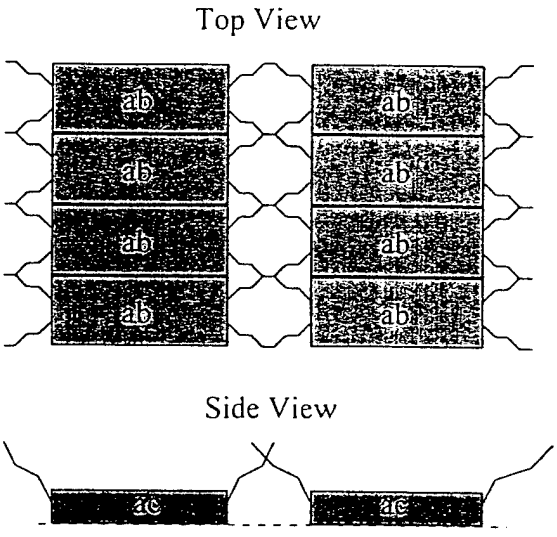

Fig. 4. The proposed close packing of TSQ molecules in air-subphase interface. The letters *ab*, *bc*, and *ac* correspond to the views described in Fig. 3.

that TSQ adopts a triclinic lattice. The above analysis suggests a packing of molecules as shown in Fig. 6C. This type of packing means each TSQ molecule lies down flat with its four tails tangled with neighbour molecules' tails. The unit cell area for this type of packing is 1.03 nm^2 which is slightly larger than the measured limiting area. In this type of arrangement, the condensing process induced by cadmium seems not to take place. This could be due to the tails interaction preventing the condensation by cadmium from happening in certain areas (Fig. 6C).

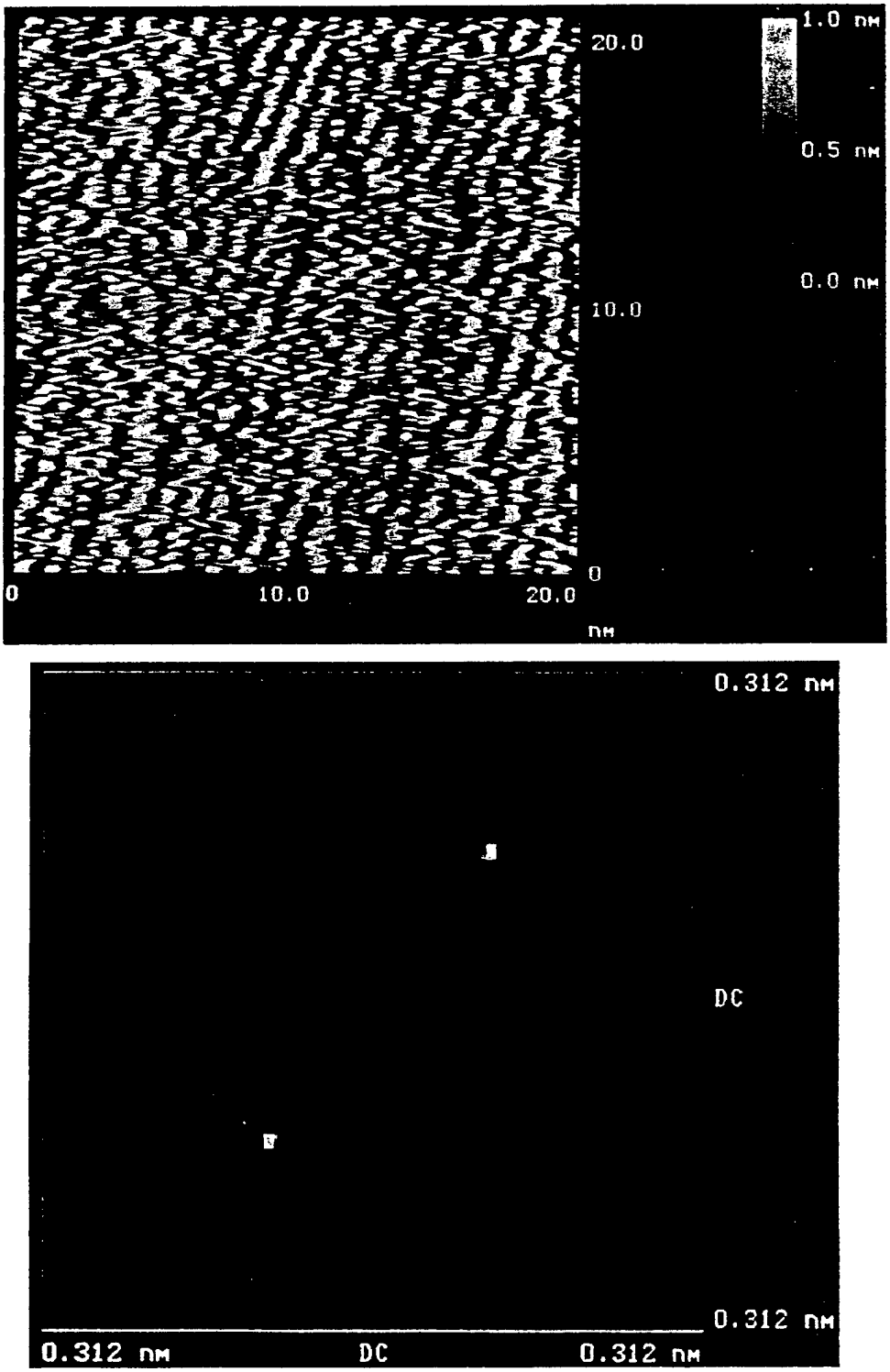

Fig. 5. (A) An AFM image (20 nm by 20 nm) of bimonolayer TSQ LB film deposited on Si(100). (B) 2D FFT of (A).

Images less ordered than Fig. 5A and Fig. 6A were also observed. The disorder could be caused by reorganization of the film after deposition. No ordered structures have been observed in either TSQ films formed on mica without cadmium or monolayer TSQ formed on silicon with cadmium.

4. Conclusion

The stability of TSQ monolayers on an air-phase interface has been shown increase substantially by adding cadmium chloride to the subphase. The π-A isotherm analysis shows that there are two limiting areas (0.58 and

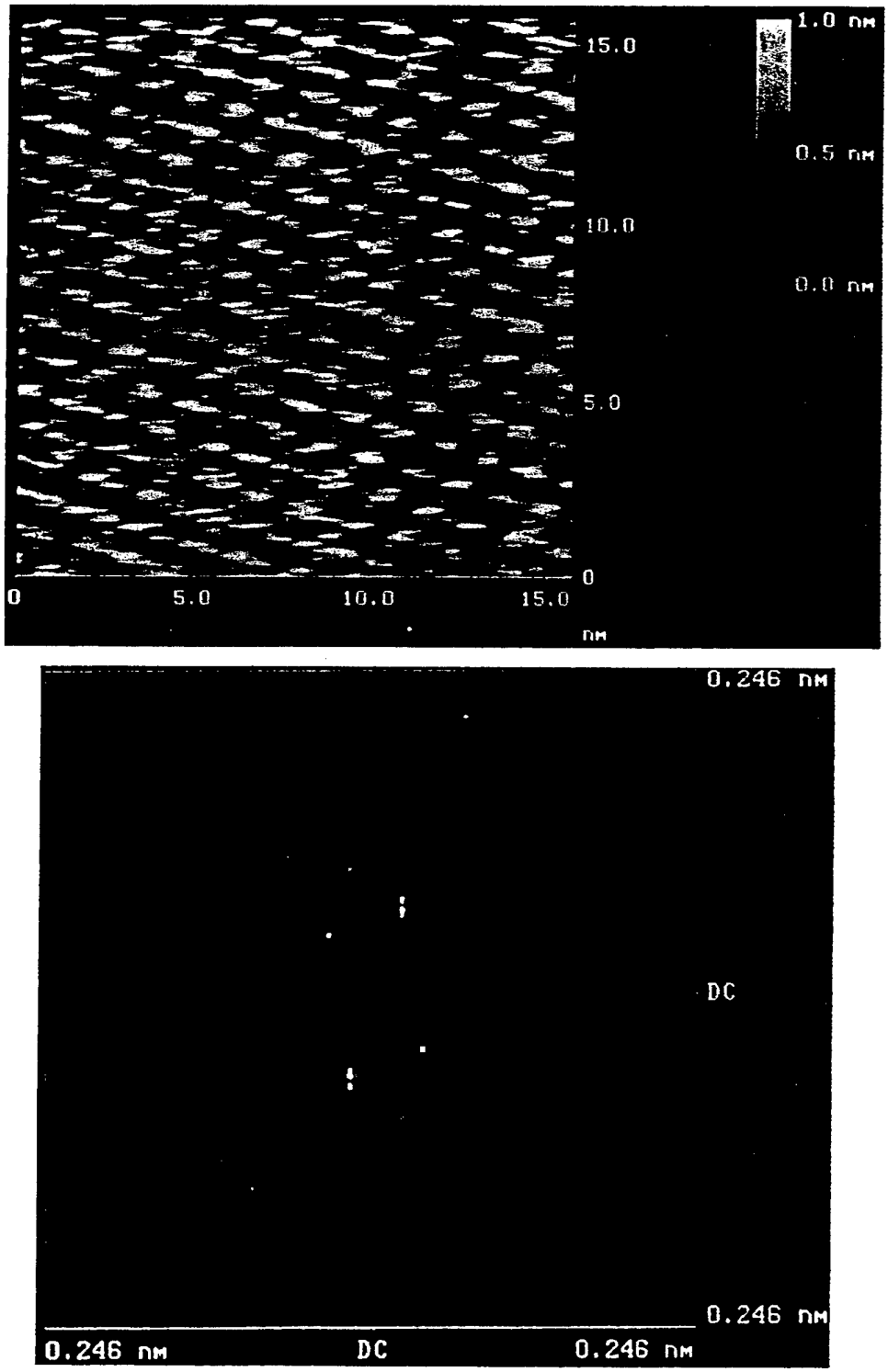

Fig. 6. (A) Image (15 nm by 15 nm) of bimonolayer TSQ LB film deposited on Si(100). (B) 2D FTs of (A). (C) A possible packing arrangement of TSQ molecules based on analysis of (A).

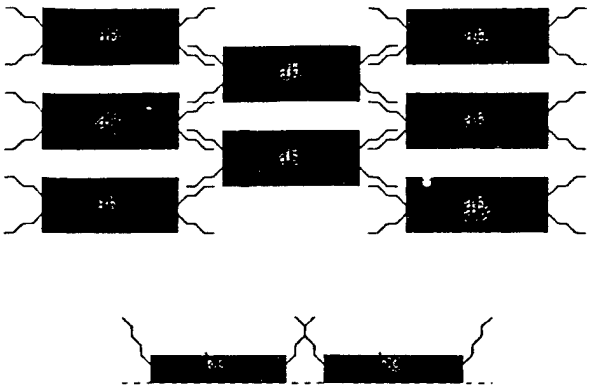

Fig. 6C.

0.39 nm^2/molecule) for TSQ monolayer formed without cadmium. Multilayer TSQ films were observed after the first limiting area in these types of films. The limiting area measured for TSQ monolayer formed with cadmium is 0.95 nm^2/molecule. This is in good agreement with the limiting area defined from AFM image analysis and the calculated limiting area. The analysis suggest that TSQ molecules lie flat in the air-subphase interface with its tail groups bending away from the subphase. Two types of periodic structures were found in a bimonolayer TSQ LB film deposited on Si(100) and a 2D FFT analysis shows that these periodical structures are triclinic.

Acknowledgements

The authors would like to thank NIMA Technology for lending us the LB trough for this research, Dr. Charles Dodd from CTC Technologies and Ms. Rebecca Spresser for their technical advice. We acknowledge the partial support of US Office of Naval Research (ONR) through the Center for Advanced Multifunctional Nonlinear Optical Polymers and Molecular Assemblies (CAMP), Air Force Office of Scientific Research, Texas Higher Education Coordination Board, and National Science Foundation (NSF-MRCE).

References

[1] K.Y. Law, C.C. Chen, J. Phys. Chem. 93 (1989) 2533.
[2] H. Chen, W.G. Herkstroeter, J. Perlstein, K.Y. Law, D.G. Whitten, J. Phys. Chem. 98 (1994) 5138.
[3] C.W. Dirk, W.C. Herndon, F.C. Lee, H. Selnau, S. Martinez, P. Kalamegham, A. Tan, G. Campos, M. Velez, J. Zyss, I. Ledoux, L.T. Cheng, J. Phys. Chem. 117 (1995) 2214.
[4] M.A. Schoondorp, A.J. Schouten, J.B.E. Hulshof, B.L. Feringa, Thin Solid Films 210/211 (1992) 166.
[5] K.Y. Law, J. Phys. Chem. 92 (1988) 4226.
[6] M.C. Petty, Langmuir–Blodgett Films, 1996, pp. 1–49.
[7] S.F. Kramarenko, V.A. Tkachev, A.V. Tolmachev, N.I. Voronkina, M.A. Afanasyeva, I.P. Krainov, Thin Solid Films 210/211 (1992) 224.
[8] K. Takehara, K. Isomura, T. Fukuda, H. Shindome, H. Taniguchi, Thin Solid Films 210/211 (1992) 169.
[9] S. Das, T. Lekshmana Thanulingam, K. George Thomas, P.V. Kamat, M.V. George, J. Phys. Chem. 97 (1993) 13620.
[10] Y. Kawabata, T. Sekiguchi, M. Tanaka, T. Nakamura, H. Komizu, M. Matsumoto, E. Manda, M. Saito, M. Sugi, S. Iizima, Thin Solid Films 133 (1985) 175.
[11] A. Schaper, L. Wolthaus, D. Mobius, T.M. Jovin, Langmuir 9 (1993) 2178.
[12] J. Garnaes, D.K. Schwartz, R. Viswanathan, J.A.N. Zasadzinski, Nature 357 (1992) 54.
[13] C.A.J. Putman, H.G. Hansma, H.E. Gaub, P.K. Hansma, Langmuir 8 (1992) 3014.
[14] R. Viswanathan, L. Madsen, J.A. Zasadzinski, D.K. Schwartz, Science 269 (1995) 51.
[15] E. Meyer, L. Howald, R.M. Overney, H. Heinzelmann, J. Frommer, H.J. Guntherodt, T. Wagner, H. Schier, S. Roth, Nature 349 (1991) 398.
[16] D.K. Schwartz, J. Garnaes, R. Viswanathan, J.A.N. Zasadzinski, Science 257 (1992) 508.
[17] J.A. Zasadzinski, R. Viswanathan, J. Garnaes, D.K. Schwartz, Science 263 (1994) 1726.
[18] S.N. Magonov, Surface Analysis with STM and AFM: Experimental and Theoretical Aspects of Image Analysis, VCH, New York, 1996, p. 20.

Mechanisms of the nonlinear optical properties of squaraine dyes in poly(methyl methacrylate) polymer

K. S. Mathis* and M. G. Kuzyk

Department of Physics and Materials Science Program, Washington State University, Pullman, Washington 99164-2814

C. W. Dirk, A. Tan, S. Martinez, and G. Gampos

Department of Chemistry, University of Texas, El Paso, Texas 79968-0513

Received March 3, 1997; revised manuscript received June 4, 1997

We report on the nonlinear optical characterization experiments of squaraine dyes in solid poly(methyl methacrylate) solutions. We find that a quantum three-level model of a squaraine best agrees with the quadratic electroabsorption measurements when the isomer composition is taken into account. We compare the nonlinear response of several dyes with the three- and four-level models to help determine which models are most suitable for predicting nonlinear behavior. Four-level models that include either two one-photon states or two two-photon states are inconsistent with quadratic electroabsorption spectroscopy. Furthermore, we find that the effect of isomers is more significant than molecular reorientation at room temperature and that the isomer model best agrees with the experimental results. © 1998 Optical Society of America [S0740-3224(98)00702-4]

OCIS codes: 190.0190, 160.5470, 190.4710, 160.2100.

1. INTRODUCTION

Organic dye-doped polymer systems have been the focus of considerable research because of their highly nonlinear optical response, facility of fabrication (into fibers, thin films, etc.), and ease of integration into electro-optical devices.[1,2] More specifically, the nonlinearity of squarylium dyes has received much attention because of the large electronic oscillator strength transitions of these dyes, their narrow transition widths, and their large molecular third-order nonlinear optical susceptibility γ.[3,4] In addition to having large dipole moments, the squaryliums (a class of zwitterionic polymethine dyes) possess a structural flexibility with which they can be tailored to meet certain spectral requirements. The x-ray analysis of squarylium structures indicates that such structures have extensive electron delocalization and a low bond-length alternation.[5] This fact plays a significant role in the nonlinear response because the bond-length alternation can be varied to optimize the susceptibility of these polymethine dyes for a given conjugation length.[6]

Various types of experiment have been performed to fully characterize the electronic properties and the nature of the excited states of squaraines that contribute to γ. A convenient method for measuring the nonlinear optical properties of organic materials in a suitable polymer matrix was outlined by Luong *et al.*[7] That study involved the determination of the electro-optic coefficients of a dye-doped polymer. Characterization of these quadratic electro-optic (QEO) parameters could then be used to determine the third-order susceptibilities. It was also concluded that the second-order susceptibility of these organic nonlinear optical materials depended on (and varied greatly with) the polarity of the polymer matrix.

Analysis (using several types of measurement, including QEO modulation) was performed on polymer thin-film solutions of dye compounds by Dirk and Kuzyk.[8] Results for the two-level model calculations suggested that the complex damping corrections (which arise from various broadening mechanisms) cannot be ignored. More specifically, they demonstrated that larger damping corrections are necessary for noncentrosymmetric molecules and that calculation of the third-order nonlinear optical susceptibility $\chi^{(3)}$ depends on the optical process, the molecular symmetry, and the transition widths and energies between the ground and the excited states. Squaraines were shown to be more promising organic materials owing to their greater susceptibilities,[2,3] relatively large solubilities, and the linear dependence of $\chi^{(3)}$ on dye concentration. Because of the predominantly electronic response at room temperature from the QEO process, it was suggested that squaraines could prove useful for other third-order processes. In particular, a two-level model of the third-order susceptibility predicted a maximum (negative) response for centrosymmetric structures (whose ground- and excited-state dipole moments vanish).[9] For this model, which includes the ground state and a one-photon state, the susceptibility depends only on the transition moment between the ground and the first-excited states. QEO measurements [of the magnitude of the real part of $\chi^{(3)}$] also showed that the dispersion of the ISQ squaraine was approximated by a two-level model,[2] thereby permitting a sound estimation of

0740-3224/98/020871-13$10.00 © 1998 Optical Society of America

the electronic $\chi^{(3)}$ (taking into account a quasi-static approximation of the orientational effects).

Subsequently it was found that the two-level model is too restrictive, and electric-field-induced second-harmonic measurements[10] suggested that the large negative microscopic susceptibility γ is dominated by a term that depends on the transition moment from the ground to the first-excited state. For the squarylium dyes it was proposed that the three-level model expression for γ is dominated by this two-level term.

Using quantum many-electron calculations, Zhou *et al.*[4] confirmed that squaraines possess an inherently large and negative third-order susceptibility (even in the zero-frequency limit). More importantly, in the calculation of γ there exists a competition between the two types of virtual transition: type I is $g \rightarrow m \rightarrow g \rightarrow m \rightarrow g$, i.e., one-photon transitions; type II is $g \rightarrow m \rightarrow n \rightarrow m \rightarrow g$, i.e., two-photon transitions, where $n \neq g$ (g labels the ground state, and m and n are the excited states). One needs to consider this competition carefully to predict correctly $\gamma_{ijkl}(-\omega_4; \omega_1, \omega_2, \omega_3)$, which was verified to be dominated by its first term (involving a type I transition). Experimental observation of the type II transitions (by a femtosecond excited-state pump–probe method) was used to verify the quantum many-electron calculations, which included positive triple summations of the type II sequences.[11] This observation provided evidence of the suspected strong coupling between the one-photon state and higher-lying two-photon states (which, in fact, was comparable with the coupling between the ground and the one-photon states). Note, however, that this experiment, by design, was not sensitive to the low-lying two-photon state. Furthermore, because this is an on-resonance experiment, in which the sum of the two input frequencies matches the energy of the high-lying two-photon state, it overemphasizes the contribution of this state. Similarly, an electro-optic or third-harmonic-generation (THG) experiment, in which the light frequency does not match the energy of the high-lying two-photon state, may not have a large contribution from this state. THG experiments located the lowest-lying two-photon-like transition for ISQ in chloroform,[12] which appears energetically just above the one-photon state. The transition moment between this state and the one-photon state is found to be smaller than that between the ground and the one-photon states. Moreover, these experiments indicated that at least one high-lying two-photon state must be included in modeling the third-order nonlinearity and that the simple three-level model is inadequate.

Quadratic electroabsorption (QEA) spectroscopy also shows evidence of a two-photon state near the one-photon state for ISQ,[13] with an energy difference less than 0.2 eV. QEA spectroscopy (which has the advantage of the optical probe wavelength's being tunable to enhance the contribution of only one state) was used to show that the squarylium's electronic excited states are approximated by a three-level model for probe wavelengths in the visible. Poga *et al.*[13] concluded that these two excited states dominate the near-resonant third-order susceptibility. Determining the room-temperature tensor ratio $a = \chi^{(3)}_{3333}/\chi^{(3)}_{1133} \approx 3$, showed that the electronic mechanism dominates the susceptibility throughout most of the visible region.

By expanding on the general theoretical framework of the three-level model, we analyze several squaraine molecules in an attempt to find a unifying principle that describes the electronic nonlinear optical properties. First we outline several theoretical models, including four-level representations, a three-level model that takes reorientational effects into account, and a *cis–trans* model that considers squaraines existing as sets of *cis–trans* isomers. We then show that a second two-photon state is incompatible with our measured QEA spectra and that the *cis–trans* model is consistent with our results. We therefore conclude that a mixture of isomers in our samples is responsible for some of the spectral features that we observe in our QEA data and that isomers must be taken into account when one is modeling the nonlinear optical response.

2. THEORY

In this section we present the theoretical three- and four-level models of the imaginary third-order nonlinear optical susceptibility $\mathrm{Im}[\chi^{(3)}]$. The three-level model is chosen as a starting point because, for a centrosymmetric molecule, a minimum of three states is needed to describe $\chi^{(3)}$. This requirement arises from the nature of the parity (even or odd with respect to inversion symmetry) of the excited-state wave functions of a centrosymmetric molecule: Since the even- (odd-) parity wave function is invariant (variant) under inversion, and the photon absorption operator changes the parity of the wave function on which it acts, then a photon absorption can occur only between states of opposite parity. The three-level model, then, has excited states of opposite parity.

With the convention that the ground-state wave function is symmetric, then (for nonzero dipole transitions) the first excited state is antisymmetric, the second excited state is symmetric, etc. The excited states having the opposite (the same) parity as that of the ground state are termed one-photon (two-photon) states; a transition between states of the same parity is allowed only if two photons are absorbed. The dopant molecules can be modeled as one dimensional (a consideration that is valid for many dye-doped polymer systems): The transition moments are nonzero only along one axis.[2]

The two-level model of the linear susceptibility of a one-dimensional molecule is

$$\chi^{(1)}(-\omega; \omega) \propto \frac{N\mu_{1g}{}^2\Gamma_{1g}}{\hbar}\left[\frac{1}{(\omega_{1g}-\omega)^2+\Gamma_{1g}{}^2} - \frac{1}{(\omega_{1g}+\omega)^2+\Gamma_{1g}{}^2}\right], \quad (1)$$

where μ_{1g} is the transition dipole moment $\int \psi_1(er)\psi_g dr$ between states 1 and g, ω_{1g} is the transition frequency between state ψ_1 and state ψ_g, Γ_{1g} is the transition width, N is the number density, ω is the photon frequency, $\hbar$ is Planck's constant, and r and e are, respectively, the electron position and charge. For a nonzero transition moment, 1 has to be a one-photon state. Fig-

ure 1 shows the absorption spectra (divided by their number densities for comparison) of the squaraine dyes PYSQ, TSQ, HSQ, PSQ, and BSQ, where the peaks are due to a strong one-photon transition (from the ground to the first excited state) in the visible. The transition energy and width obtained from the absorption spectrum of each squaraine are listed in Table 1. Note that the number density is calculated by use of a dye concentration of 1% for each squaraine (with the exception of 0.5% for TSQ). The corresponding dipole transition moments are obtained from molecular orbital calculations.

We calculate the transition width Γ_{01} (damping parameter) of the one-photon state that appears in the absorption spectra by finding the energy difference between the half-maximum points. This analysis is made somewhat difficult by the vibronic sideband (the shoulder near 600 nm) that appears in the linear spectra; hence the values for Γ_{01} are most likely an underestimation of the ground to first-excited-state transition widths.

It should be noted that the squaraines (with the exception of PYSQ) have similar electronic properties, as can be seen by the small variations, over the set of dyes, in transition energy and dipole transition moment values. Squaraines, being polymethine dyes, have a narrow isolated peak in the electronic absorption spectrum. Other characteristic similarities of squaraines include their highly polar and electron-withdrawing central moiety as well as their symmetric arrangement ($D^+ \rightarrow A^- \quad D^+$), which can lead to extensive intramolecular charge transfer.[14] The induced dipole moment (along a particular axis), which results from this charge transfer, can contribute to both the electronic and the reorientational mechanisms of the electric-field dependence of the refractive index. The electronic mechanism occurs when the electron cloud deforms in the presence of an applied optical field, thereby changing the refractive index. Similarly, when the molecules tend to align because of the applied electric field, the refractive index of the medium changes.[15] Electroabsorption is the process by which a static electric field induces change in the electronic cloud structure and induces molecular reorientation.

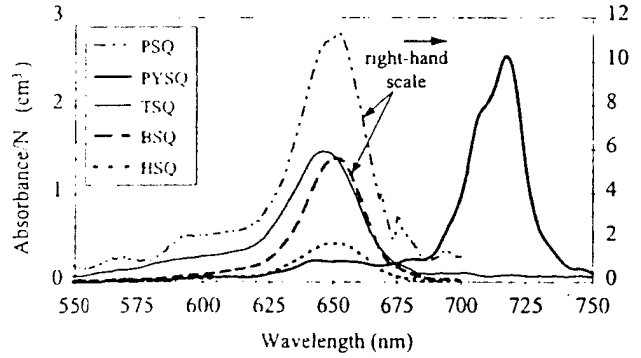

Fig. 1. Comparison of squaraine absorption spectra normalized by their number densities.

Poga *et al.*[16] showed (for the case of a dye molecule dispersed in a polymer matrix, taking the interaction between the dye and the polymer into account) that the third-order susceptibility ratio $a = \chi^{(3)}_{3333}/\chi^{(3)}_{1133}$ is unique for each mechanism. For pure electronic and reorientational mechanisms the ratio was calculated to be

$$a = \frac{\chi^{(3)}_{3333}}{\chi^{(3)}_{1133}} = \begin{cases} 3 & \text{purely electronic} \\ -2 & \text{purely reorientational} \end{cases}. \tag{2}$$

Because the electronic mechanism dominates at temperatures below the glass transition temperature ($T_g \approx 90\,^\circ\text{C}$) and the reorientational contributions dominate at high temperatures where the polymer softens, Poga *et al.* expected to see a change in the ratio as the sample was heated through T_g. Indeed, they reported that $a \approx 3$ below T_g and $a \approx -2$ above T_g. The data presented here were obtained at room temperature, so we conclude that we are measuring a predominantly electronic response.

Because QEA is also sensitive to two-photon states, it can be used to determine the energies and transition moments of all states. The three-level model used to describe the nonlinear electroabsorption spectrum includes the ground state, a one-photon state, and a two-photon state. For a one-dimensional, centrosymmetric system the perturbation theory expression of the molecular third-order susceptibility is[9]

$$\gamma = \frac{K}{\hbar^3}\left(\sum_{l,m,n} D_{l,m,n}\mu_{gl}\mu_{lm}\mu_{mn}\mu_{ng} - \sum_{l,n} D_{l,n}\mu_{gl}\mu_{lg}\mu_{gn}\mu_{ng}\right), \tag{3}$$

where l, m, and n are excited states and the D represent energy denominators described below. For reasons mentioned above, l and n ($=1$) are required to be one-photon states and m ($=2$) is required to be a two-photon state. The constant K($=3$ for the dc Kerr effect) corresponds to

Table 1. Transition Values of Squaraine Dyes as Determined by Absorption Spectroscopy

Dye	Number Density (cm^{-3})	Energy E (λ) [eV (nm)]	Half-Width Γ_{g1} (meV)	Transition Moment μ_{g1} (D)
PYSQ	1.47×10^{19}	1.727 (718.2 ± 1.0)	46.0 ± 4.0	11.40
HSQ	1.39×10^{19}	1.907 (650.1 ± 1.5)	50.0 ± 4.0	11.58
PSQ	1.19×10^{19}	1.909 (649.5 ± 1.5)	47.2 ± 4.0	11.58
BSQ	1.10×10^{19}	1.904 (651.4 ± 1.5)	39.0 ± 4.0	11.65
TSQ	6.50×10^{18}	1.921 (645.5 ± 1.5)	53.0 ± 4.0	11.52
ISQ[a]	1.94×10^{19}	1.880 (657.0 ± 1.0)	45.0 ± 5.0	11.50

[a] Ref. 13

the number of distinct permutations of the input frequencies (two static field components probed by a propagating optical field). The ground state is excluded in the summation:

$$\gamma(-\omega;\ \omega,\ 0,\ 0) = \frac{3\mu_{01}^{\ 2}}{\hbar^3}(D_{121}\mu_{12}^{\ 2} - D_{11}\mu_{01}^{\ 2}). \quad (4)$$

The imaginary part of the second-order hyperpolarizability is then of the form

$$\mathrm{Im}(\gamma)_{3\text{-level}} = \frac{3\mu_{01}^{\ 2}}{\hbar^3}[\mu_{12}^{\ 2}\,\mathrm{Im}(D_{121}) - \mu_{01}^{\ 2}\,\mathrm{Im}(D_{11})]. \quad (5)$$

The energy denominators (D_{11} and D_{121}) are given by the double and triple sums, respectively, of the time-dependent perturbation theory damped dispersion terms of Orr and Ward[17]:

$$\begin{aligned} D_{11}(-\omega_\sigma;\ \omega_1,\ \omega_2,\ \omega_3) &= \hat{I}_{1,2,3}\{[(\Omega_{1g} - \omega_\sigma)(\Omega_{1g} - \omega_3)(\Omega_{1g} - \omega_1)]^{-1} \\ &+ [(\Omega_{1g} - \omega_3)(\Omega_{1g}^{\ *} + \omega_2)(\Omega_{1g} - \omega_1)]^{-1} \\ &+ [(\Omega_{1g}^{\ *} + \omega_\sigma)(\Omega_{1g}^{\ *} + \omega_3)(\Omega_{1g}^{\ *} + \omega_1)]^{-1} \\ &+ [(\Omega_{1g}^{\ *} + \omega_3)(\Omega_{1g} - \omega_2)(\Omega_{1g}^{\ *} + \omega_1)]^{-1}\}, \end{aligned} \quad (6a)$$

$$\begin{aligned} D_{121}(-\omega_\sigma;\ \omega_1,\ \omega_2,\ \omega_3) &= \hat{I}_{1,2,3}\{[(\Omega_{1g} - \omega_\sigma)(\Omega_{2g} - \omega_1 - \omega_2)(\Omega_{1g} - \omega_1)]^{-1} \\ &+ [(\Omega_{1g}^{\ *} + \omega_3)(\Omega_{2g} - \omega_1 - \omega_2)(\Omega_{1g} - \omega_1)]^{-1} \\ &+ [(\Omega_{1g}^{\ *} + \omega_1)(\Omega_{2g}^{\ *} + \omega_1 + \omega_2)(\Omega_{1g} - \omega_3)]^{-1} \\ &+ [(\Omega_{1g}^{\ *} + \omega_1)(\Omega_{2g}^{\ *} + \omega_1 + \omega_2)(\Omega_{1g}^{\ *} + \omega_\sigma)]^{-1}\}, \end{aligned} \quad (6b)$$

where $\Omega_{ng} = \omega_{ng} - i\Gamma_{ng}$, $\omega_\sigma = \omega_1 + \omega_2 + \omega_3$, and * denotes complex conjugation. The damping term Γ_{ng} is obtained from the one-photon absorption spectrum, and the energy between the ground state and the excited state, n, is given by $\hbar\omega_{ng}$. For QEA, ω_1, ω_2, and ω_3 can take on the value of 0 or ω. The intrinsic permutation operator $\hat{I}_{1,2,3}$ indicates an average of the summation over $[(\omega, 0, 0); (0, \omega, 0); (0, 0, \omega)]$. The final imaginary terms are

$$\mathrm{Im}(D_{11}) = \frac{16\gamma_1\omega\omega_1[-2\Gamma_1^{\ 6} - \Gamma_1^{\ 4}(2\omega^2 + \omega_1^{\ 2}) - 2\Gamma_1^{\ 2}\omega_1^{\ 2}(\omega^2 - 2\omega_1^{\ 2}) - \omega^2\omega_1^{\ 2}(4\omega_1^{\ 2} - \omega^2) + 3\omega_1^{\ 6}]}{3\{(\omega_1^{\ 2} + \Gamma_1^{\ 2})[(\omega_1 - \omega)^2 + \Gamma_1^{\ 2}][(\omega_1 + \omega)^2 + \Gamma_1^{\ 2}]\}^2}, \quad (7a)$$

$$\begin{aligned} \mathrm{Im}(D_{121}) &= \frac{2\Gamma_1(\omega_1\omega_2 - \Gamma_1\Gamma_2)[(\omega_2 - \omega)^2 + \Gamma_2^{\ 2}] + 2\omega_1(\omega_2^{\ 2} + \Gamma_2^{\ 2})[\Gamma_1(\omega_2 - \omega) + \Gamma_2(\omega_1 - \omega)]}{3(\omega_1^{\ 2} + \Gamma_1^{\ 2})(\omega_2^{\ 2} + \Gamma_2^{\ 2})[(\omega_1 - \omega)^2 + \Gamma_1^{\ 2}][(\omega_2 - \omega)^2 + \Gamma_2^{\ 2}]} \\ &+ \frac{-2\Gamma_1(\omega_1\omega_2 - \Gamma_1\Gamma_2)[(\omega_2 + \omega)^2 + \Gamma_2^{\ 2}] - 2\omega_1(\omega_2^{\ 2} + \Gamma_2^{\ 2})[\Gamma_1(\omega_2 + \omega) + \Gamma_2(\omega_1 + \omega)]}{3(\omega_1^{\ 2} + \Gamma_1^{\ 2})(\omega_2^{\ 2} + \Gamma_2^{\ 2})[(\omega_1 + \omega)^2 + \Gamma_1^{\ 2}][(\omega_2 + \omega)^2 + \Gamma_2^{\ 2}]} \\ &+ \frac{\Gamma_1^{\ 2}\Gamma_2(3\omega^2 - 6\omega\omega_1 + 2\omega_1^{\ 2}) + 2\Gamma_1(\omega - \omega_1)(\omega - \omega_2)(\omega_1^{\ 2} + \Gamma_1^{\ 2}) + [\Gamma_2(\omega - \omega_1)^2(\omega^2 - 2\omega\omega_1 + 2\omega_1^{\ 2})]}{3(\omega_1^{\ 2} + \Gamma_1^{\ 2})[(\omega_1 - \omega)^2 + \Gamma_1^{\ 2}]^2[(\omega_2 - \omega)^2 + \Gamma_2^{\ 2}]} \\ &+ \frac{-\Gamma_1^{\ 2}\Gamma_2(3\omega^2 + 6\omega\omega_1 + 2\omega_1^{\ 2}) - 2\Gamma_1(\omega + \omega_1)(\omega + \omega_2)(\omega_1^{\ 2} + \Gamma_1^{\ 2}) - [\Gamma_2(\omega + \omega_1)^2(\omega^2 + 2\omega\omega_1 + 2\omega_1^{\ 2})]}{3(\omega_1^{\ 2} + \Gamma_1^{\ 2})[(\omega_1 + \omega)^2 + \Gamma_1^{\ 2}]^2[(\omega_2 + \omega)^2 + \Gamma_2^{\ 2}]}, \end{aligned} \quad (7b)$$

where we have defined $\omega_n = \omega_{ng}$, the transition frequency between states n and g, and $\Gamma_n = \Gamma_{ng}$, the transition width.

Plots of the dispersion terms $\mathrm{Im}(D_{11})$ and $\mathrm{Im}(D_{121})$ as a function of wavelength are shown in Fig. 2 for $\hbar\omega_1 = 1.909$ eV, $\hbar\omega_2 = 2.092$ eV, $\hbar\Gamma_1 = 47.2$ meV, and $\hbar\Gamma_2 = 55.0$ meV. The microscopic susceptibility can be determined as a function of the dipole transition moments μ_{01} and μ_{12} from Eqs. (5) and (7). The value μ_{01} is taken, as a starting point, to be the one given in Table 1. By varying this parameter and μ_{12}, one can find a best fit to the experimental data.

A. Four-Level Model 1

The four-level model is also represented by the perturbation theory for the molecular susceptibility [Eq. (3)]. The fourth state, considered in addition to the states included in the three-level model, can be a higher-lying two-photon state or another one-photon state (discussed below). With the three-level model, the summation variables in Eq. (3) are given by $l = 1$, $m = 2$, and $n = 1$, whereas the four-level model has $m = 2, 3$ (where 3 denotes the high-lying two-photon state).

The investigation of the role of the fourth state as a two-photon state is prompted by Andrews *et al.*,[12] whose

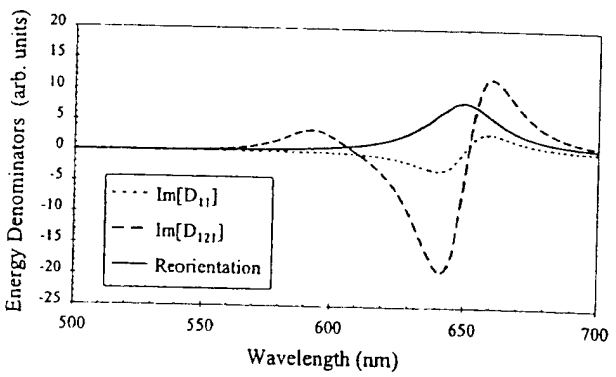

Fig. 2. Dispersion of $\mathrm{Im}(D_{11})$, $\mathrm{Im}(D_{121})$, and the molecular reorientation term relative to probe wavelength.

data (using THG) for the ISQ molecule best fit the theory when a two-photon state at 375 nm, which has a transition energy of 360 meV and a dipole transition μ_{13} of 9.5 D, is included. Because squaraines have similar electronic properties, this second two-photon state should generally be near 375 nm for most squaraines. This fourth state introduces an additional term into Eq. (5):

$$\mathrm{Im}(\gamma)_{4\text{-level}} = \frac{3\mu_{01}^2}{\hbar^3}[\mu_{12}^2\,\mathrm{Im}(D_{121}) + \mu_{13}^2\,\mathrm{Im}(D_{131}) - \mu_{01}^2\,\mathrm{Im}(D_{11})]. \quad (8)$$

The damped dispersion term D_{131} has the form of Eq. (6b) with Ω_{3g} replacing Ω_{2g}, so the corresponding imaginary part $\mathrm{Im}(D_{131})$ is given by an expression similar to Eq. (7b), with $\Gamma_2 \rightarrow \Gamma_3$ and $\omega_2 \rightarrow \omega_3$.

B. Four-Level Model 2

The second possible four-level model includes the ground state, a two-photon state (which is the same one as in the three-level model), and two one-photon states (close in energy). The basis for this approach is the speculation that the hump that appears in the PYSQ dye's absorption spectrum (Fig. 1) consists of a second one-photon state very close in energy to the original one-photon state. For this particular model, the susceptibility [given in Eq. (3)] is summed over the excited states l (=1 or 1′), m (=2), and n (=1 or 1′), where 1′ denotes the second one-photon state.

The final expression for γ includes four more terms than in the previously discussed four-level model:

$$\gamma(-\omega;\,\omega,\,0,\,0) = \frac{3}{\hbar^3}(-\mu_{01}^4 D_{11} - 2\mu_{01}^2\mu_{01'}^2 D_{11'} - \mu_{01'}^4 D_{1'1'} + \mu_{01}^2\mu_{12}^2 D_{121} + \mu_{01}\mu_{12}\mu_{21'}\mu_{1'0} D_{121'} + \mu_{01'}\mu_{1'2}\mu_{21}\mu_{10} D_{1'21} + \mu_{01'}^2\mu_{1'2}^2 D_{1'21'}), \quad (9)$$

where the imaginary terms of D_{11} and D_{121} are given in Eqs. (7). The energy denominators $D_{1'1'}$ and $D_{1'21'}$, of course, have forms equivalent to Eq. (6) (with 1′ replacing 1 in those equations). The terms $D_{11'}$ and $D_{121'}$ and their imaginary counterparts are more intricate and are obtained in analogy to Eqs. (6) and (7). The transition widths and energies calculated from the experimental spectra of PYSQ, assuming two one-photon states, are shown in Table 2.

The one-photon state parameters are obtained from the linear spectra (Fig. 1), and the two-photon state parameters are determined from the nonlinear QEA spectra. For example, the transition energy of the two-photon state, which appears as a shallow dip in the PYSQ spectrum, occurs at 628.5 nm. This dip feature is recognized to be a two-photon state because there is no corresponding peak in the linear absorption spectra at that wavelength. (A two-photon peak should not appear in the absorption spectrum because it has the same symmetry as the ground state, and therefore no transitions are allowed between the two states.) Poga *et al.* determined that this shallow feature, which occurs at 596 nm for ISQ, is constant with temperature, which is consistent with a two-photon state peak (of electronic origin) whose properties should not depend on temperature.[18]

Table 2. Spectroscopic Designation of the PYSQ Molecule[a]

State n	Energy E (λ) [eV (nm)]	Half-Width Γ_n (meV)
1	1.73 (718.6 ± 0.5)	15.5 ± 0.5
1′	1.75 (707.1 ± 0.5)	16.0 ± 0.5
2	1.97 (628.5 ± 1.0)	50.0 ± 5.0

[a] Four-level model 2 and *cis–trans* model.

C. *cis–trans* Model

The hypothesis that the presence of a mixture of *cis* and *trans* isomers explains the features of the data is based on the observation that a shoulder—especially pronounced for PYSQ—appears in some of the absorption spectra. Because the absorption peak of each isomer is different, the shoulder would be consistent with the presence of two distinct isomers (different structures of the same molecule). We assume that the material is predominantly composed of two classes of isomer: the *cis* and *trans* forms. In particular, Dirk *et al.* have concluded, on the basis of their molecular mechanics calculations, that ISQ and BSQ exist primarily as mixtures of these isomers.[5] It is thought that the excited-state characteristics could be evaluated by incorporation of both the three-level model for the *cis* molecule and a distinctly separate three-level model for the *trans* isomer. The *cis–trans* model would then be given by the (concentration-weighted) linear addition of both the *cis* and the *trans* three-level models.

The three-level model for both the *cis* and the *trans* configurations includes the ground state, a one-photon state, and a two-photon state. The one-photon states for the *cis* and the *trans* isomers are denoted 1 and 1′, respectively. The transition widths and energies for these states (of PYSQ) are again taken to be those values listed in Table 2. If the two-photon states are identical in each molecule, the expression for γ is given by

$$\mathrm{Im}(\gamma) = \frac{3}{\hbar^3}\{[\mu_{01}^2\mu_{12}^2\,\mathrm{Im}(D_{121}) - \mu_{01}^4\,\mathrm{Im}(D_{11})] + [\mu_{01'}^2\mu_{1'2}^2\,\mathrm{Im}(D_{1'21'}) - \mu_{01'}^4\,\mathrm{Im}(D_{1'1'})]\}, \quad (10)$$

which is simply the sum of the individual three-level model contributions of the *cis* and the *trans* molecules.

D. Molecular Reorientation

In addition to the models outlined above, reorientational effects on the third-order nonlinear optical susceptibility are investigated. In this case the susceptibility of a collection of molecules in an elastic host polymer includes not only the electronic contributions of $\mathrm{Im}(\gamma)$ but those of the chromophore reorientation as well[18]:

$$\mathrm{Im}[\chi^{(3)}(-\omega;\ \omega,\ 0,\ 0)] \propto \frac{N}{15}\left\{\mathrm{Im}[\gamma(-\omega;\ \omega,\ 0,\ 0)] - \frac{4}{3k_\theta}\,\mathrm{Im}[\alpha(-\omega;\ \omega)\alpha(0;\ 0)]\right\}, \tag{11}$$

where k_θ is the microscopic polymer elasticity and $\mathrm{Im}(\gamma)$ is given in Eq. (5). In the sum-over-states perturbation model the polarizability is[19]

$$\alpha(\omega) = \frac{1}{\hbar}\sum_{n,m}\rho_{mm}^{(0)}\left(\frac{\mu_{mn}{}^i\mu_{nm}{}^j}{\omega_{mn} - \omega - i\Gamma_{nm}} + \frac{\mu_{mn}{}^i\mu_{nm}{}^j}{\omega_{mn} + \omega + i\Gamma_{nm}}\right), \tag{12}$$

which, in the two-level model, reduces to

$$\alpha(\omega) = \frac{1}{\hbar}\left(\frac{\mu_{gl}{}^i\mu_{lg}{}^j}{\omega_{lg} - \omega - i\Gamma_{lg}} + \frac{\mu_{lg}{}^i\mu_{gl}{}^j}{\omega_{lg} + \omega + i\Gamma_{lg}}\right)\rho_g^{(0)}, \tag{13}$$

where $\rho_g^{(0)}$ represents the unperturbed density matrix [we assume that $\rho_{nm}^{(0)} = 0$ for $n \neq m$] and $\mu_{gl}{}^i$ is the ith Cartesian component of the electric dipole transition moment. In this two-level model, only one excited state (the one-photon state) dominates. With the static polarizability (purely real term) given by $\alpha(0) = 2\mu_{01}{}^2\omega_{01}/[\hbar(\omega_{01}{}^2 + \Gamma_{01}{}^2)]$, the reorientational term simplifies to

$$\mathrm{Im}[\alpha(-\omega;\ \omega)\alpha(0;\ 0)] = \frac{8\mu_{01}{}^4\omega\omega_{01}{}^2\Gamma_{01}}{\hbar^2(\omega_{01}{}^2 + \Gamma_{01}{}^2)[(\omega - \omega_{01})^2 + \Gamma_{01}{}^2][(\omega + \omega_{01})^2 + \Gamma_{01}{}^2]}, \tag{14}$$

where all the quantities represent the dressed ones (i.e., μ_{01} is the dressed transition moment and α is the dressed polarizability). By including the molecular reorientational term (shown in Fig. 2 for the BSQ parameters listed in Table 1) in the theoretical model, one can assess the role of reorientation in the characterization of the excited states.

E. Quadratic Electro-Optic Effect

For centrosymmetric systems the lowest-order change in the refractive index n is quadratically related to the applied dc field strength.[19] This QEO effect, which occurs when an optical wave propagates in a medium in the presence of a dc (low-frequency) applied field, leads to a voltage-induced refractive index:

$$n_{ij} = (n_0)_{ij} + \frac{(n_0)_{ij}{}^3}{2}\,s_{ijkl}E_k{}^0E_l{}^0, \tag{15}$$

where n_0 is the zero-field refractive index (summation notation does not apply to i and j) and the complex electro-optic tensor s_{ijkl} is directly proportional to the third-order nonlinear optical susceptibility $\chi^{(3)}$ (Ref. 13):

$$\mathrm{Im}[\chi_{ijkl}^{(3)}] = {}^1/_3\mathrm{Re}(n_0)\mathrm{Im}(n_0{}^3s_{ijkl}). \tag{16}$$

Inasmuch as the quadratic electroabsorption experiments discussed in this paper probe only the two tensor components $\chi_{1133}^{(3)}$ and $\chi_{3333}^{(3)}$ [where $\chi_{2233}^{(3)} = \chi_{1133}^{(3)}$ owing to azimuthal symmetry about the normal to the surface], then, for spectra taken at normal incidence, only the $\mathrm{Im}(n_0{}^3s_{1133})$ component is experimentally probed.[18]

For an isotropic distribution of one-dimensional molecules, $\mathrm{Im}(\chi)$ is related to the molecular third-order susceptibility through the relation[13]

$$\mathrm{Im}[\chi_{1133}^{(3)}] = \frac{N}{15}(f^\omega)^2(f^0)^2\,\mathrm{Im}(\gamma), \tag{17a}$$

where N is the number density and $(f^\omega)^2$ and $(f^0)^2$ are local-field factors (by means of the Lorentz–Lorenz form with $n_\omega \approx 1.48$ and $\epsilon = n_0{}^2 \approx 3$; Ref. 20):

$$(f^\omega) = \frac{n_\omega{}^2 + 2}{3} \rightarrow (f^\omega)^2(f^0)^2 \approx 7. \tag{17b}$$

In this manner the theoretical third-order susceptibility obtained from relations (17) can be directly compared with the complex electro-optic tensor in Eq. (16), whose component is proportional to experimental parameters (discussed below).

3. QUADRATIC ELECTROABSORPTION EXPERIMENT

A. Sample Preparation

Data are presented and discussed for several squaryliums, whose structures are shown in Table 3. The dyes were created to improve solubility and stability relative to ISQ. Preliminary calculations suggested that the nonlinear susceptibility of PYSQ should be larger than for previous dyes. This squaraine, in addition to being more

Table 3. Molecular Structures of Squarines

Name	Squaraine	Molecular Structure
BSQ	butyl (anilinium)	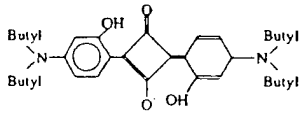
ISQ	indole	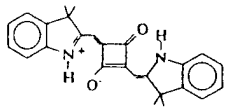
PYSQ	pyrylium	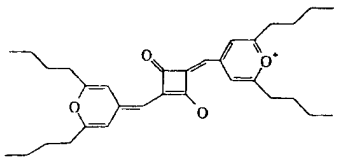
HSQ	hexyl	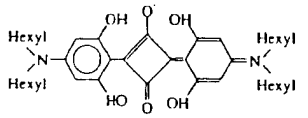
PSQ	pentyl	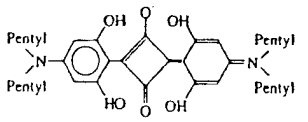
TSQ	tetrahydroxy	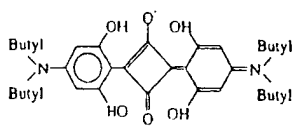

soluble (and more highly delocalized in its electronic structure than ISQ), was also made as a synthetic intermediate to pyridinium-based dyes, which are predicted to have a third-order susceptibility ten times larger than those of previously measured dyes.

We made thin films by spin coating a polymer-dye solution that comprised (by weight) 85% solvents (67% propylene glycol methyl ether acetate and 33% γ-butyrolactone) and 15% solids [1% squaraine dye and 99% poly(methyl methacrylate)]. The substrate is a glass slide with one side coated with an optically transparent layer of conducting indium tin oxide (ITO). Etching is performed on the slide to create three uniform strips of the ITO conductor layer. The dye-doped polymer solution is then spin coated onto the ITO side at 950–1000 rpm for 30 s to produce a 2–3-μm-thick layer. The samples are baked at 95 °C for at least 20 min to ensure complete evaporation of the solvent.

To form the final samples, two pieces are placed together, with the dye-coated sides in contact with each other, such that the ITO strips are perpendicular. The pieces are fused together by use of the pressing oven described in the literature.[21] With an initial uniaxial stress of ≈12.5 Torr (for an area of ≈1.1 cm^2), the temperature is raised to 150 °C for 1 h and is then cooled to room temperature. The sample is then annealed (with no applied pressure) to relieve internal stresses and render the films isotropic. The time dependence of the temperature and pressure of the sample is shown in Fig. 3. The magnitude and stability of the pressure during this process are very important to ensure that the thin-films have pressed evenly, with no air voids.

The samples are then placed in a sample holder[13] containing metal electrical contacts that attach to the ITO strips of the sample. A waveform generator is used to apply voltage (which is subsequently amplified) through the ITO strips by means of this conducting holder, creating an electric field parallel to the sample normal.

B. Experimental Apparatus

The QEA experiment (Fig. 4) has a probe beam (from either a xenon-arc lamp or a laser) that passes through the thin-film sample, to which a low-frequency oscillating voltage is applied (usually of the order of 24 V/μm). This voltage, produced by the internal oscillator of a Stanford Research Systems (SRS 850) lock-in amplifier, is amplified with a Realistic MPA-30 amplifier. The stepping motors, which are interfaced with a computer, control the wavelength and the angle of the sample. The experimental wavelength range spans the visible region (usually 450–750 nm), and for typical runs the sample is illuminated at normal incidence. The modulation of the sample transmittance by a sinusoidal electric field of 1.5 kHz at frequency Ω is detected by a silicon photodiode whose output is read by a lock-in amplifier (SRS-530 or SRS-850) referenced to twice the applied field modulation frequency, 2Ω. For field frequencies much smaller than optical frequencies this oscillating electric field can be considered a quasi-static field. The modulation of the static field and lock-in detection allow us to measure an intensity modulation that is 10^{-5} times the background.[22]

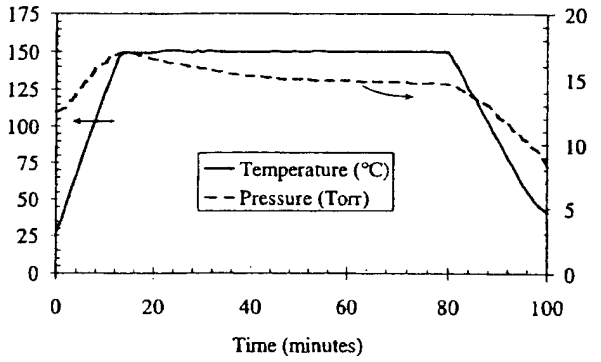

Fig. 3. Variation in pressure and temperature during the sample pressing procedure.

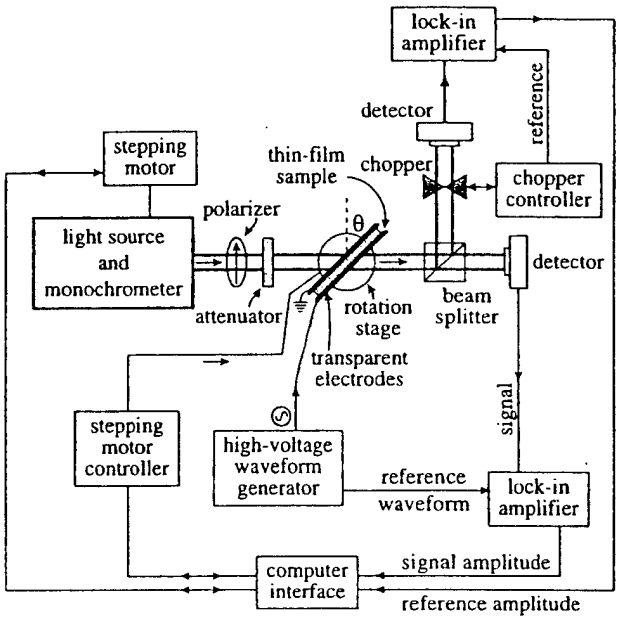

Fig. 4. Diagram of the QEA experiment.

The experimental data are related to the QEO tensor s_{ijkl} (Ref. 13) according to

$$(n_0{}^3 s)_I = \frac{\lambda d}{4\pi V_{\mathrm{rms}}{}^2} \frac{I^{2\Omega}}{I_{\mathrm{sig}}}, \tag{18}$$

where V_{rms} is the root-mean-square voltage that is applied to the sample, I_{sig} is the light intensity transmitted through the sample with no applied voltage, d is the sample thickness, λ is the wavelength of the modulated light, and $I^{2\Omega}$ is the amplitude of the transmitted light modulated at 2Ω. The lock-in amplifier reading $I^{2\Omega}$ is referenced to twice the modulation frequency because the transmitted intensity ($I \propto |E_0|^2$) $\propto |V_{\mathrm{rms}} \cos(\Omega t)|^2$ is related to the applied quasi-static field at Ω. The experimental third-order nonlinear optical susceptibility [Eq. (17)] can then be obtained. Note that, at normal incidence, the electric field is perpendicular to the beam polarization and $s = s_{1133}$.

The magnitude of a typical QEA response (related to $n_0{}^3 s_{1133}$) as a function of frequency, read by the lock-in amplifier, is shown in Fig. 5. The relative phase between the signal and the applied voltage is shown in Fig. 5(b). To measure absolute values of s_{1133}, we must perform a

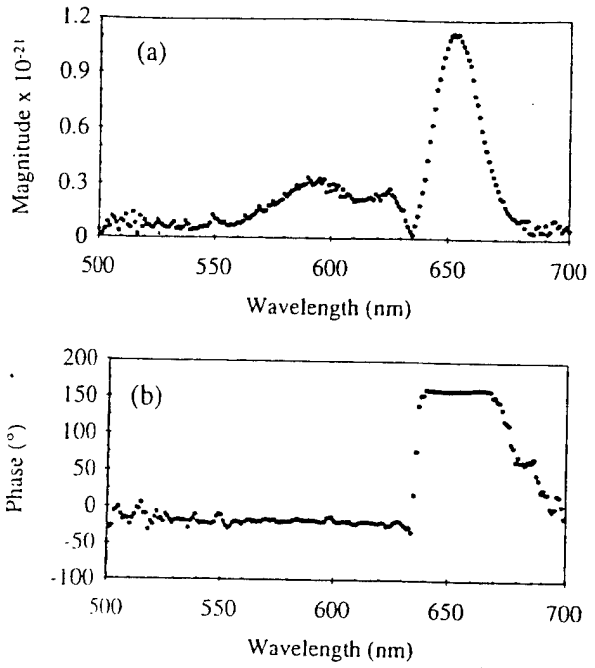

Fig. 5. (a) Magnitude (square meters per square volt) of the QEA spectrum of 0.5% TSQ at room temperature and modulating frequency Ω = 1.5 kHz. (b) Relative phase between the signal and the applied voltage.

calibration run of the detectors, without application of the external field, to obtain the zero-field transmitted light intensity I_0 (whose root-mean-square value is proportional to the transmitted intensity I_{sig}). For the calibration run the chopper is placed before the sample and the sample is removed. The intensity at each detector is then measured as a function of wavelength, and a calibration curve is generated.

4. EXPERIMENTAL RESULTS

A. Three-Level Model

The QEA spectrum for the BSQ dye is shown in Fig. 6 (points) with the theoretical three-level model (dashed curve). Initially, the original measured parameters ω_1, Γ_1, and μ_{01} are used to generate the theoretical curve (with Γ_2 = 50 meV). The two-photon state transition energy $\hbar\omega_2$, obtained from the experimental nonlinear spectrum of BSQ, is 2.094 eV, or 592.3 nm. All the squaraines (with the exception of PYSQ) have this two-photon transition energy of ~593 nm. The optimized three-level model curve, obtained by keeping ω_1 and Γ_1 fixed and adjusting the dipole transition moments as floating fit parameters, yields μ_{01} = 11.60 D and μ_{12} = 4.45 D. Because the measured values of Γ_1 may be an underestimation and Γ_2 is not necessarily equal to Γ_1, we also make them floating variables. The solid curve in Fig. 6 is the resulting best fit for Γ_1 = 57 meV, Γ_2 = 75 meV, and μ_{12} = 4.3 D (in agreement with the previous value).

Because the electronic characteristics of the squaraines (with the exception of PYSQ) are very similar, their nonlinear spectra resemble one another. For the particular case of the QEA spectrum of PSQ (points in Fig. 7), with μ_{01} = 11.58 D kept fixed, the optimization of the three-level model (dashed curve) results in a transition moment value of μ_{12} = 4.14 D. The origin of the relative shift, again, could be due to underestimation of either transition width Γ_1 or Γ_2 or to the uncertainty in ω_2 = 592.8 ± 1.5 nm. The last supposition was analytically determined to have no effect on the relative shift between the QEA spectrum and theoretical model. This relative shift depends heavily on the one-photon state parameters: The solid curve in Fig. 7 shows the three-level model best fit with μ_{12} = 4.40 D, ω_1 = 646 nm, Γ_1 = 48 meV, ω_2 = 591 nm, and Γ_2 = 75 meV. The theoretical fit for 0.5% TSQ, with the initial transition frequency variables kept fixed, is shown in Fig. 8. The parameters used for this fit are μ_{01} = 11.7 D (in agreement with the value in Table 1), μ_{12} = 4.35 D, $\hbar\omega_2$ = 2.091 eV, Γ_1 = 44 meV, and Γ_2 = 69 meV. Like that

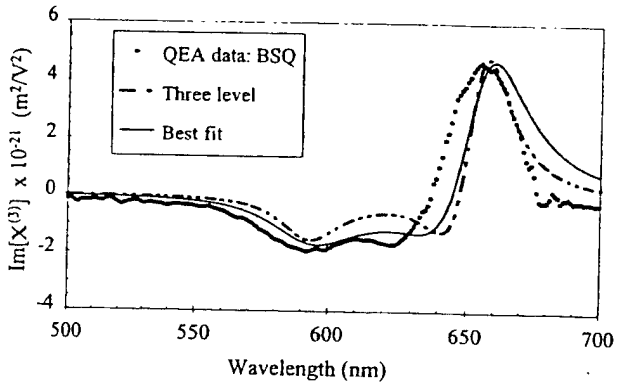

Fig. 6. QEA spectrum (points) and three-level model curves: theoretical fit (dashed curve) and best fit (solid curve) for BSQ.

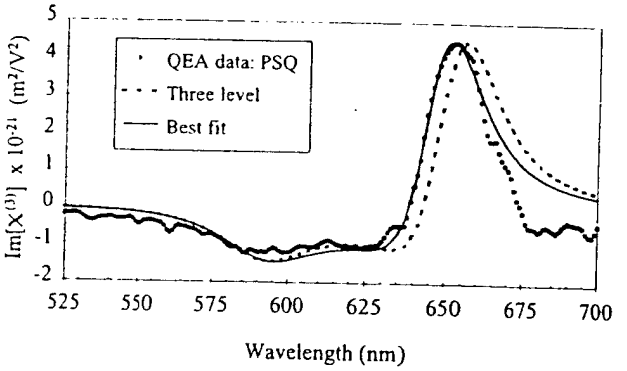

Fig. 7. Nonlinear spectrum and three-level model fits for PSQ.

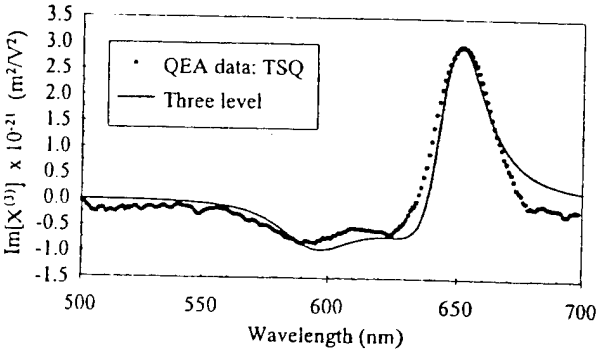

Fig. 8. Nonlinear spectrum and three-level model for 0.5% TSQ.

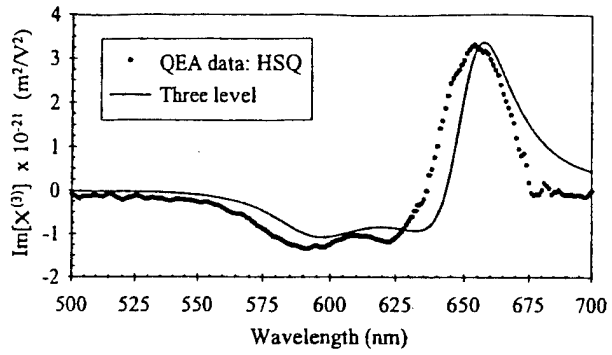

Fig. 9. QEA spectrum and three-level model fit for HSQ.

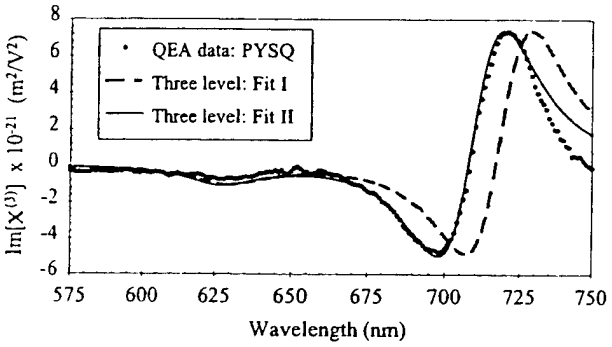

Fig. 10. QEA spectrum and three-level model fit for PYSQ.

Table 4. Parameter Values Used in the Three- and Four-Level Models for the PYSQ Dye

State n	Transition Moment $\mu_{n-1,n}$ (D)	Energy E (λ) [eV (nm)]	Half-Width Γ_n (meV)
1	11.40 ± 2.80	1.73 (718.2 ± 1.0)	46 ± 4
2	4.12 ± 0.86	1.97 (628.5 ± 1.0)	50 ± 5
3	μ_{13} varied	3.30 (375.0)	360

of PSQ, the three-level model fit of TSQ would improve if the value of ω_2 were decreased to 588 nm.

The nonlinear spectrum for HSQ is shown in Fig. 9. We optimized this three-level fit by using the one-photon parameters in Table 1, μ_{12} = 4.30 D, Γ_2 = 75 meV, and $\hbar\omega_2$ = 2.091 eV (from the two-photon hump in the nonlinear spectrum). Even though the qualitative agreement is good between the QEA spectrum and the three-level model, it is of great interest to determine what underlying electronic mechanisms are responsible for the slight discrepancy between the two. For this reason, other possibilities, such as a four-level model or *cis–trans* isomerization, are considered in the following subsections.

Figure 10 shows the QEA spectrum for 1% PYSQ; the theoretical model (dashed curve) parameters of the one- and two-photon states are listed in Table 4. The energy of the one-photon state, used in fit I of Fig. 10 (dashed curve), is fixed by its value obtained from the linear absorption spectrum. Even though it has dipole transition moments similar to those of the other dyes, its nonlinear spectrum is unique. The displacement in energy of the three-level model relative to the data is also slightly greater than for the other squaraines. When the transition energy of the one-photon state is made an adjustable parameter, the theory agrees well with the data for $\hbar\omega_1$ = 1.75 eV (solid curve in Fig. 10). The dipole transition moment is μ_{12} = 3.80 D for this fit (in agreement with the previous value), and Γ_2 = 48 meV. The transition width Γ_2 was also varied (50 ± 20 meV), with all the other parameters held constant: In this range the molecular susceptibility remains fairly constant, with no noticeable shift in the nonlinear peak or width. Again, consideration of a fourth state or *cis–trans* isomerization, without use of $\hbar\omega_1$ as a floating parameter, may lead to a better fit between theory and the experimental QEA spectrum.

One may ask why the transition moment to the first one-photon state may be different when it is determined with linear absorbance or QEA. The main problem with the linear absorption spectrum is the shoulder: It is difficult to determine the area under the main absorption peak without making assumptions about how to account for this shoulder. When the one-photon-state variables are used as fitting parameters in the QEA spectrum, the results can be considered reasonable, provided that the difference in these parameters is not substantial between fits to the linear and nonlinear data. In all the data analyzed in this paper, this provision was found to be satisfied.

B. Four-Level Model 1

The QEA spectrum for ISQ is shown in Fig. 11, as is the theoretical three-level model (solid curve) that uses data from Ref. 13. The four-level model [Eq. (8)], as applied to the same data, is represented by the dashed curves. For illustrative purposes, three reasonable values for μ_{13} are depicted, assuming a two-photon state at 375 nm ($\hbar\omega_3$ = 3.3 eV) with a transition width of Γ_3=360 meV, as measured by Andrews *et al.*[12] Clearly, as the variable μ_{13} is increased, the four-level model fit becomes inconsistent with the QEA measurement. The same analysis of this second two-photon state was also performed for the HSQ dye, resulting in the same qualitative findings as for the ISQ squaraine.

Using the same three-level model values listed in Table 4 (with μ_{12} = 4.4 D), we also consider the same fourth state mentioned above for PYSQ. A comparison of the dispersion terms [energy denominators Im(D_{11}), Im(D_{121}), and Im(D_{131})] is shown in Fig. 12. The four-level model fits are shown in Fig. 13 for several values of

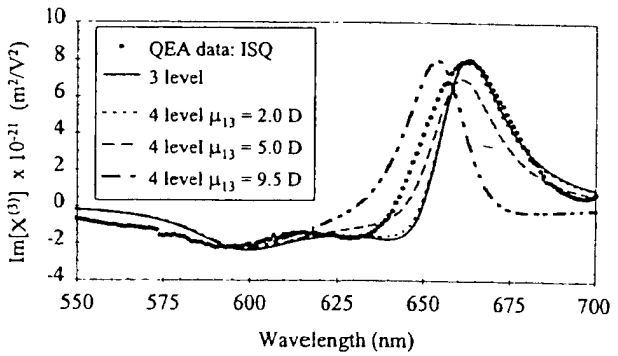

Fig. 11. Nonlinear spectrum of ISQ versus three-level model and four-level model 1.

μ_{13}. For very small μ_{13} (for example, up to 2.0 D), the four-level model 1 appears the same as the three-level; yet as this transition moment increases, the theoretical plot strays from the experimental data: It decreases in value (with the valley shrinking faster than the peak). Also, analysis of the molecular susceptibility indicates that $\mathrm{Im}(\gamma)_{4\text{-level}}$ remains constant as $\hbar\omega_3$ is varied from 3 to 15 eV (for example, with $\mu_{13} = 5$ D). Clearly, having this second two-photon state does not improve the fit to the data and is inconsistent with the QEA spectrum for $\mu_{13} > 3.0$ D.

We conclude from these measurements that the high-lying two-photon state cannot have a transition moment from the dominant one-photon state larger than ~3 D if the data are to be consistent with theoretical results. It is instructive to compare our results with those of Zhou *et al.*,[4] Yu *et al.*,[11] and Andrews *et al.*[12] Before doing this we must point out that our measurements are all done for molecules in solid polymer solution, the measurements of Yu *et al.*[11] and Andrews *et al.*[12] are in liquid solution, and the calculations of Zhou *et al.*[4] are in gas phase. Furthermore, the squaraines measured by Yu *et al.*[11] and calculated by Zhou *et al.*[4] are not identically the same molecules as in our measurements. We therefore would expect at best a qualitative agreement among the results.

First, the energies and the transition moments of the one-photon state and the low-lying two-photon state are consistent between our results and those of Andrews *et al.*[12] On the other hand, Yu *et al.*[11] do not discuss the low-lying two-photon state. Because this state is ~50 nm higher in energy than the one-photon state, it would appear at 7000 nm in their excited-state spectrum. Clearly, their experiments were not performed at this extreme wavelength.

The transition moment between the one-photon state in our measurement and the high-lying two-photon state is lower than that measured by Andrews *et al.* with THG[12] and by Yu *et al.*[11] with excited-state absorption. There are several possible explanations for this difference. We note that the third-harmonic experiments and our experiments deduce the excited-state values by using these values as adjustable parameters and fitting the observed spectrum to a multiple-level theory. Such a method is inherently inaccurate if the excited-state energy in question is much larger than the energy of the light used to probe the state. Small experimental uncertainties near the wavelengths measured can lead to large uncertainties in excited-state parameters of states that are far away in energy. The excited-state measurements of Yu *et al.*[11] do not suffer from this problem. The fact that those authors observe a differential spectrum with a peak corresponding to a two-photon state clearly shows the high-lying two-photon state. It is difficult, however, to determine the absolute transition moment from such measurements because it is difficult to determine the excited-state population that is being probed. Even simple single-beam two-photon absorption experiments, which are much easier to implement than two-beam excited-state experiments, are notorious for not being able to get accurate, absolute measurements. On the basis of these arguments, it is no surprise that our results vary by a factor of 2–3.

We believe that a proper analysis of the data in all three measurements needs to take account of the *cis–trans* composition of the sample. In Subsection 5.C, we show that such a model results in good agreement between experiment and theory.

C. Four-Level Model 2

As a starting point, a different four-level model (two one-photon states and a two-photon state) includes the values listed in Table 2. Figure 14 shows this plot (solid curve) for the values of $\mu_{01} = 11.5$ D, $\mu_{01'} = 8.6$ D, $\mu_{12} = 2.7$ D, and $\mu_{1'2} = 4.2$ D. It should be noted that the data have been rescaled to permit comparison of the relative shapes of the four-level model and the QEA spectrum. An important aspect that this model lacks is the distinct ap-

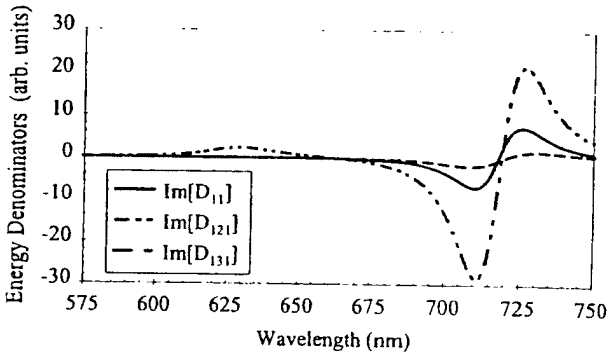

Fig. 12. Comparison of the dispersion terms used in the PYSQ three- and four-level 1 models.

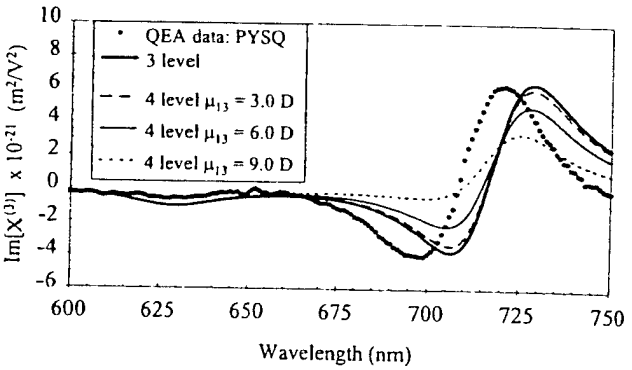

Fig. 13. Four-level model 1 for PYSQ as μ_{13} is varied.

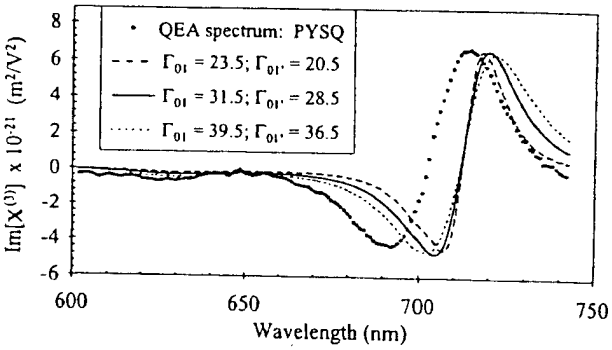

Fig. 14. Four-level model 2 of PYSQ using two one-photon states, with increasing transition widths (in millielectron volts).

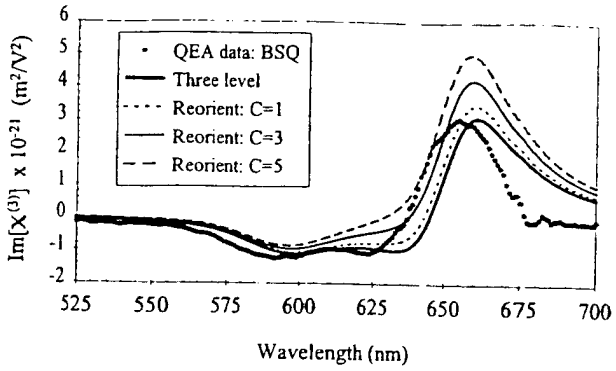

Fig. 15. BSQ three-level model including molecular reorientation.

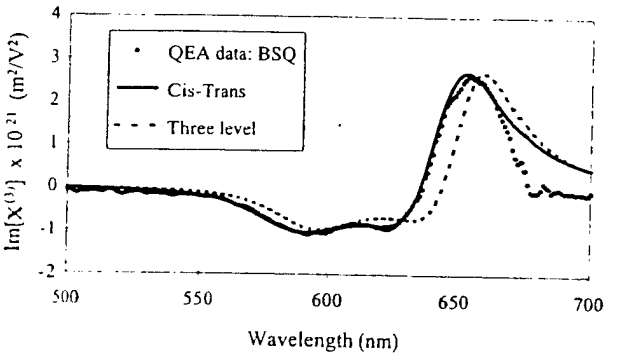

Fig. 16. Comparison of the three-level models (original and *cis–trans*) for BSQ.

pearance of the two-photon state, which can clearly be seen in the three-level model (Fig. 10). Various values of Γ_1 and $\Gamma_{1'}$ are used to expand the width of the model (dashed curves in Fig. 14) to fit the data, which occurs for the approximate values of $\Gamma_1 = 39.5$ and $\Gamma_{1'} = 36.5$ meV. In a similar fashion, we also modify the transition energies, $\hbar\omega_1$ and $\hbar\omega_{1'}$ to determine whether shifting of the theoretical plot occurs (with the best-fit transition width values mentioned above). The four-level fit does indeed get closer to the experimental QEA spectrum as the one-photon states get closer together in energy. For example, the transition energy values of $\hbar\omega_1 = 1.734$ and $\hbar\omega_{1'} = 1.742$ eV (separated by ~3 nm) give a theoretical plot that is similar to that of the three-level model for PYSQ.

D. Molecular Reorientation Model

Because molecular reorientation is thought to play a role in the distinct shift between the three-level model and the experimental QEA spectra, the reorientational term [Eq. (14)] is included in the original three-level model. We can vary the constant of proportionality c, which relates this term to $\mathrm{Im}[\chi^{(3)}]$ and which includes the elasticity of the polymer, to determine whether the reorientational term improves the level of agreement between theory and data. Since all the dyes (excluding PYSQ) have similar electronic properties, BSQ is selected as a representative of the squaraines. Figure 15 shows the experimental BSQ spectrum as well as the three-level model that includes molecular reorientation (with the multiplicative factor C varied for illustrative purposes). When the reorientational term is added, the three-level model is displaced upward with respect to the experimental curve, and there is no appreciable shift in wavelength. Because of the level of disagreement between this model and the nonlinear spectrum, we conclude that reorientational effects do not contribute substantially to our QEA measurements at room temperature.

E. *cis–trans* Model

Because it has been demonstrated that the molecules BSQ and ISQ can exist as a mixture of isomers,[5] we investigate these molecules with a comprehensive three-level model. Based on the linear optical and proton NMR spectral studies of Dirk *et al.*, a distribution of 21% *trans* and 79% *cis* isomers is assumed for BSQ (whose *trans* isomer is shown in Table 3). It was also determined that TSQ does not undergo *cis–trans* isomerization. Because TSQ, HSQ, and PSQ differ only in the length of alkyl groups attached to the nitrogens, we did not attempt to use the *cis–trans* model for these squaraines. From linear addition of the individual three-level models for the *cis* and *trans* isomers, the number of floating parameters, of course, doubles. Despite the increasing complexity of this model, Fig. 16 shows that the best fit is obtained for BSQ when the two slightly shifted spectra of the *cis* and the *trans* isomers are added according to the weight fraction of 21% *trans* and 79% *cis*. Table 5 lists the corresponding spectroscopic values of the parameters used in this theoretical fit. The theoretical model that includes *cis–trans* isomerization does provide a considerably closer fit for the nonlinear response of BSQ.

Because the ISQ molecule has been demonstrated to undergo *cis–trans* isomerization, the three-level *cis–trans* model is also applied to it, assuming a distribution of approximately 36% *trans* (the centrosymmetric ISQ6 struc-

Table 5. Parameters Used in the *cis* (C)–*trans* (T) Isomerization Model for BSQ

State n	Transition Moment $\mu_{n-1,n}$ (D)	Energy E (λ) [eV (nm)]	Half-Width Γ_n (meV)
1 (C)	11.40	1.93 (642.5 ± 1.0)	67 ± 3
2 (C)	3.75	2.12 (579.5 ± 1.0)	80 ± 4
1′ (T)	11.10	1.92 (643.5 ± 1.0)	65 ± 3
2′ (T)	3.63	2.09 (593.0 ± 1.0)	71 ± 3

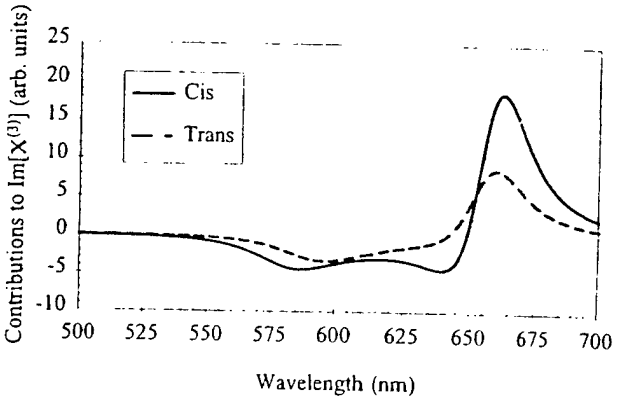

Fig. 17. Contributions of the ISQ *cis* and *trans* isomers to $\mathrm{Im}[\chi^{(3)}]$ for the *cis–trans* model.

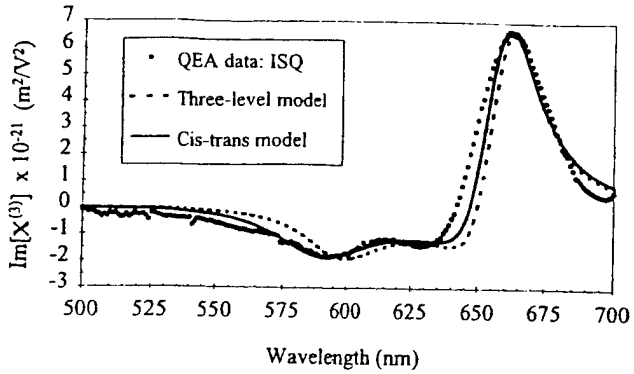

Fig. 18. Comparison of the three-level models (original and *cis–trans*) for ISQ.

Table 6. Parameters Used in the *cis* (C)–*trans* (T) Isomerization Model for ISQ

State n	Transition Moment $\mu_{n-1,n}$ (D)	Energy E (λ) [eV (nm)]	Half-Width Γ_n (meV; ±2)
1 (C)	11.80	1.89 (656.0 ± 1.0)	48
2 (C)	5.20	2.13 (583.0 ± 1.0)	80
1′ (T)	11.70	1.89 (655.0 ± 1.0)	50
2′ (T)	5.00	2.09 (593.0 ± 1.0)	74

ture) and 64% *cis* (the very polar ISQ4).[5] Even though the ISQ molecule can exist as six different *cis–trans* isomers, the two listed above are the most stable structures. Figure 17 shows the individual *cis* and *trans* contributions to $\mathrm{Im}[\chi^{(3)}]$ for the best obtainable *cis–trans* model fit. This particular model is compared in Fig. 18 with the original[13] three-level model for ISQ. From this it can be seen that, by considering a distribution of *cis–trans* isomers, this theory provides a better description of the nonlinear response than the original three-level model. Table 6 lists the values of the parameters used in the *cis–trans* model for ISQ.

The *cis–trans* model best describes the QEA spectrum for squaraines that exist as a mixture of isomers. For ISQ, the inclusion of all the possible isomers would be extremely difficult but may provide an even better description than assuming a combination of only two isomers.

5. CONCLUSION

The QEA spectra of several squaraines (including ISQ, a well-studied system known to have a large third-order nonlinear optical susceptibility) have been analyzed and compared with the theoretical molecular susceptibility. This evaluation permits the determination and verification of the excited-state characteristics of the dye-doped polymer by use of the sum-over-states perturbation theory. The set of transition widths and energies and the dipole transition moments (from the ground to the one-photon state and from the one-photon to the two-photon state) can be completely determined with the combination of linear and QEA spectroscopy. Although including as many states as possible in the perturbation theory would be most comprehensive, the three-level model provides an easy and very reasonable description of the excited states and their role in the nonlinear optical response. It appears that, for QEA spectroscopy, inclusion of a higher-lying two-photon state hinders the agreement between the theoretical nonlinear susceptibility and the QEA spectra. This result serves to verify the importance and dominance of the two-photon state in the visible region.

To fine tune our understanding of the nonlinear response, we must better model the material system. In the particular case of PYSQ, the three-level model was a good description of the data only when the transition energy $\hbar\omega_1$ was shifted by -10 nm. The reason for the shift is unclear. We used a different four-level model (with two one-photon states and a two-photon state) to determine whether this shift could be explained with two one-photon states that are very close in energy. (The two-photon state of the three-level model is used in both of the four-level models.) Transition width values needed for the agreement between theory and experiment were $\Gamma_1 = 39.5$ meV and $\Gamma_{1'} = 36.5$ meV.

The small shallow humps that appear in the absorption spectra of some squaraines are thought to be indicative of some underlying mechanism such as molecular reorientation and vibronic levels. By including the reorientation term, $\mathrm{Im}[\alpha(\omega)\alpha(0)]$, with the three-level model, we determined that addition of this term resulted in little or no improvement in the fit, implying that molecular reorientation can be ignored. This term only enhanced the one-photon peak and did not improve the fit.

The presence of *cis–trans* isomers was found best to describe the data when each isomer was treated as a separate three-level system. Two squaraines (ISQ and BSQ) are known to exist as a mixture of isomers, and when this *cis–trans* model is applied to BSQ, the theory and experiments agree well. Similarly, *cis–trans* isomerization provides a better description for the ISQ data than the three-level model alone. For squaraines, though, which do not exist as a mixture of isomers (such as TSQ), the three-level model presents a simple and acceptable representation of the nonlinear spectrum. We thus conclude that squaraine molecules are best described as three-level molecules and that the presence of isomer mixtures must be accounted for if nonlinear optical measurements are to be used to characterize the excited states of the molecule.

ACKNOWLEDGMENTS

The authors express gratitude to C. Poga for helpful discussions. We thank J. Haidar and E. Toussaere for helpful comments. We also thank the U.S. Air Force Office of Scientific Research, the Texas Higher Education Coordinating Board, and Sandia National Laboratory for generously supporting this research.

*Present address, France Telecom, Centre National d'Etudes des Telecommunications, Concepts et Dispositifs pour la Photonique/Electronique Quantique et Moleculaire, 196 rue Henri Ravera, 92225 Bagneux, France.

REFERENCES

1. J. Zyss, "Nonlinear organic materials for integrated optics: a review," J. Molec. Electron. **1**, 25 (1985).
2. M. G. Kuzyk, J. E. Sohn, and C. W. Dirk, "Mechanisms of quadratic electro-optic modulation of dye-doped polymer systems," J. Opt. Soc. Am. B **7**, 842 (1990).
3. C. W. Dirk and M. G. Kuzyk, "Squarylium dye-doped polymer systems as quadratic electrooptic materials," Chem. Mater. **2**, 4 (1990).
4. Q. L. Zhou, R. F. Shi, O. Zamani-Khamari, and A. F. Garito, "Negative third-order optical responses in squaraines," Nonlinear Opt. **6**, 145 (1993).
5. C. W. Dirk, W. C. Herndon, F. Cervantes-Lee, H. Selnau, S. Martinez, P. Kalamegham, A. Tan, G. Campos, M. Velez, J. Zyss, I. Ledoux, and L. Cheng, "Squarylium dyes: structural factors pertaining to the negative third-order nonlinear optical response," J. Am. Chem. Soc. **117**, 2214 (1995).
6. S. Marder, J. W. Perry, G. Bourhill, C. B. Gorman, B. G. Tiemann, and K. Mansour, "Relation between bond-length alternation and second electronic hyperpolarizability of conjugated organic molecules," Science **261**, 186 (1993).
7. J. C. Luong, N. F. Borrelli, and A. R. Olszewski, "Quadratic electro-optical characterization of molecular nonlinear optical materials," Mater. Res. Soc. Symp. Proc. **109**, 251 (1988).
8. C. W. Dirk and M. G. Kuzyk, "Damping corrections and the calculation of optical nonlinearities in organic molecules," Phys. Rev. B **41**, 1636 (1990).
9. M. G. Kuzyk and C. W. Dirk, "Effects of centrosymmetry on the nonresonant electronic third-order nonlinear optical susceptibility," Phys. Rev. A **41**, 5098 (1990).
10. C. W. Dirk, L.-T. Cheng, and M. G. Kuzyk, "A simplified three-level model describing the molecular third-order nonlinear optical susceptibility," Int. J. Quantum Chem. **43**, 27 (1992).
11. Y. Z. Yu, R. F. Shi, A. F. Garito, and C. H. Grossman, "Origin of negative $\chi^{(3)}$ in squaraines: experimental observation of two-photon states," Opt. Lett. **19**, 786 (1994).
12. J. H. Andrews, J. D. V. Khaydarov, K. D. Singer, D. L. Hull, and K. C. Chuang, "Characterization of excited states of centrosymmetric and noncentrosymmetric squaraines by third harmonic spectral dispersion," J. Opt. Soc. Am. B **12**, 2360 (1995).
13. C. Poga, T. M. Brown, M. G. Kuzyk, and C. W. Dirk, "Characterization of the excited states of a squaraine molecule with quadratic electroabsorption spectroscopy," J. Opt. Soc. Am. B **12**, 531 (1995).
14. R. W. Bigelow and H. Freund, "An MNDO and CNDO/S(S+DES CI) study on the structural and electronic properties of a model squaraine dye and related cyanine," Chem. Phys. **107**, 159 (1986).
15. Y. R. Shen, *Principles of Nonlinear Optics* (Wiley-Interscience, New York, 1984).
16. C. Poga, M. G. Kuzyk, and C. W. Dirk, "Quadratic electroabsorption studies of third-order susceptibility mechanisms in dye-doped polymers," J. Opt. Soc. Am. B **11**, 80 (1994).
17. B. J. Orr and J. F. Ward, "Perturbation theory of the nonlinear optical polarization of an isolated system," Mol. Phys. **20**, 513 (1971).
18. C. Poga, "Mechanisms of the third-order nonlinear optical response in dye-doped polymers," Ph.D. dissertation (Washington State University, Pullman, Wash., 1994).
19. R. W. Boyd, *Nonlinear Optics* (Academic, San Diego, Calif., 1992).
20. K. D. Singer, M. G. Kuzyk, and J. E. Sohn, "Second-order nonlinear-optical processes in orientationally ordered materials: relationship between molecular and macroscopic properties," J. Opt. Soc. Am. B **4**, 968 (1987).
21. K. Zimmerman, F. Ghebremichael, and M. G. Kuzyk, "Electric-field-induced polarization current studies in guest–host polymers," J. Appl. Phys. **75**, 1270 (1994).
22. M. G. Kuzyk and C. Poga, "Quadratic electro-optics of guest–host polymers," in *Molecular Nonlinear Optics: Materials, Physics, and Devices*, J. Zyss, ed. (Academic, San Diego, Calif., 1993), pp. 299–337.